Examination of Factors Influencing Environmental Stability of the 2009 H1N1 Pandemic Influenza Virus and its Pathogenesis in the Ferret Model

by

Andrea J. French

B.S., University of Wisconsin, Madison, 2017

Submitted to the Graduate Faculty of the

School of Medicine in partial fulfillment

of the requirements for the degree of

Doctor of Philosophy

University of Pittsburgh

2023

UNIVERSITY OF PITTSBURGH

SCHOOL OF MEDICINE

This dissertation was presented

by

Andrea J. French

It was defended on

April 14, 2023

and approved by

JoAnne L. Flynn, PhD, Professor, Microbiology and Molecular Genetics

John V. Williams, MD, Professor, Pediatrics

Jennifer M. Bomberger, PhD, Professor, Microbiology and Immunology, Dartmouth College

N. Luisa Hiller, PhD, Professor, Biological Sciences, Carnegie Mellon University

Michael M. Myerburg, MD, Professor, Pulmonary, Allergy, and Critical Care Medicine

Dissertation Director: Seema S. Lakdawala, PhD, Microbiology and Immunology, Emory University

Examinations of Factors Influencing Environmental Stability of the 2009 H1N1 Pandemic Influenza Virus and its Pathogenesis in the Ferret Model

Andrea J. French, PhD

University of Pittsburgh, 2023

Influenza virus is an ongoing global disease burden. It circulates annually as a seasonal respiratory virus and has caused most major pandemics within the last century. Influenza infection is often complicated by secondary bacterial infection with *Streptococcus pneumoniae,* resulting in increased morbidity and mortality. This dissertation investigates factors influencing transmission and severe disease of the 2009 H1N1 pandemic influenza virus (H1N1pdm09) by assessing how co-infection with *S. pneumoniae* impacts H1N1pdm09 pathogenesis and environmental stability and by defining the role of droplet size on H1N1pdm09 environmental stability. First, research investigating co-infection's impact on morbidity established tissue-specific trends towards increased bacterial burden in the upper respiratory tract of co-infected ferrets compared to mono-infection. The relationship between viral and bacterial burden varied by tissue and was associated with altered host responses. Exploration of host responses showed that they were critical components of increased morbidity during co-infection and the altered host responses varied by tissue. These data establish previously unknown aspects of pathogenesis and host immune response to influenza virus and *S. pneumoniae* co-infection in the ferret model. Additional work focusing on the environmental persistence and prevalence of H1N1pdm09 and *S. pneumoniae* in respiratory emissions revealed that both microbes were detected in aerosols from co-infected ferrets. In addition, *S. pneumoniae* in respiratory fluid droplets exhibited a trend towards increased persistence in the presence of H1N1pdm09. Co-infections with these microbes can therefore result

in spread of both pathogens and may lead to increased bacterial stability outside the host. Finally, to evaluate virus persistence, I compared H1N1pdm09 decay in 50 µL, 5 µL, and 1 µL droplets at variable relative humidity to decay of bacteriophage Phi6. Results show virus within larger droplets is more sensitive to relative humidity-mediated decay than smaller droplets. Additionally, Phi6 decay differed from H1N1pdm09 at low relative humidity. These findings highlight the importance of using relevant droplet sizes and appropriate surrogates to evaluate half-lives for pathogens. Taken together, the results of this dissertation further the field of influenza virus transmission and pathogenesis and can ultimately inform future mitigation measures to reduce overall disease burden.

Table of Contents

1.0 Introduction....1

1.1 Influenza Viruses....1

1.1.1 Influenza virus lifecycle....1

1.1.2 Influenza Virus Pathogenesis....2

1.1.3 Animal Models of Influenza....3

1.1.4 Pathogenesis of Influenza Virus in the Ferret....4

1.1.5 Host Response to Influenza Virus....6

1.1.5.1 Innate Response to Influenza Virus....6

1.1.5.2 Adaptive Response to Influenza Virus....7

1.1.6 Ferret Host Responses to Infection....8

1.1.7 Immunopathology....9

1.1.8 Factors influencing Pathogenesis and Immune Responses....10

1.2 Influenza and *Streptococcus pneumoniae* Co-infection....11

1.2.1 Morbidity and Mortality of Influenza and *S. pneumoniae* Co-infection....11

1.2.2 *S. pneumoniae*, the Primary Source of Community-acquired Pneumonia...11

1.2.3 Timing of Influenza and *S. pneumoniae* Co-infection....13

1.2.4 Impact of Co-infection on *S. pneumoniae*....14

1.2.5 Impact of Co-infection on Influenza Virus....15

1.2.6 Immune Response to Co-infection....16

1.2.6.1 Immune Response to *S. pneumoniae*....16

1.2.6.2 Bacterial Modulation of the Antiviral Immune Response....17

1.2.6.3 Immune Responses to Influenza Facilitate *S. pneumoniae* Secondary Infection 19

1.2.7 Reducing Burden of Disease 21

1.3 Transmission of Respiratory Pathogens 21

1.3.1 Modes of Transmission 22

1.3.2 Spread of Influenza Viruses 23

1.3.3 Transmission Experiments with Ferrets 25

1.3.4 Transmission during Co-infection 26

1.3.4.1 Impact of Co-infection on *S. pneumoniae* Transmission 26

1.3.4.2 Impact of Co-infection on Influenza Virus Transmission 27

1.3.5 Environmental Stability of Microbes 28

1.3.6 Respiratory tract droplet sizes and composition 31

1.4 Statement of the Problem 32

2.0 Tissue-specific responses and microbial relationships during influenza virus and *Streptococcus pneumoniae* co-infection in the ferret model 34

2.1 Abstract 34

2.2 Introduction 35

2.3 Results 38

***2.3.1* Co-infected ferrets display greater morbidity and more severe pathology than ferrets infected with only influenza virus or *S. pneumoniae* 38**

2.3.2 Co-infection leads to tissue-specific increased bacterial burden in the upper respiratory tract 46

2.3.3 Tissue site is an important determinant of viral/bacterial titer relationship and host response to infection.....52

2.3.4 Host response to co-infection varies by tissue 53

2.3.5 Host response to co-infection is synergistic compared to mono-infection....56

2.3.6 Co-infection broadly heightens immune response pathways in the nasal turbinates but not the soft palate or lungs 60

2.3.7 Immune cell migration and chemotaxis pathways are highly enriched in the nasal turbinates of co-infected animals.....62

2.4 Discussion 67

2.5 Materials and Methods 67

2.5.1 Viruses and bacteria.....70

2.5.2 Ferrets.....71

2.5.3 Histology and immunohistochemistry 72

2.5.4 RNA Sequencing.....73

2.5.5 Acknowledgements.....73

3.0 Detection of Influenza virus and Streptococcus pneumoniae in air sampled from co-infected ferrets and analysis of their influence on pathogen stability.....74

3.1 Abstract 74

3.2 Importance 75

3.3 Observation and Discussion.....75

3.3.1 Co-infected ferrets shed H1N1pdm09 and Spn into expelled aerosols. 76

3.3.2 Environmental stability of H1N1pdm09 is not impacted by the presence of Spn.....80

3.4 Materials and Methods 86

3.4.1 Virus and Bacteria 86

3.4.2 Animals 86

3.4.3 Air Sampling 87

3.4.4 Stability Experiments 88

3.4.5 Data Availability 89

3.4.6 Acknowledgements 89

4.0 Environmental stability of enveloped viruses is impacted by the initial volume and evaporation kinetics 91

4.1 Abstract 91

4.2 Introduction 92

4.3 Results 94

4.3.1 Relative humidity alters morphology of evaporating droplets and drying kinetics 94

4.3.2 Virus decay is more sensitive to relative humidity in large droplets 98

4.3.3 Virus decay rates differ during the wet and dry phases and depend on droplet volume and virus 105

4.3.4 H1N1pdm09 decays similarly to SARS-CoV-2 at intermediate RH 111

4.4 Discussion 117

4.5 Materials and Methods 123

4.5.1 Cells and viruses 123

4.5.2 Evaporation experiment 125

4.5.3 Stability studies 125

4.5.4 Calculations and modeling 126

4.5.5 Quantitative RT-PCR 128

4.5.6 Multivariate analysis 128

4.5.7 Data Availability 129

4.5.8 Acknowledgements and funding 129

5.0 Summary and Implications 130

5.1 Summary 130

5.1.1 Influenza virus and *S. pneumoniae* co-infection has complex impacts on pathogenesis 132

5.1.2 Analysis of microbial stability in the environment requires careful consideration of experimental conditions 133

5.2 Future Directions 135

5.2.1 Bacterial evolution during co-infection 135

5.2.2 Sampling aerosols to assess for presence of commensal bacteria during influenza infection 136

5.2.3 Impact of droplet size on microbial stability in the presence of biologically relevant solutions 137

5.3 Conclusion 138

Appendix A 139

Bibliography 140

List of Tables

Table 1 ..... **50**

Table 2 ..... **51**

Table 3 ..... **59**

Table 4 ..... **65**

Table 5 ..... **72**

Table 6 ..... **83**

Table 7 ..... **98**

Table 8 ..... **98**

Table 9 ..... **103**

Table 10 ..... **105**

Table 11 ..... **110**

Table 12 ..... **111**

Table 13 ..... **115**

Table 14 ..... **123**

List of Figures

Figure 1. Characterizing abundance and environmental stability of respiratory emissions during co-infection could help reduce incidence. 30

Figure 2. Morbidity of co-infected ferrets compared to H1N1pdm09 or D39 only. 40

Figure 3. Pathology of co-infected ferrets compared to H1N1pdm09 or D39 only.....44

Figure 4. Viral and bacterial burden in nasal washes of infected animals.....48

Figure 5. H1N1pdm09 and D39 titers in infected ferret tissues. 49

Figure 6. Determination of tissue-specific relationships between viral and bacterial burden. 53

Figure 7. RNA sequencing of infected tissues reveals tissue-specificity. 55

Figure 8. RNAseq in nasal turbinates, soft palate, and lungs shows that many genes differentially expressed during co-infection overlap with genes altered during H1N1pdm09-only infection. 58

Figure 9. Gene set variation analysis of sequenced RNA samples.....61

Figure 10. Comparison of co-infection to H1N1pdm09-only in the nasal turbinates shows enrichment of genes involved in immune cell migration. 63

Figure 11. Co-infected ferrets shed H1N1pdm09 and Spn. 78

Figure 12. Condensation air sampling.....79

Figure 13. Stability of S. pneumoniae and influenza viruses in droplets. 84

Figure 14. Macroscale physico-chemical characteristics of DMEM droplets vary with RH but not initial volume.....96

Figure 15. Initial droplet volume impacts drying kinetics.....97

Figure 16. Virus decay varies more with relative humidity in large droplets than in small droplets.....100

Figure 17. Environmental conditions of H1N1pdm09 and Phi6 droplets were within an average of 5% of the target RH and maintained temperatures between 20 and 25°C. 101

Figure 18. Mechanistic first-order decay modeling of viral decay in 5x5 µL droplets at 40% RH and 10x1 µL droplets at 65% RH shows that viral decay during the wet phase is greater than decay during the dry phase. 108

Figure 19. Mechanistic, first-order exponential decay modeling shows that the decay during the wet phase is greater or similar to the rate of decay the dry phase.....109

Figure 20. SARS-CoV-2 and H1N1pdm09 decay similarly across RH in 1x50 µL droplets. 114

Figure 21. SARS-CoV-2 and H1N1pdm09 decay similarly across droplet volume at intermediate RH. 117

Figure 22. Evaporation is major determinant of virus decay regardless of initial droplet volume.....122

Figure 23. Disseration summary.....131

Equations

Equation 1 126

Equation 2 127

Equation 3 127

Equation 4 127

Preface

Every PhD is a rollercoaster, and this one is no exception. I am extremely grateful to my thesis committee for guiding my project and providing critical feedback. None of this work would have been possible without the guidance of my mentor, Dr. Seema Lakdawala, who taught me to think critically, become a storyteller, and always encouraged me to celebrate with bubbles. Thank you for always providing opportunities to grow.

I would like to thank our wonderful collaborators at Virginia Tech (Dr. Linsey Marr and Alex Longest) and Carnegie Mellon University (Dr. Luisa Hiller and Karina Mueller Brown) for working together with us through long review processes and always pushing to produce a better product.

I would also like to thank all our lab members, both past and present, but I would especially like to acknowledge Dr. Valerie Le Sage and Dr. Nicole Rockey for the many memorable times together in the lab. These two have been steadfast allies in my pursuit of graduation. Thank you for always providing honest feedback and guidance.

Thanks should also go to my friends and cohort, for making me laugh until I cried, and crying with me until we laughed. Finally, I would like to express my profound gratitude to my partner, Megan, for moving out to Pittsburgh during a tumultuous time in the world. This dissertation is a testament to your unwavering support.

1.0 Introduction

1.1 Influenza Viruses

Influenza virus is a significant global health burden. Influenza A virus has caused four major pandemics since the advent of the 20th century, with the most severe of these in 1918 leading to an estimated 25-50 million deaths worldwide[1]. Influenza virus also circulates annually, contributing to increased morbidity and mortality. The most recent influenza pandemic occurred in 2009, when a novel influenza A H1N1 virus emerged in California and Mexico[2]. During the 2009 pandemic, infection with the 2009 influenza A virus was typically a self-limiting infection that included cough, sore throat, fever, and malaise[2,3]. In severe cases, infection leads to pneumonia, respiratory failure, multi-organ failure, or death[2,4]. During the 2009 H1N1 pandemic, approximately 11% of people admitted to the hospital died[5]. Influenza virus is also an agricultural burden, as infection of birds in the 2014-2015 season led to the death or culling of over 50.4 million poultry in the United States and an economic cost of $3.3 billion[6]. The current avian influenza outbreak is even more severe[7]. As such, prevention of influenza virus infection has broad implications for human and animal health.

1.1.1 Influenza virus lifecycle

Influenza A virus is an eight-stranded negative sense RNA virus that infects epithelial cells in the respiratory tract through binding of the viral hemagglutinin (HA) protein to its host entry receptor: α2,3 or α2,6 sialic acids. Upon binding the entry receptor, the virus undergoes receptor-

mediated endocytosis[8]. Once endocytosed, endosomal acidification leads to cleavage of the receptor binding protein, HA, to its fusion form[9]. The virus then fuses with the endosome and is released into the cell cytosol[10]. Influenza virus then traffics to the nucleus[11], where it undergoes most of its lifecycle: protein production and genome replication.

Once in the nucleus, the genomic RNA generates messenger RNA that is exported to the cytosol and translated into the viral proteins[11]. Some of these viral proteins then return to the nucleus to facilitate genome replication[12]. Genome replication occurs first through transcription of complementary RNA that are complements of the genomic RNA segments. The complementary RNA is then used as a template for production of new genomic RNA[13]. Once the new genomic RNA is transcribed and assembled into viral ribonucleoprotein complexes, they are transported out of the nucleus in a process dependent on CRM-1 and the Nuclear Export Protein[14]. The eight genomic ribonucleoprotein complexes assemble in the cytoplasm before budding to form new virions[15]. Finally, the viral neuraminidase (NA) protein is essential to prevent budding virions from sticking to the cells from which they are exiting[16,17].

To date, 18 HA proteins and 11 NA proteins have been identified for influenza A viruses[18]. These proteins are then used to name influenza A virus strains (HxNx), as these proteins are major determinants of virus tropism[19,20] and pathogenesis[21]. These proteins are the major viral proteins detected by antibodies and therefore are major determinants of susceptibility to pre-existing immunity[22].

1.1.2 Influenza Virus Pathogenesis

Human challenge studies have given us valuable insight into the pathogenesis of influenza virus in humans. While there is some variation by virus subtype, infection with H1N1, H3N2, or

H2N2 viruses typically led to a peak in virus shedding into nasal wash on day 2 post-infection and an average shedding duration of 4.80 days[23]. Clinical symptoms follow virus shedding by 24-48 hours and can sometimes last much longer than virus shedding[23,24]. Experimental infections have shown that infection can initiate in the upper or lower respiratory tract, as both small volume intranasal inoculations that don't drain into the lungs and aerosol inoculation can initiate infection[25]. However, it seems that the dose required for infection of the lungs via aerosol is lower than the dose required for intranasal infection by up to 100-fold[26,27], suggesting that the lungs might be more sensitive to infection.

Upon entering the body, influenza infection first begins in epithelial cells of the respiratory tract[28]. This leads to high levels of infectious virus present in the nasal passages, soft palate, trachea, and lungs that typically resolves around day seven post-infection[27,29,30]. Histological analysis of lung tissues has shown that epithelial cells in the bronchioli are the most likely to be infected in the lungs, with only rare detections of infected cells in the lung parenchyma[31]. In cases of influenza leading to hospitalization, the most common symptoms are fever, cough, and shortness of breath[5,32]. Nausea/vomiting, muscle aches, sore throat, chills, diarrhea, and rhinorrhea are also common[5].

1.1.3 Animal Models of Influenza

Human challenge experiments provide extremely valuable insight into influenza pathogenesis, but due to the high cost, ethical considerations, and challenging logistics, these are often not possible. Much of what is known about influenza virus pathogenesis and host response comes from animal models of infection. The most commonly studied animal models for studying

influenza virus pathogenesis include the mouse (*Mus musculus*) and the ferret (*Mustela putorius furo*).

Use of the ferret model offers many advantages over the other models[33]. Unlike mice, which require adaptation of influenza virus for infection, ferrets are naturally susceptible to influenza virus infection[33]. Ferrets have a sneeze reflex[21], a symptom also observed during infection in humans. Pathogenesis of influenza virus in ferrets is also more similar to humans than the pathogenesis in guinea pigs, as highly pathogenic influenza viruses are not fatal in guinea pigs[33].

Given that ferrets are not as widely used in biomedical research as mice, there is more limited availability for ferret-specific reagents, and the ferret genome has not been as well annotated as those of mice and humans. Subsequently, the murine model is commonly used to study the immune response to influenza virus due to their genetic tractability, ease of use, and their well characterized genome. However, a comparison of mouse, ferret, and human genomes found that for 75% of genes, the ferret sequences are closer to the human sequences than are the mouse sequences[34], suggesting the study of ferret responses to infection is valuable to understanding respiratory viruses.

1.1.4 Pathogenesis of Influenza Virus in the Ferret

Ferrets are naturally susceptible to seasonal influenza viruses and avian influenza viruses[35,36]. Most experiments use animals naïve to influenza virus infection to assess pathogenesis. Infection of ferrets has been performed using small volume intranasal inoculation to initiate infection only in the nose[37], large volume intranasal inoculation to flush the respiratory tract system[37], or aerosol infection[25]. Interestingly, studies in ferrets showed that the dose of

influenza required to initiate infection when infecting with an intranasal liquid suspension was similar to the dose required when infecting with inhaled aerosols[25]. However, increased inoculum volume correlates with more severe clinical signs[37].

Once infection is initiated, ferrets display clinical symptoms similar to humans: fever, anorexia, weight loss, sneezing, nasal discharge, and lethargy[38]. Infection is typically tracked by nasal washing anesthetized animals (passing PBS through the nostrils and collecting flow-through). While there is some variability, experimentally infected animals typically display peak virus shedding into nasal wash on day two post-infection of seasonal influenza viruses, and infection resolves around day seven post-infection[39]. Assessment of seasonal influenza virus replication in tissues shows a similar trend of virus replication, although there is variation by virus[37]. Virus titers in tissues peak between day one and day three post-infection, leading to resolution in the lower respiratory tract around day seven[29], although RNA remains detectable through day 11[40]. Viral RNA in the upper respiratory tract peaks sooner than the lower respiratory tract[21,40]. Resolution of infection, as measured by no longer detecting infectious virus, in the upper respiratory tract (nasal turbinates and soft palate) does not necessarily occur at the same time as the lower respiratory tract[29,37]. Whether differences in resolution of infection are due to slower clearance or sustained replication in the tissue is unclear.

Histological analysis of tissues from ferrets infected with seasonal H1N1 and H3N2 viruses showed that inflammatory changes in the nasal turbinates begins on day three and is most evident on day six[37]. The nasal turbinates display cellular hyperplasia and loss of cilia. There is also significant infiltration of inflammatory cells (primarily neutrophils and necrotic cellular debris) and edema into the nasal turbinate lumen[37]. The lungs display inflammation at timing similar to the nasal turbinates, with little to no inflammation noticeable on day one, and most severe

pathology on day six post-infection[37]. Lung inflammation primarily presented as neutrophils present around the small airways, edema, and epithelial hyperplasia[37,41].

1.1.5 Host Response to Influenza Virus

Host defenses again influenza virus are both physical and cellular. To initiate infection, influenza must bypass physical barriers in the respiratory tract, such as the mucus layer atop the epithelial cells[42]. It has been demonstrated that overexpression of a specific mucin, MUC1, leads to reduced influenza infection of human lung epithelial cells, and mice deficient in MUC1 have enhanced disease severity during influenza infection[43]. Once the virus traverses the mucus, it can infect epithelial cells of the respiratory tract and spread to alveolar macrophages[28].

1.1.5.1 Innate Response to Influenza Virus

Upon initiating infection, the host innate immune response will kick in. At least three different classes of pattern recognition receptors recognize influenza virus infection: toll-like receptors (TLR3, TLR7, and TLR8; sensing single-stranded RNA and double-stranded RNA), retinoic acid-inducible gene I (RIG-I; sensing 5'-triphosphate RNA), and the NOD-like receptor family member, NOD-, LRR- and pyrin domain-containing 3 (NLRP3; multiple stimuli)[44,45]. TLR3, TLR7, and TLR8 all detect virus within endosomes of innate immune cells like dendritic cells and macrophages. RIG-I and NLRP3 detect virus within the cytoplasm of cells[44]. These pattern recognition receptors then signal through NFκB, interferon-regulatory factor 3 and 7 (IRF3, IRF7) to initiate transcription of type 1 interferons (such as interferon-α and β: IFNα, IFNβ), which then lead to transcription of interferon-stimulated genes (ISGs)[44]. Some of the ISGs with important antiviral effects against influenza virus include MX1 (suppresses viral mRNA transcription), OAS

(degrades viral RNA), and PKR (suppresses protein translation), although there are many more[44,46–48]. Transcription of pro-IL-1β and pro-IL-18 occurs through NFκB and then together with the NLRP3 inflammasome cleaves them to their active forms which are then secreted. This has been observed in human bronchial epithelial cells and in ferrets during influenza infection[49]. The NLRP3 inflammasome then contributes to initiation of adaptive immunity by establishing T-helper type 1 (Th1) cell, cytotoxic T lymphocyte, and IgA responses[50].

1.1.5.2 Adaptive Response to Influenza Virus

Detection of virus by alveolar macrophages leads to release of cytokines and chemokines[48]. These cytokines, such as tumor necrosis factor alpha (TNFα), are pro-inflammatory[48]. Upon induction of inflammation, neutrophils will be some of the first white blood cells to reach the site of infection, followed by monocytes[48]. IL-1[51], IL-6[52] and IL-18[53] promote the host adaptive immune response by attracting and activating $CD8^+$ T lymphocytes at the site of infection. IL-1 promotes adaptive responses by inducing an antibody response from B cells and cytotoxic activity from T cells[44].

Antigen presenting cells such as tissue-resident dendritic cells and macrophages traffic to the lymph nodes where they provide stimulation for $CD4^+$ T cells and $CD8^+$ T cells. The $CD4^+$ T cells both produce IL-2, which drives $CD8^+$ T cell proliferation, and help activate the $CD8^+$ T cells[48,54]. T-follicular helper cells (T_{FH}), a subset of $CD4^+$ T cells, assist B cells in generating certain immunoglobulins[48]. So, $CD4^+$ T cells are a critical component that coordinates the adaptive immune response to infection. Once activated, B cells differentiate into plasma cells that produce antibody and memory B cells[48]. Antibodies both assist in viral clearance and contribute to future protection against influenza virus[55]. The type of antibody present in the upper respiratory tract, IgA, differs from the type dominating the lower respiratory tract, IgG[22]. Together, the antiviral

effects of innate effector molecules combined with the adaptive killing response helps the host clear influenza virus.

1.1.6 Ferret Host Responses to Infection

Investigation of ferret immune responses to influenza infection has been hampered by a limited availability of ferret specific reagents. In 2014, a panel of qPCR primers from previous publications[56] were further validated to address a subset of cytokines, chemokines, and housekeeping genes in ferrets[57]. Subsequently, these primers were used to look at the ferret response to influenza A and influenza B infection[40]. They found that inflammatory cytokines peaked at similar times as peaks in viral RNA: around day two in the upper respiratory tract and day five in the lower respiratory tract[40]. Granzyme A, one of the enzymes released by $CD8^+$ T cells to kill infected cells, peaks slightly after the peak in viral RNA, which likely corresponds to the immune system working to clear the virus[40]. Then IL-10 peaks at day nine to ten, corresponding to the start of the anti-inflammatory response and tissue repair[40,48]. A comparison of seasonal H3N2, 2009 pandemic H1N1, and two avian H5N1 viruses in ferrets also found that TNFα and IL-6 mRNA in the upper respiratory tract correlated with virus shedding, sneezing, rhinorrhea, and virus transmission[21]. Influenza virus strains that induced the greatest clinical signs and peak virus shedding in the upper respiratory tract induced much higher levels of IFNα and IFNβ than less severe infections[21].They also found that the chemokines CXCL9, CXCL10, and CXCL11 peaked for all four virus infections at day two[21].

When looking at cellular responses, lymphopenia in the peripheral blood of animals infected with an H3N2 or H1N1 virus suggests that these $CD8^+$ and $CD4^+$ T cells are trafficking to the respiratory track or lymph nodes to fight infection[58]. There also appeared to be

granulocytosis/neutrophilia in infected ferrets. The presence of B cells in the peripheral blood were more scattered and trends were not interpretable[58]. Another study found that, following H3N2 influenza infection, B cells were trafficking to the spleen and lymph nodes of the infected regions[59]. Together, studies of immune responses in ferrets suggest that infection causes a type one interferon response that then leads to leukocyte chemotaxis to the respiratory tract. Neutrophils, alveolar macrophages, T cells, and antibody-producing B cells contribute to viral clearance. The antibody response then provides protection against future infection[39]. Further study of the cellular immune responses in ferrets will require improved tools to determine T cell subsets, B cell subsets, and more accurately characterize innate immune cells.

1.1.7 Immunopathology

While an immune response is critical to prevent a pathogen from overtaking and killing an infected host, this response needs to be balanced. An overly strong immune response can hurt the host and lead to tissue damage or death, as was observed by the "cytokine storm" that contributes to influenza deaths[60,61]. While influenza infection kills epithelial cells, the host is also harmed by the strength of the immune response. For example, detection of virus by TLR3 helps control viral replication. However, mice deficient in TLR3 have demonstrated improved survival following influenza infection, suggesting that while TLR3 helps control replication, it also leads to a detrimental immune response[62]. The TLR3 deficient mice had reduced levels of IL-6, a cytokine that's been shown to correlate with increased symptom scores and temperature in experimental human infection[62,63]. Some of the signaling components during influenza infection have been identified as modulating lung pathology, demonstrating the fine balance between protection and

damage[64]. So, extreme immune responses can be harmful even if they're meant to control infection.

1.1.8 Factors influencing Pathogenesis and Immune Responses

A number of risk factors have been identified to influence the pathogenesis of influenza virus[65]: age, obesity, sex, pregnancy, microbiome, and co-infection. Influenza infection is typically most severe in elderly adults, corresponding to immunosenescence[66]. However, the age group most impacted can vary, as the 1918 H1N1 pandemic was particularly severe amongst young adults[67]. Obesity also contributed to worsened outcomes during the 2009 H1N1 pandemic[68]. Sex differences during influenza infection can be difficult to assess, as these differences likely vary by age, as sex hormones fluctuate. An assessment of pediatric mortality found that female sex was a significant predictor of mortality[69]. Studies in mice have shown that female mice have greater antibody responses than male mice in response to vaccination[70]. Reports from the 1918 and 2009 H1N1 pandemics demonstrate the increased risk of mortality due to pregnancy[71,72]. More recently, there has been a growing interest in the role the microbiome plays in health and disease. Research has suggested that the commensal microbiome can alter susceptibility to influenza infection[73,74] and it can modulate the immune response to influenza[75]. One of the greatest risk factors for severe disease during influenza infection is bacterial co-infection[76,77].

1.2 Influenza and *Streptococcus pneumoniae* Co-infection

1.2.1 Morbidity and Mortality of Influenza and *S. pneumoniae* Co-infection

S. pneumoniae significantly increases the morbidity and mortality of influenza virus, both historically and more recently. Between 23.2% and 50.1% of fatalities during the 1918 H1N1 influenza pandemic involved *S. pneumoniae*[76]. More recently, *S. pneumoniae* has been implicated in increased morbidity during the 2009 H1N1 influenza pandemic[32,77], and increased morbidity during seasonal influenza virus infection[78]. Approximately 10% of pediatric deaths from seasonal influenza infection during 2016-2020 involved *S. pneumoniae*[79].

Animal studies of influenza and *S. pneumoniae* co-infection have also demonstrated that influenza and *S. pneumoniae* co-infection greatly increases morbidity[80–82]. Ferrets infected with only influenza virus or only *S. pneumoniae* showed only minimal clinical signs (decreased playfulness and sneezing), whereas co-infected ferrets showed discoordination, severe lethargy, and death[81,82]. Co-infected mice demonstrated a similar increase in morbidity during co-infection, although sequence of infection had significant impact on survival following co-infection[80]. However, the exact mechanism of this increased morbidity is unclear and addressing this gap in knowledge could generate therapeutic targets to reduce severe disease.

1.2.2 *S. pneumoniae*, the Primary Source of Community-acquired Pneumonia

In 2019, the leading cause of death, accounting for 14% of fatalities, for children less than five years of age was community-acquired pneumonia[83]. *Streptococcus pneumoniae* (*S. pneumoniae*), a gram-positive, capsular, spherical bacterium, is a major causative agent of

community-acquired pneumonia[83]. In addition to causing pneumonia, *S. pneumoniae* contributes greatly to otitis media in children[84]. Even with an available vaccine, the World Health Organization listed *S. pneumoniae* as one of twelve priority pathogens of concern in a 2017 assessment, due to development of penicillin resistance[85].

Research has suggested that acquisition or colonization with *S. pneumoniae* greatly increases the probability of otitis media[84] or respiratory illness[86,87]. Colonization is much more common in children than adults[84,88], with 21-52% of children carrying *S. pneumoniae* and only 8% of adults[89]. Fortunately, the first pneumococcal vaccine was licensed in the United States in 2000 (called "Prevnar") and vaccinated against 7 of the most common serotypes of *S. pneumoniae*, of which there are now over 90 identified serotypes[90]. The bacterial capsule determines the serotype and is a source of antigenic variation that allows it to evade antibody recognition[48]. Vaccination against *S. pneumoniae* has since evolved to include 23 different serotypes and reduced the health burden of pneumococcal disease[91]. Interestingly, vaccination of children against *S. pneumoniae* also reduced pneumonia due to influenza A virus, respiratory syncytial virus, and parainfluenza virus, suggesting a role for *S. pneumoniae* in the development of viral pneumonia[92].

The capsule serotype of *S. pneumoniae* is a major determinant of clinical outcomes and virulence[90,93,94]. The capsule influences pathogenesis by altering biofilm formation[95], susceptibility to neutrophil traps[96], and bacterial interaction with the epithelium[97]. The capsule also prevents complement deposition on the bacterial surface, thereby avoiding clearance by the complement arm of the immune system[48]. The genome of *S. pneumoniae* is also highly variable, with more than 20% of genes in a given clone part of the accessory genome, leading to diverse gene expression across a bacterial community[98]. The transfer of genomic material has been shown to create virulence in a previously avirulent strain[98]. Given the importance of the capsule and the

pangenome in pathogenesis, it's often important to study multiple serotypes to understand if the observed effect varies by capsule type. A few particular strains of *S. pneumoniae* are studied most often, allowing for in-depth characterization: D39 (serotype 2) and TIGR4 (serotype 4) being the most common. Use of these strains in research facilitates reproducibility and depth of understanding *S. pneumoniae*.

1.2.3 Timing of Influenza and *S. pneumoniae* Co-infection

The order and timing between infection with influenza and *S. pneumoniae* is extremely important to the outcome of co-infection. The timing also determines whether the infections are concurrent and therefore co-infections or whether it's a secondary bacterial infection. Animal studies of influenza and *S. pneumoniae* secondary bacterial infection have tested a range of durations between infections: anywhere from *S. pneumoniae* infection 9 days before influenza infection[99] to *S. pneumoniae* 10 days after influenza infection[100]. Studies have been done in such a wide range because it has been commonly thought that co-infection occurs either when colonizing *S. pneumoniae* in the nasopharynx replicate to cause severe disease upon infection with influenza[101] or *S. pneumoniae* can be newly acquired after influenza infection. It has been documented that acquisition rather than prolonged carriage has been more strongly associated with bacterial infection in children[102]. A prospective cohort study of infants found that acquisition of *S. pneumoniae* in the nasopharynx was more strongly correlated with general practitioner consultations for infection than was carriage of *S. pneumoniae* (odds ratio of 2.1 and 1.4, respectively)[87], suggesting that new introductions of *S. pneumoniae* may be more likely to contribute to disease.

Mouse models of *S. pneumoniae* and influenza infection suggest that *S. pneumoniae* infection prior to influenza infection can lead to expansion of bacterial burden and severe disease[99], but the data of severe disease in mice when *S. pneumoniae* infection occurs before influenza are conflicting, as other groups did not detect severe disease or mortality when *S. pneumoniae* infection occurred first[80]. Experiments infecting ferrets first with *S. pneumoniae* then influenza did not observe expansion of *S. pneumoniae* burden nor severe disease[82].

When examining only *S. pneumoniae* infections after influenza, assessment of infection intervals with 2009 pandemic H1N1 or seasonal H3N2 showed that ferrets were most susceptible to severe disease when secondary bacterial infection was performed on day five or day ten post-influenza, but bacterial infection on day 16 post-influenza did not cause severe disease in animals infected with H1N1[103]. Additionally, development of fatal outcomes following co-infection is serotype dependent, as not all *S. pneumoniae* serotypes lead to death following co-infection[104].

1.2.4 Impact of Co-infection on *S. pneumoniae*

The relationship between influenza virus and *S. pneumoniae* is complex. Epidemiological studies indicate that influenza infection is correlated with increased odds of acquiring a new serotype of *S. pneumoniae* in the nasopharynx[105]. A small study examining oropharyngeal bacteria in humans experimentally infected with influenza found that experimental infection led to a heavy density of *S. pneumoniae* on day six post-influenza, however the sample size was small, and the effect was non-significant[106]. Animal studies of influenza and *S. pneumoniae* co-infection have allowed for a much more thorough investigation of this complex relationship.

Investigation of co-infection in mouse models has demonstrated that when influenza infection precedes bacterial infection, influenza infection increases the bacterial burden of *S.*

pneumoniae in the nasopharynx, lungs[80], and blood[80]. Some groups have also seen increased bacterial burden in the nasopharynx[99,107,108] and lungs[107] of mice when *S. pneumoniae* infection precedes influenza infection.

Experiments in ferrets have shown similar results. When influenza infection occurs prior to *S. pneumoniae*, there is an increase in bacterial burden in nasal washes[81,82,104,109]. Limited work has been done looking at *S. pneumoniae* infection followed by influenza infection, but the available study demonstrated that when *S. pneumoniae* infection occurred first, there was no expansion of bacterial burden in nasal washes[82]. However, there appear to be no studies on *S. pneumoniae* replication in the tissues during co-infection in ferrets. Addressing this gap in knowledge could inform best treatment practices for patients with severe bacterial pneumonia following influenza infection.

1.2.5 Impact of Co-infection on Influenza Virus

Studies of co-infection often use the term "synergistic" to discuss co-infection, but they have mostly focused on how co-infection increases the pathogenicity and transmission of *S. pneumoniae*. Very few studies have addressed whether co-infection impacts influenza virus, either by altering viral replication or transmission.

While co-infection promotes *S. pneumoniae* replication and transmission, it appears to be more complex for influenza. Infection of mice with *S. pneumoniae* first then influenza led to protection from severe disease[80]. When mice were infected with *S. pneumoniae* nine days before influenza infection, there was a significant decrease in influenza virus detected in the nasal homogenates[110]. However, when influenza infection occurs before *S. pneumoniae* infection, severe disease develops, often leading to fatal outcomes[104]. When *S. pneumoniae* infection occurred seven

days after influenza infection in mice, there appeared to be a rebound of virus titers in the lungs, although this effect was modest[111].

Protection from severe disease when influenza infection occurs after *S. pneumoniae* has also been observed in ferrets[82], but work studying co-infection in ferrets has primarily focused on outcomes when influenza infection occurs before *S. pneumoniae*[81,82,104,109,112,113]. Work in ferrets confirmed enhanced disease severity when *S. pneumoniae* infection occurs after influenza infection[81,82,104]. Interestingly, there seemed to be reduced virus in nasal washes of co-infected ferrets compared to influenza-only infection when *S. pneumoniae* infection occurred two days after influenza[82]. So, there appears to be a complex relationship in which sometimes *S. pneumoniae* increases virus burden during co-infection and sometimes it decreases virus burden. However, this relationship needs further examination to understand the mechanisms behind the effect of *S. pneumoniae*.

1.2.6 Immune Response to Co-infection

1.2.6.1 Immune Response to *S. pneumoniae*

S. pneumoniae carriage during colonization can last for weeks to months[114]. The time to clearance is more dependent on bacterial factors than host factors[115]. Colonization leads to increased levels of neutrophils and macrophages in upper respiratory tract lavages of *S. pneumoniae*-infected mice[116]. Sensing of *S. pneumoniae* occurs through TLR2 sensing and Nod2, which senses peptidoglycan[117]. One of the bacterial virulence factors, pneumolysin, acts by forming pores in macrophages that take up the bacteria, thereby killing them[118]. Conversely, it also contributes to clearance by inducing inflammation[114]. Bacterial mutants that don't express the pneumolysin toxin display prolonged colonization, due to the decreased activation of the monocyte

attractant CCL2[119]. Colonization by *S. pneumoniae* leads to increased IFNα and IFNβ[116]. It also is cleared by opsonophagocytosis from the complement system[120]. The bacterial capsule shields some of the bacterial components and decreases the binding of antibodies and components of the complement system[120].

Colonization by *S. pneumoniae* leads to antibody production against both the capsule and other bacterial components[121]. Antibodies against *S. pneumoniae* can be detected in the nose and blood of previously colonized humans, and these antibodies prevent future colonization[89,121]. Colonization also leads to the development of *S. pneumoniae*-specific CD4 T cells[122]. A subset of CD4 T cells, T helper 17 cells, are reduced in mice without Nod2 sensing of the bacteria[117] and are required for clearance of the colonizing bacteria[123]. These cells are less common in children when colonization by *S. pneumoniae* is more common, and T helper 17 cells become more common in adults, when colonization becomes less frequent[124]. So, for non-invasive *S. pneumoniae* colonization, the bacteria induce a mild immune response that leads to eventual clearance through elimination by monocytes and the development of an adaptive immune response.

1.2.6.2 Bacterial Modulation of the Antiviral Immune Response

As the importance of the microbiome has become more evident, research has expanded to include studies on the respiratory tract microbiome. Given that *S. pneumoniae* commonly colonizes the nasopharynx of children[89], understanding how the microbiome regulates the immune system is important to understanding how primary infection/colonization with *S. pneumoniae* might protect against influenza infection. Broad-spectrum oral antibiotic treatment of mice for four weeks prior to influenza infection led to decreased production of influenza-specific antibody development and influenza-specific T cells[75], indicating that the microbiome is important for

respiratory tract immune responses. Application of lipopolysaccharide (TLR4 agonist), CpG (TLR9 agonist), PolyI:C (TLR3 agonist), and peptidoglycan (TLR2 agonist) either locally (intranasal) or distally (intrarectal) restored immune responses to influenza infection[75]. Given that the distal application of the TLR agonists restored immune responses, the systemic oral antibiotics were likely altering systemic immune responses instead of just local immune responses. So, further examination of the specific role of the respiratory tract microbiome was necessary. When mice were given intranasal antibiotics to deplete nasal bacteria and subsequently infected with influenza virus, mice had elevated nasal IgA and serum IgG levels compared to no-antibiotics controls[125]. This increased antibody production appeared to be due to the lysis of the commensal bacteria, thereby activating more innate immune sensors and sensitizing the immune response[125]. So, while the role of the nasal microbiome in modulating infection is still unclear, primary infection with *S. pneumoniae* may be sensitizing the immune response by activating innate immune sensors prior to influenza infection, similar to the intranasal administration of antibiotics[125].

Instead of administering antibiotics to measure respiratory tract microbiome impact on the antiviral response, one group colonized human volunteers with *S. pneumoniae* prior to vaccinating with live-attenuated influenza virus, which is a replication-competent, non-pathogenic virus, or they vaccinated with a tetravalent-inactivated influenza vaccine[126]. They found that *S. pneumoniae* colonization did not alter immune responses to the inactivated vaccine, but there were decreased antibody responses in the colonized individuals that received the live-attenuated influenza virus. They also found that colonized individuals that had detectable *S. pneumoniae* in nasal wash had increased expression of TLR2, TLR4, TLR9, IFNα, IFNβ, IFNγ, and RIG-I/MDA5 pathways[126]. The authors examined influenza virus RNA levels on day three-post vaccination with live-attenuated influenza virus, they saw no differences. Quantification of RNA may have not

accurately assessed replication of the live-attenuated influenza virus between the groups, since RNA levels are not indicative of infectious virus. So, the difference between primary *S. pneumoniae* infection being protective from influenza or expanding and causing full bacterial co-infection may be a complex interplay of dose and serotype, as some serotypes are more invasive[93].

1.2.6.3 Immune Responses to Influenza Facilitate *S. pneumoniae* Secondary Infection

Studies of immune responses to co-infection have primarily focused on how influenza infection weakens host defenses to facilitate infection by *S. pneumoniae*. They often fail to address how the host response to co-infection differs from the response to individual pathogens, which would improve our ability to mediate immunopathology due to co-infection. Studies examining the relative contribution of influenza and *S. pneumoniae* to co-infection are complicated by the many different timing intervals and doses used between the two infections. One group attempted to model the outcomes of secondary infection with *S. pneumoniae* based on the dose and time between influenza infection, but this model is based primarily on murine data and is not necessarily reflective of what happens in humans[127].

However, murine models have provided valuable insight into how co-infection alters the immune system. When mice were infected with influenza, then seven days later infected with *S. pneumoniae*, there was significantly more TNFα and IL-1 in the co-infection group 48 hours after the *S. pneumoniae* infection compared to *S. pneumoniae* (48 hours after infection) or influenza (nine days after infection) alone[128], indicating that co-infection synergistically upregulated TNFα and IL-1. IL-1 induces strong inflammation in the lung and aids in attracting T cells to help clear infection, but it can also contribute to pathology[129]. While IL-1 is not necessary for clearance of *S. pneumoniae* in the absence of influenza, mice lacking the IL-1 receptor 1 have significantly increased burdens of *S. pneumoniae* in the lungs compared to mice with IL-1 receptor 1[130]. So, IL-

1 helps to clear infection while simultaneously causing tissue damage. Other work has demonstrated that influenza infection leads to depletion of alveolar macrophages and dysfunction[131], which allows *S. pneumoniae* to replicate to high levels[111]. When mice were treated with GM-CSF to replenish alveolar macrophages following influenza infection, there was reduced incidence of pneumonia during secondary bacterial infection[131]. The IL-1 signaling upon secondary infection with *S. pneumoniae* prevented further depletion of alveolar macrophages following influenza infection[130]. So, loss of alveolar macrophages contributes to susceptibility to secondary infection, and IL-1 signaling to sustain the remaining alveolar macrophages then causes tissue damage.

One study infected humans with the live-attenuated influenza virus or inactivated vaccine (the control) three days before *S. pneumoniae* infection and subdivided groups based on those that became *S. pneumoniae* carriage-positive or remained carriage-negative. They found that there is decreased neutrophil degranulation in individuals who received live-attenuated influenza virus then became carriage-positive compared to controls that became carriage-positive[132], indicating that neutrophils function is impaired following influenza infection, which may contribute to *S. pneumoniae* susceptibility. This group also demonstrated that individuals infected with the live-attenuated influenza virus and shed detectable *S. pneumoniae* had significantly higher levels of CXCL10, and significantly lower levels of IL-10 compared to those that did not shed detectable *S. pneumoniae*[132]. CXCL10 levels had a positive correlation with increased bacterial burden[132] and were, separately, associated with increased death of monocyte-derived macrophages[133]. Together, published work seems to show that influenza facilitates *S. pneumoniae* infection by impairing innate immune cell function, especially alveolar macrophages and neutrophils. Then, the host

responds by increasing interleukins and chemokines in an attempt to counteract this impairment, which may lead to immunopathology.

1.2.7 Reducing Burden of Disease

Laboratory-confirmed viral and bacterial co-infection contributes to increased rates of intensive care unit admission and 30-day mortality[134]. Medical care for co-infection offers several treatment options when a patient presents with influenza and *S. pneumoniae*. Oseltamivir can be administered to reduce influenza burden, but this is most effective if administered within two days of symptom onset[135]. Antibiotics can also be administered to reduce bacterial burden during co-infection which leads to mortality outcomes being similar to viral infection alone[134]. Prevention of co-infection is another method of reducing the health burden of influenza and *S. pneumoniae*. To do this, we must understand how these pathogens transmit.

1.3 Transmission of Respiratory Pathogens

Transmission is the process by which a pathogen is transferred to an uninfected host from an infected host, and efficient transmission is required for the epidemiological success of a pathogen[136]. Multiple factors influence transmissibility of a pathogen: susceptibility of an exposed individual, infectious dose required to initiate infection, microbial burden of the infected host, and transmission mode[137]. A combination of epidemiological analysis and laboratory experiments can be used to determine the transmission mode of a pathogen, which has important implications for infection prevention and control when a new pathogen emerges into a population.

1.3.1 Modes of Transmission

Transmission of pathogens can be broadly broken down into 5 categories: direct contact transmission, indirect contact transmission (fomite transmission), vector transmission, droplet transmission, and aerosol/airborne transmission[138]. A pathogen can use one or more of these transmission modes to spread to a new host. Direct contact transmission involves an infected host transferring a pathogen to an uninfected host through touch. For indirect contact transmission, an infected host would touch an inanimate object, thereby transferring the pathogen to the surface, and an uninfected host becomes infected by then touching that inanimate object. Vector transmission involves transfer of an infection through an animal such as mosquitoes, ticks, or fleas that primarily carries the pathogen without necessarily allowing pathogen replication. Droplet spread and aerosol/airborne transmission commonly refer to transmission for respiratory pathogens. Droplet transmission involves transmission through large droplets that quickly fall out of the air, while aerosol/airborne transmission requires transmission through aerosols that stay suspended in the air for longer periods of time. Frequently, multiple modes of transmission are at play simultaneously. So, confirmation of an individual transmission mode through experimentation is extremely challenging.

Given the difference in droplet sizes required for droplet transmission and airborne transmission, a cut-off is required to differentiate the two modes. The classical cut-off for droplet sizes belonging to these transmission modes was that droplets >5 μm in diameter were droplet transmission, and droplets <5 μm in diameter were considered aerosols[139]. However, studies examining the length of time droplets of different sizes stay suspended in the air have shown that this cut-off is likely arbitrary and have suggested that the cut-off be moved to 100 μm droplet diameter, as droplets larger than this fall out of the air within 5 seconds (given a height of 1.5

m)[139,140]. The longer a droplet or aerosol stays in the air, the more likely it is that an uninfected host will inhale that contaminated air and become infected[137,140].

1.3.2 Spread of Influenza Viruses

Once an influenza virus circulating in animals becomes capable of human infection, human-to-human transmission is required for the virus' epidemiological success. It's commonly accepted that direct contact, indirect contact, droplet, and aerosol transmission contribute to influenza transmission among humans[141,142]. However, the relative contributions of the different modes of microbial transmission to influenza virus transmission are not well understood.

Evidence exists to support several of these transmission modes. Direct contact experiments, in which an uninfected animal is placed in the same cage as an infected animal provide evidence of direct contact transmission[39,143]. However, these experiments do not exclude other modes of transmission. Studies have been done measuring influenza virus persistence on skin[144] and surfaces[145,146], supporting the idea of indirect contact transmission. Indirect contact transmission has also been suggested by studies placing uninfected animals in the cages of infected ferrets after the infected animal has been removed[147].

Several research groups have studied influenza virus airborne transmission in humans through direct inoculation of human donors and subsequent exposure of these donors to uninfected recipients. Infection of donors with a seasonal H3N2 influenza virus led to transmission rates between 3%[148] and 25%[149] to naive recipients, with discrepancies in the air ventilation rate given as a possible source of the observed variation[148]. Experimental aerosol infection of humans has also resulted in seroconversion and clinical symptoms[27], supporting aerosol transmission as a mode of transmission for influenza. Droplet transmission is difficult to assess, as instances of droplet

transmission also include aerosol transmission. However, pharmaceutical studies of zanamivir showed that intranasal administration prevented intra-nasal droplet infection by influenza virus, demonstrating that droplet infection is possible[150].

Since influenza virus has been shown to replicate in both the upper and lower respiratory tract, groups have tried to determine which anatomical site is responsible for the infectious droplets or aerosols. This information would be valuable to better engineer public spaces to reduce influenza virus transmission. Studies utilizing recombinant viruses have shown that the upper respiratory tract, especially the soft palate[29] and the nasal epithelium[151], are responsible for aerosol transmission of influenza virus in ferrets.

There are many factors known to influence transmission of influenza virus, even if we don't know exactly which modes of transmission are being altered. Other than some of the environmental factors described above, there are many host factors influencing transmission of influenza virus. For example, previous influenza infection[39,152] or some types of vaccination[153] have been shown to reduce recipient animals' susceptibility to new infection from donor animals. Similarly, previous influenza infection of donor animals reduces transmission to recipient animals[39], possibly through decreased virus in saliva[154]. The respiratory tract microbiome also appears to play a role in influenza susceptibility, as human cohort studies found that nasal/oropharyngeal microbiome abundance and diversity altered susceptibility to influenza infection[73], the length of time for household contacts to become infected with influenza[74], and virus shedding duration[74]. More specifically, some clinical symptoms such as fever, runny nose, and sore throat were even associated with specific bacterial taxa[74]. The effects of pre-existing immunity, through prior infection or vaccination, and the effect of the microbiome are likely caused by alterations in the host immune responses[75,155].

1.3.3 Transmission Experiments with Ferrets

Ferrets are uniquely suited for use studying transmission of respiratory viruses due to their ability to sneeze. There exist a number of different caging set-ups to study different modes of transmission. To study transmission of all modes (direct contact, indirect contact, droplet, and aerosol transmission), an infected animal may be placed in the same cage as an uninfected animal. To study only droplet and aerosol transmission, an infected animal is typically placed in a cage alone, with perforations in one wall. The perforated side is connected to another adjacent cage with perforations and contains an uninfected animal. This set-up allows droplets and aerosols to pass from the infected animal to the uninfected animal without allowing the animals to touch each other (to prevent direct contact transmission) or to touch any of the same items (to prevent indirect contact transmission). Droplet transmission can be prevented by reducing the perforations in the cage to exclude large droplets. To sample animals and prevent indirect contact transmission during transmission experiments, thorough cleaning between infected and uninfected animals must also be performed[36].

There is a lot of variation in the exact caging set-up used by different laboratories[36]. The distance between cages used during airborne transmission experiments varies, and some laboratories use directional airflow during these experiments. Directional airflow typically carries air from infected donors towards uninfected recipients and then out of the system through a HEPA filter. Directional airflow might increase probability of infection by carrying contaminated air from the donor animal to the recipient animal, while simultaneously decreasing the probability of infection by removing contaminated air from the space[156]. Exhaust rates for airborne transmission experiments using ferrets have ranged from 12 to 180 air changes per hour, but air exchange rate

has not been demonstrated as having a significant impact on variation within ferret transmission experiments[36].

The length of time that an uninfected animal is exposed to an infected animal is another important parameter of transmission experiments. Historically, groups used very long exposure periods of 14 days[136], which does not align with common human exposure to infectious pathogens. Further, groups typically use naïve animals as the uninfected recipients, when humans have more complex immune histories that involve prior infection and vaccination against influenza [38,136,153]. Work examining exposure duration and pre-existing immunity has shown that shorter exposure durations of 2 days or 5x8 hours (to simulate workplace exposure) is sufficient for the 2009 H1N1 pandemic virus to transmit[39]. Pre-existing immunity in uninfected recipient animals to the 2009 pandemic H1N1 virus also reduced transmission of a seasonal H3N2 virus, but pre-existing immunity to H3N2 did not fully block transmission of the H1N1 virus[39]. So, transmission experiments involve many factors that reflect the complexity of studying transmission in humans: exposure type, air flow, exposure duration, natural immunity, vaccination, and duration since prior exposure. Studying the impact of each component on transmission helps us understand the complex transmission dynamics of influenza virus in humans.

1.3.4 Transmission during Co-infection

1.3.4.1 Impact of Co-infection on *S. pneumoniae* Transmission

While ferrets are the preferred model for influenza virus transmission, infant mouse models have also been developed to study transmission during co-infection[99,107,157]. Experiments of *S. pneumoniae* mono-infection in infant mice have shown that contact transmission does not occur when there is only one donor pup in a cage, but the addition of another infected animal to the cage

allows some instances of transmission. These studies are limited to direct contact transmission with a limited subset of mouse-adapted viruses. However, they found that when recipient mice were experimentally infected or naturally infected with influenza, they were more susceptible to direct contact transmission of *S. pneumoniae*[99,107].

Transmission experiments using ferrets have allowed investigation of airborne transmission in addition to contact transmission. Transmission of *S. pneumoniae* in the absence of influenza infection has not been observed in ferrets[82,104]. It was demonstrated that influenza infection in recipients made ferrets more susceptible to direct contact transmission of *S. pneumoniae* and airborne transmission up to 10 meters away[104]. Influenza infection of donor animals three days before *S. pneumoniae* infection also increased transmission of *S. pneumoniae*, but to a lesser extent than recipient animals being infected with influenza[104]. This effect was also serotype dependent, as *S. pneumoniae* BHN97 (serotype 19F) transmitted but BHN54 (serotype 7F) did not transmit in any cases, regardless of influenza infection[104]. Together, these data demonstrate that influenza infection facilitates transmission of *S. pneumoniae* through multiple mechanisms. When recipients are healthy, co-infection in donor animals is likely aiding transmission through increased bacterial burden. When recipient animals are infected with influenza, the virus primes the host for *S. pneumoniae* infection, possibly through immune-mediated pathways.

1.3.4.2 Impact of Co-infection on Influenza Virus Transmission

Ferrets are the preferred model organism for studying influenza virus transmission, but some experiments have utilized mice to examine direct contact transmission. Mice that were experimentally infected with *S. pneumoniae* before acting as recipients for influenza infection were less likely to acquire influenza infection[157], which was dependent on the bacterial neuraminidase

activity. This suggests a microbial cause of the protection rather than host immune-mediated protection.

Experiments examining transmission of influenza virus during co-infection in ferrets have been limited[82,112]. One study administered topical mupirocin, which primarily targets *Staphylococcus* and *Streptococcus* species[158], to influenza-infected donor ferrets and saw an ablation of influenza virus transmission to uninfected recipient animals[112]. When mupirocin-resistant *S. pneumoniae* was then used to infect the influenza-infected, mupirocin-treated ferrets two days after influenza infection, influenza virus transmission returned[112]. Therefore, these authors said that respiratory tract bacteria therefore promote influenza A virus transmission. However, it has previously been shown that antibiotic treatment can lead to modulation of the host immune response through depletion of the commensal microbiota[75,155]. So, these results are more informative about the impact of nasal microbiota depletion on influenza transmission rather than *S. pneumoniae* co-infection on influenza virus transmission. One other study examined influenza transmission during *S. pneumoniae* co-infection and found that co-infection with *S. pneumoniae* two days after influenza potentially diminished influenza transmission, but this effect was non-significant[82]. When *S. pneumoniae* infection occurred two days prior to influenza infection, there was no change in influenza transmission[82].

1.3.5 Environmental Stability of Microbes

Once a contaminated droplet or aerosol enters the environment, the pathogen within the droplets must maintain infectivity in order to initiate infection in a new host (Figure 1). Environmental stability of a pathogen is also key for fomite transmission, as the microbe must maintain infectivity on surfaces until coming into contact with an uninfected host and initiating

infection. Environmental factors such as temperature[137,159–161], humidity[137,159,161–164], air exchange[148], and ultraviolet radiation impact microbial stability in droplets[137,139]. When examining virus stability, increased temperature and greater exposure to ultraviolet radiation leads to greater decay (loss of virus infectivity)[159,160,165]. The association between humidity and environmental stability of viruses is more complex, showing a U-shaped relationship with the greatest decay occurring at low and high humidities and decreased decay occurring at intermediate humidity[146,161]. However, this U-shaped relationship is not observed for bacteria[162] or in all droplet solutions[146].

In addition to the environmental determinants, host factors such as droplet composition[146,163,166], pathogen type[145], and host origin alter the dynamics of pathogen decay[145]. Different locations in the respiratory tract are lined with different fluids: lung airway cells secrete airway surface liquid[167,168], while saliva is secreted from salivary glands into the oral cavity[168,169]. When airway surface liquid from human bronchial epithelial cells was added to virus-laden droplets, it negated the impact of humidity[146], indicating that droplet composition is a major determinant of microbial stability in the environment. Studies have identified salt content, protein content, pH, and surfactant concentration as mediators of environmental decay[163] (Figure 1). As such, determining an absolute time that a microbe maintains stability in the environment is difficult, as droplet composition may change between individuals and environmental conditions will vary.

Pathogen type is also a major determinant of microbial stability because viruses and bacteria do not undergo decay from the same pressures[162,170]. Specifically, bacterial stability can be altered by a specific bacterium's respiration; for example, some anaerobic bacteria are highly sensitive to oxygen and will decay rapidly when exposed to it[166,170]. There is also some limited

evidence that bacteria and viruses may interact to stabilize each other from desiccation[112] or heat-inactivation[171,172]. Given the presence of commensal microbes in the respiratory tract[173] and the frequency of viral-bacterial co-infection[134], especially influenza virus and *S. pneumoniae*, it is possible that respiratory viruses and respiratory tract bacteria are present within the same droplets. However, the abundance of influenza and *S. pneumoniae* in respiratory emissions has never been determined from co-infected hosts. Further, it is not known whether these two pathogens might influence each other's environmental stability. Characterizing these environmental factors is crucial for determining best practices for disinfection and engineering safer conditions indoors to reduce occurrence of influenza and *S. pneumoniae* co-infection.

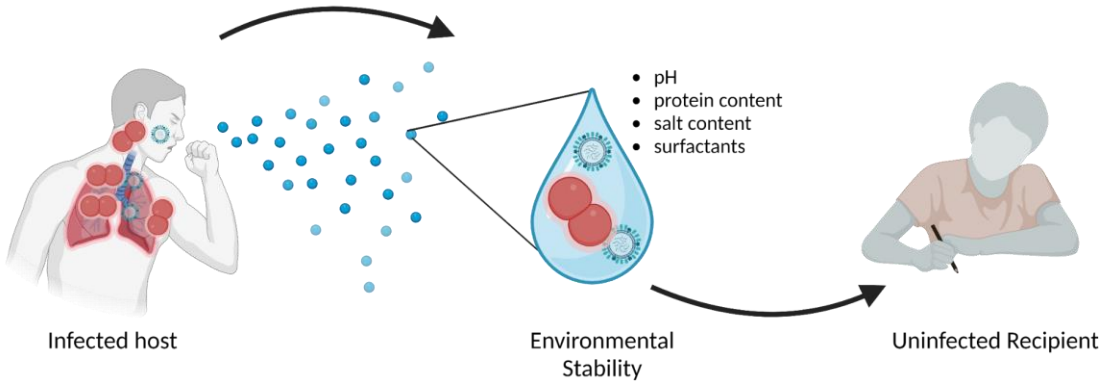

Figure 1. Characterizing abundance and environmental stability of respiratory emissions during co-infection could help reduce incidence. For transmission of respiratory microbes to occur, a pathogen starts by infecting a host and must be released into the environment. Then, the pathogen(s) must maintain stability and infectivity in the environment. Finally, an uninfected host must come into contact with the respiratory emissions to allow the microbe(s) to initiate a new infection.

1.3.6 Respiratory tract droplet sizes and composition

Droplet size is another determinant of airborne transmission. The respiratory tract generates a large range of droplet sizes, from aerosols <1 μm in diameter up to droplets of 1 mm in diameter. However, these droplet sizes are not present in equal amounts. Previous work has shown the droplet sizes expelled from the respiratory tract are multimodal and change depending on whether an individual is breathing, talking, sneezing, or coughing[139,174]. Aerosols are generated during all these activities, while larger droplets are generated more during sneezing and coughing[139]. Upon exiting the respiratory tract, droplets do not maintain their original size. Instead, droplets are part of a dynamic respiratory cloud that undergo fragmentation due to strong forces present during exhalation[140]. As a result, droplets measured immediately exiting the oral and nasal cavities might differ in size from those measured further away.

Viral copy number within droplets also varies[175,176]. For example, past work has shown there is a greater amount of influenza virus RNA in fine aerosol fractions (i.e., <5 μm) than in coarse air fractions (i.e., >5 μm) from infected humans[148,175]. Droplet size is therefore an important factor in defining how much virus may be inhaled by an uninfected individual.

When comparing the quantity of infectious virus necessary to initiate infection, intranasal infection required approximately 100 times more virus than aerosol infection[177]. This difference is likely due to aerosols being able to penetrate deeper into the respiratory tract and deposit in the lungs unlike large droplets, which are more likely to deposit in the upper respiratory tract[139,178]. So, increased generation of smaller aerosols may contribute to greater transmission. Given that droplet size can impact movement of contaminated air, virus load in droplets, and deposition site, the size of expelled droplets is a major determinant of transmission.

Droplet size is correlated with droplet composition, as different locations in the respiratory tract are lined with different fluids and generate different size particles. For example, particles generated in the lower respiratory tract contain airway surface liquid and develop when airways containing mucus films come together and then separate, creating fine aerosols less than 10 μm in diameter[179]. Larger droplets generated during coughing and sneezing are more commonly generated in the upper respiratory tract and therefore likely contain more saliva[174]. Airway surface liquid in the lungs and saliva differ in their composition in both organic and inorganic components[168]. These components can alter microbial stability in a relative humidity-dependent manner[163]. While droplet size may correlate with droplet composition, it is not known whether droplet size alters viral stability in the environment given the same composition. Characterizing the role droplet size plays in environmental persistence of influenza virus would allow for improved public health measures to reduce transmission.

1.4 Statement of the Problem

Understanding factors influencing pathogenesis and microbial transmission is required to decrease the public health burden of infection. Despite the availability of vaccines for both influenza virus and *S. pneumoniae*, an estimated 389,000[180,181] and 294,000[182] people around the world die annually from infections with each pathogen, respectively. Further characterizing the factors influencing their transmission and disease burden will allow the design of improved public policy and engineering controls to reduce the relative burden of both pathogens.

First, I examine how co-infection with *S. pneumoniae* alters influenza virus pathogenesis and host responses in the ferret model to better understand what drives the increased morbidity

and mortality observed during co-infection. Next, I assess the presence of influenza virus and *S. pneumoniae* in air collected from co-infected ferrets and perform stability studies to determine transmission risks during co-infection. Finally, I compare influenza virus decay in droplets of variable sizes to both increase our knowledge of influenza fomite transmission and to propose improved methodologies for future characterization of pathogen decay in the environment. Together, this work adds valuable insight into host and environmental factors influencing severe disease and transmission of influenza virus.

2.0 Tissue-specific responses and microbial relationships during influenza virus and *Streptococcus pneumoniae* co-infection in the ferret model

2.1 Abstract

Secondary bacterial infection following influenza virus infection has contributed to significant increases in morbidity and mortality during seasonal and pandemic influenza seasons, though the mechanisms behind this are not well understood. To improve our understanding of the increased morbidity, we undertook an analysis of ferrets either mono-infected or co-infected with the 2009 H1N1 pandemic influenza virus and *Streptococcus pneumoniae*, analyzing pathology, microbial replication, and gene expression. As expected, co-infected animals displayed more severe clinical signs compared to animals infected with only one pathogen, and increased pathological changes in the nasal turbinate tissues. Co-infection did not alter virus burden in the upper and lower respiratory tract tissues tested, indicating that morbidity is not driven by changes in virus replication. However, a tissue-specific trend towards greater bacterial burden in the upper respiratory tract was found. Tissue-specific gene expression profiles revealed that while host responses to co-infection were primarily driven by influenza virus, there was a unique enrichment of immune response pathways during co-infection. This study demonstrates that host responses to co-infection are associated with increased pathology and gene expression changes in a tissue-specific manner, providing a molecular basis for the increased morbidity seen during co-infection.

2.2 Introduction

Influenza A viruses have caused four pandemics since the start of the 20th century. The 1918 H1N1 influenza pandemic, the most severe, led to 25-50 million deaths worldwide[1]. Almost half of the deaths attributed to the 1918 H1N1 influenza pandemic included secondary bacterial infection with *Streptococcus pneumoniae* or mixed pneumopathogens, indicating that secondary bacterial infection was a primary contributor to mortality[76]. Secondary bacterial infection includes bacterial infection that occurs concurrently with viral infection (co-infection) and bacterial infection that begins after the resolution of viral infection. *S. pneumoniae* has also been implicated in increased mortality during seasonal influenza infection as well[79]. During the 2009 H1N1 pandemic, *S. pneumoniae* was one of the most commonly identified bacteria in patients with co-infection and contributed to severe disease[32,77,183]. Co-infected patients were more likely to present with shock, require mechanical ventilation, and have longer stays in the ICU than patients without bacterial co-infection[32,77]. Epidemiological studies of the 2009 H1N1 pandemic showed that bacterial co-infection occurred within 1.2-11.1 days after influenza infection[32,183]. These data indicate that bacterial co-infection with *S. pneumoniae* greatly increases the health burden of both seasonal and pandemic influenza A viruses.

Despite the disease severity observed during influenza virus and *S. pneumoniae* co-infection, our understanding of the mechanisms underlying the increased morbidity and mortality is still limited. Work examining immune responses to co-infection in mice have primarily focused on changes in the lungs and how prior influenza infection facilitates *S. pneumoniae* infection by increasing susceptibility to infection[116,184–186]. Influenza virus has been shown to increase *S. pneumoniae* burden in influenza-infected mice through increased IFNβ production, leading to a decrease in macrophage recruitment and subsequent increased bacterial burden[116,187]. It has also

been observed that neutrophils limit susceptibility to *S. pneumoniae* following influenza virus infection, and that neutrophil production of reactive oxygen species is impaired by influenza virus, likely creating a more favorable environment for *S. pneumoniae* to infect, grow, and colonize[186]. Increases in IL-10 production following influenza infection dampen the host immune response, impairing the ability to clear bacteria[186,188,189]. Taken together, many host responses may be responsible for the increased disease burden associated with secondary bacterial infection.

While immune responses are important for clearing virus and bacteria, an excessive immune response can negatively affect the host too. Compared to influenza alone, co-infection has been shown to increase tumor necrosis factor-α (TNFα)[128,187], interferon-γ[185], IL-6[189], and MIP-1α/CCL3[189], which promote inflammation. Knock-out of the MCP-1/CCL2 receptor CCR2 also improved survival following co-infection[190,] highlighting the importance of monocytes on the immunopathology responsible for mortality of mice during a bacterial secondary infection.

While mouse models have been helpful in identifying these host factors due to their genetic tractability, they are limited in their ability to recapitulate disease symptoms associated with influenza virus infection and focus on a single tissue site. Specifically mice are not susceptible to many human influenza viruses, so host responses and pathological changes associated with secondary bacterial infections must be studied in other systems. Another concern is the focus on one tissue site, which may not represent the response present in other regions of the respiratory tract; thus, a comprehensive evaluation of host responses within distinct tissue sites is warranted.

Ferrets are a valuable model for studying influenza virus and *S. pneumoniae* co-infection due to their natural susceptibility to human influenza virus strains, their similar respiratory tract physiology to humans, and their clinical signs exhibited during infection[33]. Additionally, cross-species comparison of protein sequences has shown that for 75% of proteins, ferret sequences are

closer than mouse to human sequences[34]. Previous work with the ferret model has primarily focused on pathogen replication, shedding, and transmission, as well as the impact of co-infection timing. Animals pre-infected with influenza virus shed more bacteria in nasal washes after secondary infection, and transmitted *S. pneumoniae* more often than animals infected with only the bacteria[103,104,109]. Another study found that ferrets co-infected with influenza virus and *S. pneumoniae* have decreased levels of virus in the nasal wash compared to animals infected with only influenza[82]. Studies done in both mice and ferrets have suggested that secondary infection with *S. pneumoniae* is most severe when concurrent with influenza infection[103,116]. Despite this work, we have a limited view of how co-infection alters pathogenesis throughout the respiratory tract and which host responses drive increased morbidity and mortality in this animal model. Whether the same host factors identified in mice also impact co-infection pathogenesis in ferrets remains to be determined. Investigations addressing these issues are critical to understanding the disease progression of co-infection in humans.

To gain a more comprehensive view of the factors underlying morbidity during co-infection, we utilized ferrets that were infected with the 2009 pandemic H1N1 virus (H1N1pdm09) and subsequently infected with *S. pneumoniae* D39 two days later. We investigated viral and bacterial replication, tissue damage throughout the respiratory tract, and tissue-specific host responses. We found that co-infection with *S. pneumoniae* caused increased morbidity but did not alter virus replication in tissues. *S. pneumoniae* replication was limited to the upper respiratory tract, and co-infection with H1N1pdm09 led to greater bacterial burden in the soft palate and trachea compared to D39-only. Furthermore, the pathogenesis and host response to co-infection was tissue-specific and correlated with increased immune cell infiltration and enrichment of inflammatory pathways. Overall, our results show that multiple tissue-specific changes contribute

to the increased morbidity observed during co-infection, and they demonstrate that more global analysis of infection and host-pathogen interactions would help elucidate the mechanisms involved in disease progression.

2.3 Results

2.3.1 Co-infected ferrets display greater morbidity and more severe pathology than ferrets infected with only influenza virus or *S. pneumoniae*

To investigate the mechanisms underlying increased morbidity and mortality observed during co-infection, we used the ferret model because of its natural susceptibility to influenza virus infection and its display of clinical signs observed in humans: weight loss, mucus accumulation, coughing, and sneezing[33]. Ferrets were first infected with H1N1 A/CA/07/2009 (H1N1pdm09) intranasally or mock infected. Two days later, these animals were either mock infected or infected intranasally with 10^7 CFU *S. pneumoniae* D39 (D39) (Figure 2A). Animals were assessed for clinical signs each day, and then sacrificed on day 3 or day 5 to measure tissue-specific titers and pathology changes over time.

We quantified total clinical scores of each animal, using previously published metrics that include willingness to initiate play, coughing, sneezing, nasal discharge, diarrhea, and weight loss (Figure 2B-F)[82]. D39-infected ferrets displayed limited clinical signs: only sneezing was observed on day 5 (Figure 2D). H1N1pdm09-infected ferrets only displayed a slight increase in clinical score (Figure 2B) due to a mild decrease in willingness to initiate play, sneezing, diarrhea, and weight loss greater than 10% but less than 15% (Figure 2C-D, F-H). Co-infected ferrets displayed

the greatest morbidity, with cumulative clinical scores significantly greater than H1N1pdm09-infected ferrets on days 3, 4, and 5 and significantly greater than D39-infected ferrets on days 3, and 4 (Figure 2B). Ferrets co-infected with both pathogens displayed increased inactivity, nasal discharge, sneezing, and weight loss compared to animals infected with a single pathogen (Figure 2C-H). Overall, these results complemented previous work [81,112] and confirmed that co-infected ferrets experience significantly greater morbidity than animals infected with only H1N1pdm09 or D39.

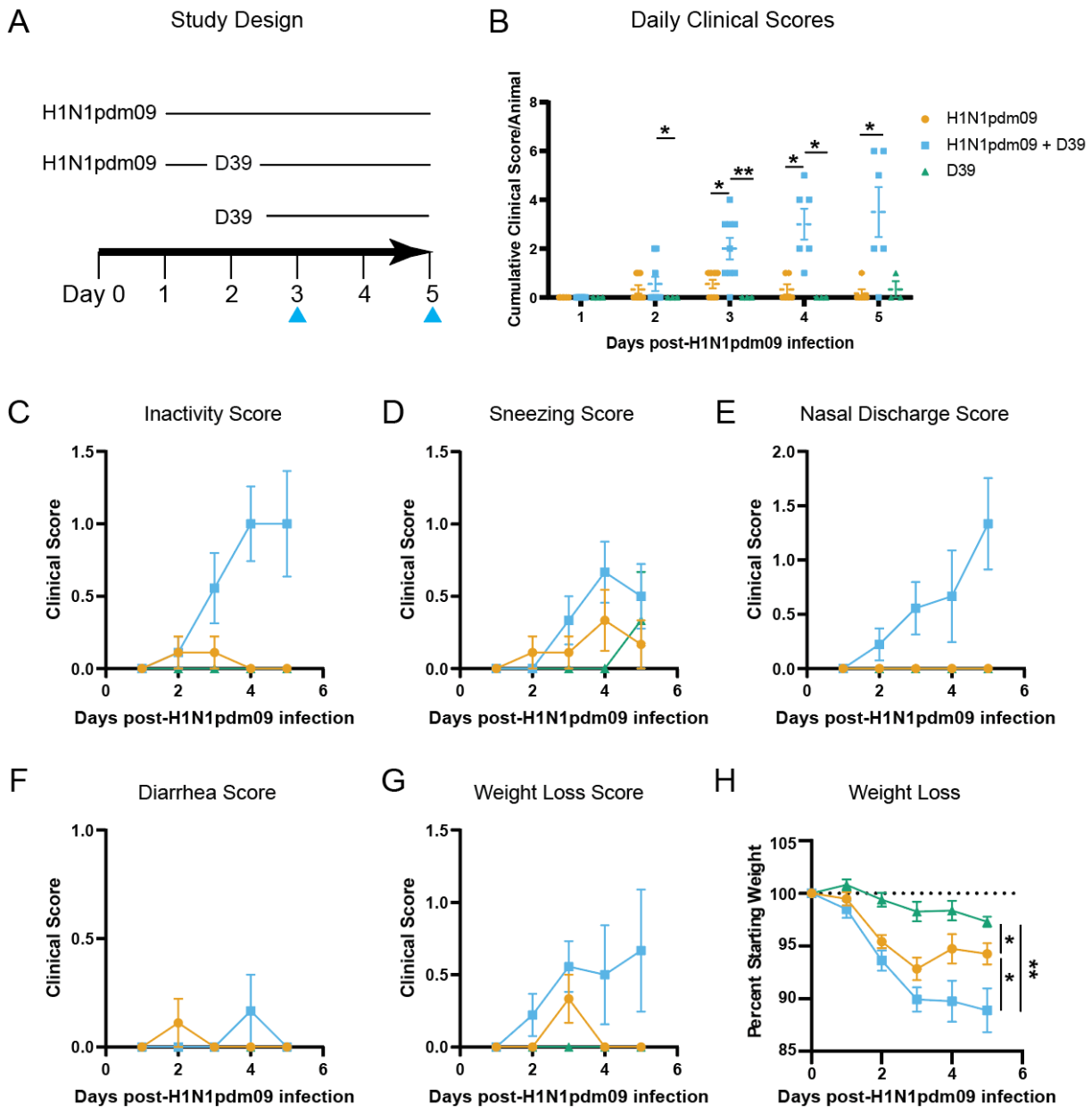

Figure 2. Morbidity of co-infected ferrets compared to H1N1pdm09 or D39 only. (A) Ferrets were intranasally infected on day 0 with 10^6 $TCID_{50}$ of A/CA/07/2009 (H1N1pdm09) or mock infected. Two days later, animals were either intranasally infected with 10^7 CFU *S. pneumoniae* D39 (D39) or mock infected. Animals were then sacrificed on day 3 (H1N1pdm09: N=3; co-infection: N=3) or day 5 post-influenza virus infection (H1N1pdm09: N=6; co-infection: N=6; D39: N=3) (blue arrows). (**B**) Clinical signs were assessed for all animals each day and a total score was calculated as described in materials and methods. The mean is shown with standard error. Significance was determined using multiple unpaired Welch's t-tests. *p<0.05; **p<0.01. Animals were evaluated for (**C**) inactivity score, (**D**) sneezing, (**E**) nasal discharge, (**F**) diarrhea, and (**G-H**) weight loss. Mean and standard error are shown.

Multiple Mann-Whitney t-tests were used to assess statistical significance of **C**-**G**. Two-way ANOVAs were used to assess differences in **H**.

To correlate the increased clinical signs to pathological changes within the respiratory of infected ferrets, hematoxylin and eosin staining was performed on tissue sections from day 5 (except in limited cases of D39-only tissues), and the results were read by a pathologist blinded to the conditions (Figure 3). Pathological changes in the nasal turbinates appeared distinct between each infection condition (Figure 3A). Nasal turbinates from animals infected with D39-only displayed mild lymphoplasmacytic infiltrates in the submucosa with some fibrin present in the lumen. Ferrets infected with H1N1pdm09-only displayed squamous metaplasia and attenuation of the epithelium with edema in the submucosa and bone remodeling in their nasal turbinate tissue. In contrast to each single infection condition, co-infection with both pathogens resulted in severe changes within the nasal turbinate tissue, with similar attenuation and loss of epithelium as in H1N1pdm09-only infected animals, but with greater necrosis, fluid accumulation, and immune cell infiltrate in the luminal space (Figure 3A). To quantify these observed differences between animals infected with H1N1pdm09 or co-infection, we scored inflammation in the submucosa, inflammatory cells in the lumen, and fluid in the lumen from day 3 and day 5 tissue. Scores from day 3 and day 5 were combined since results were similar (Figure 3E). Inflammation in the submucosa was similar between H1N1pdm09-only and co-infected nasal turbinate sections (Figure 3E). In co-infected animals, there was a trend towards greater fluid accumulation, which periodic acid-schiff staining indicated was mucous (data not shown), and more inflammatory cells (Figure 3A,E), primarily consisting of neutrophils and macrophages (per pathologist assessment).

Histology of the soft palate did not observed differences in pathological changes in animals infected with H1N1pdm09, D39, or co-infected (Figure 3B). There were mild lymphoplasmacytic infiltrates in all sections examined. Soft palate tissue from H1N1pdm09 infected animals also displayed mild multifocal erosion on the nasal surfaces (Figure 3B). When lung sections were

examined, animals infected with D39-only appeared to be unaffected, with limited sections displaying rare perivascular lymphocytic infiltrates and interstitial pneumonia (Figure 3C-D). In contrast, the pathology of lung tissue from co-infected and H1N1pdm09-only animals was similar: bronchi and bronchioles were filled with neutrophils, macrophages, lymphocytes, and debris (Figure 3C). Large airways exhibited loss of epithelium, and alveolar walls were filled with edema (Figure 3D). Together, these data demonstrate that animals co-infected with these H1N1pdm09 followed by D39 display increased morbidity and unique pathological changes in the nasal turbinates compared to mono-infection with either pathogen.

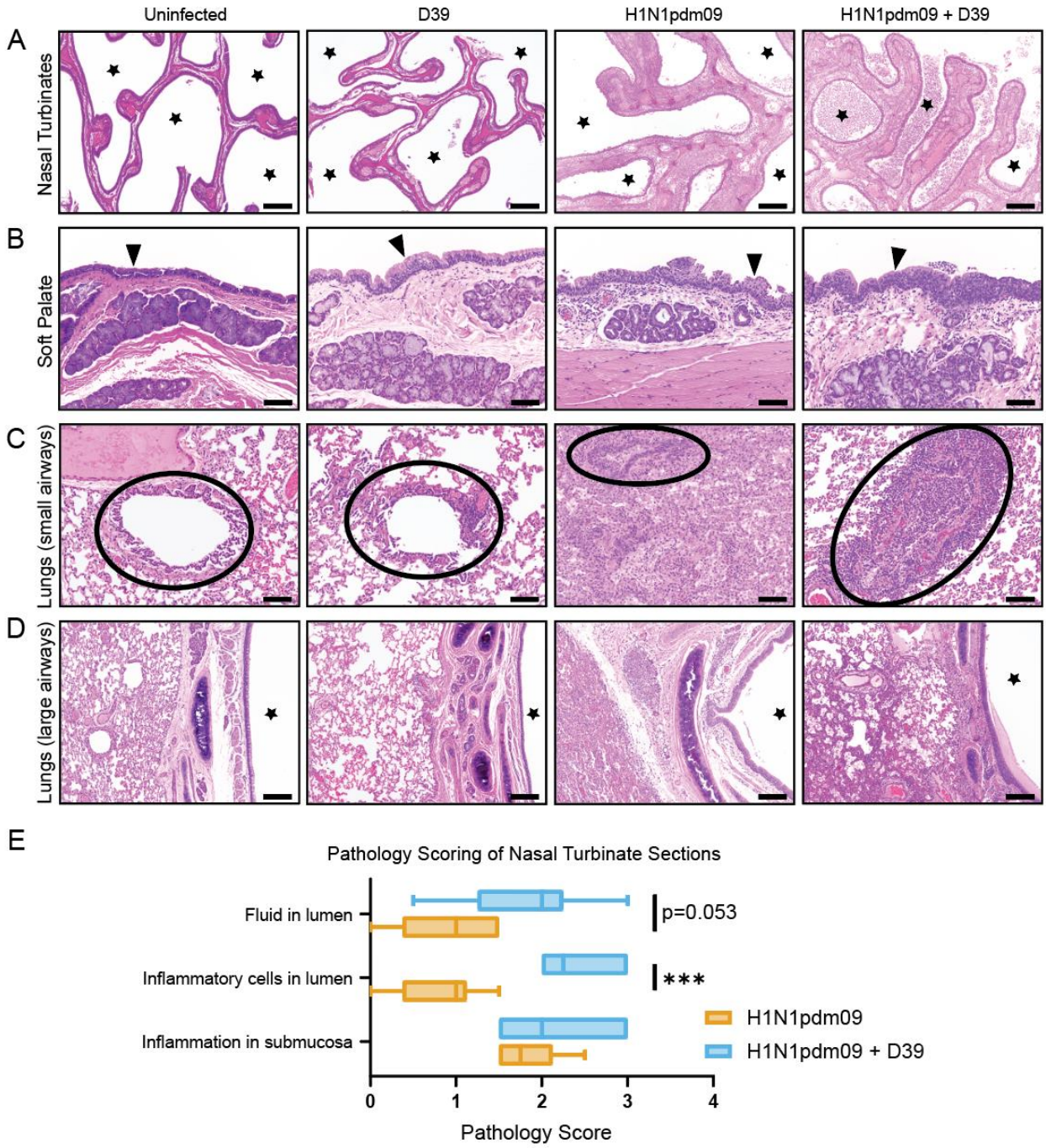

Figure 3. Pathology of co-infected ferrets compared to H1N1pdm09 or D39 only. Hematoxylin and eosin staining was performed on uninfected, D39, H1N1pdm09, and co-infected tissues. All tissues are from day 5 post-influenza virus infection, except the D39 nasal turbinate and lung (from 2 days post-D39 infection). (**A**) In nasal turbinates, stars indicate the lumen of the tissue, and scale bars indicate 200 µm. (**B**) Soft palates are oriented such that the nasal surface faces up with scale bars representing 100 µm. (**C**) Small airways of the lung are circled, and scale bars indicate 100 µm. (**D**) Large airways of the lungs are marked by a star and have scale bars indicating 200 µm. All scale bars represent

100 μm. (**E**) Scoring of nasal turbinates (day 3 and day 5 scored combined) was performed by a blinded pathologist with 0 = “none present”, 1 = “mild”, 2 = “moderate”, and 3 = “severe.” Significance was determined with multiple unpaired t-tests. N=6. *p<0.05; **p<0.01; ***p<0.001

2.3.2 Co-infection leads to tissue-specific increased bacterial burden in the upper respiratory tract

While greater morbidity and pathology during co-infection might suggest increased virus replication during co-infection, previous work in ferrets and mice found a reduction in viral titers in nasal washes of co-infected animals [82,110]. Conversely, previous work in mice suggested that bacterial co-infection leads to a rebound in viral burden in the lungs [191]. To better understand how co-infection impacts both influenza virus and D39 replication, we measured bacterial and viral titers in nasal wash (Figure 4) or homogenized tissues of infected animals on day 3 or day 5 post-infection (Figure 5 and Table 1). Not all samples were quantifiable due to the presence of contaminating bacteria (Table 1). Additionally, we measured bacterial titers from the spleen, heart, and blood to assess D39 dissemination or sepsis, although no bacteria were detected in any animals in these sites (data not shown).

Co-infected animals had similar or lower virus titers in the nasal wash compared to H1N1pdm09-infected animals (Figure 4A-B). When examining bacterial load, there was a trend towards greater bacterial burden in the nasal washes of co-infected animals (Figure 4C-D). In both H1N1pdm09-infected and co-infected ferrets, substantial virus titers were observed on days 3 and 5 in all tissues, and there were no significant differences between H1N1pdm09-infected and co-infected ferrets (Figure 5A-E), suggesting that increased morbidity during co-infection does not correspond to increased viral burden. In contrast to virus replication, we found that bacterial burden in co-infected animals varied by tissue over time. On day 3, most samples from co-infected animals exhibited detectable bacteria (Figure 5F-J). By day 5, however, only co-infected samples from the nasal turbinates, soft palate, and trachea contained detectable bacterial titers, while the left cranial lung and right middle lung had none (Figure 5F-J). This was distinct from D39-only controls where

only the nasal turbinates displayed a high bacterial burden (Figure 5B). The high bacterial burden in the D39-only group was a surprise given the trend towards decreased bacterial burden in the nasal wash of these animals. Interestingly, while the soft palate trended towards increased bacterial burden, there did not appear to be differences in pathology between co-infection and D39-infection (Figure 3B).

Together, these data suggest that the increased morbidity in co-infected animals is not simply related to viral burden, since virus replication was similar to H1N1pdm09-infected animals, but rather correlated with tissue-specific trends towards increased bacterial burden in the upper respiratory tissues.

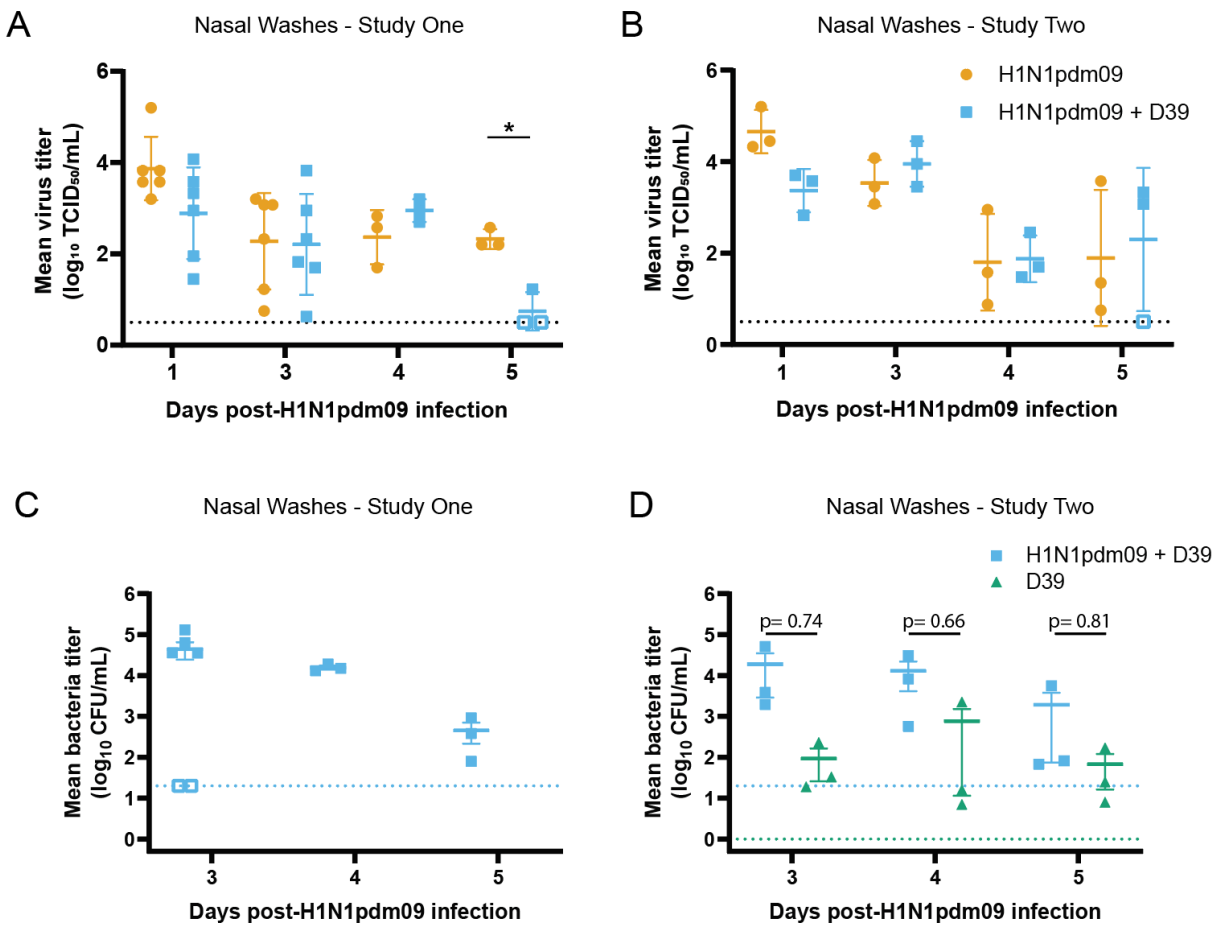

Figure 4. Viral and bacterial burden in nasal washes of infected animals. Nasal washes were collected from infected animals on days 1, 3, 4, and 5 of the study. (**A-B**) Viral burden was assessed in nasal washes of H1N1pdm09-infected and co-infected ferrets. LOD for all samples is shown with a black dotted line. (**C-D**) Bacterial load was quantified in nasal washes of D39-infected and co-infected ferrets. LOD for co-infected samples is shown with a blue dotted line and a green dotted line for D39-infected samples. Mean and standard error are shown for all samples. Open symbols indicate samples that were below the LOD.

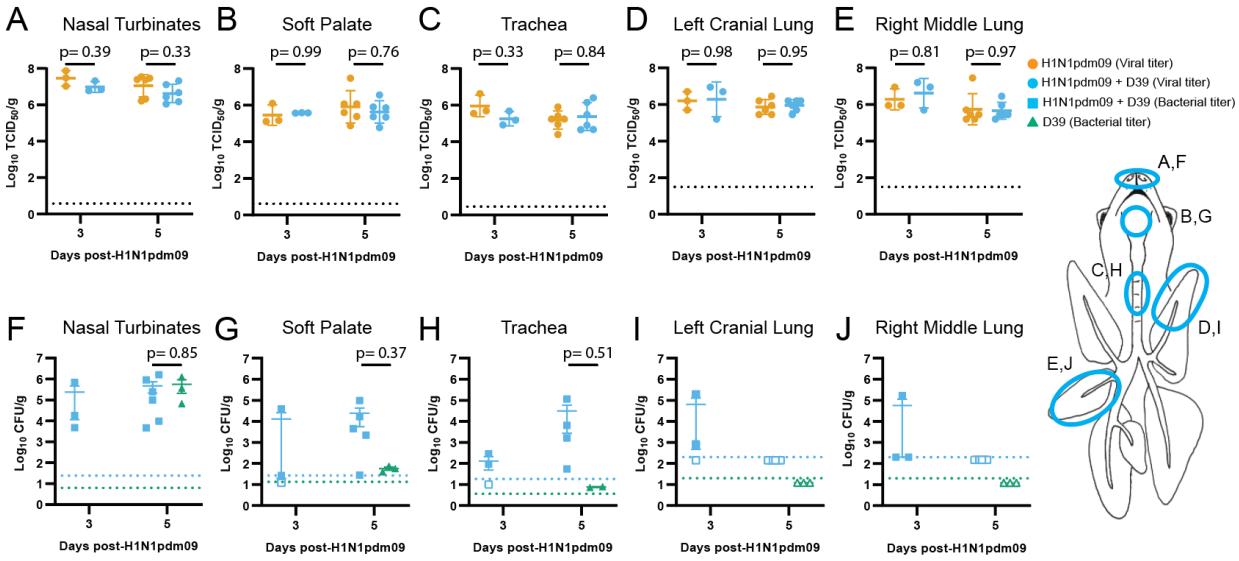

Figure 5. H1N1pdm09 and D39 titers in infected ferret tissues. Influenza titers were measured by $TCID_{50}$ assay from tissue extracts of the (**A**) nasal turbinates, (**B**) soft palate, (**C**) trachea, (**D**) left cranial lung, and (**E**) right middle lung of H1N1pdm09-only and co-infected animals. The limit of detection (LOD) is indicated by the black dotted line and varied by sample. *S. pneumoniae* titers were measured by colony formation on blood agar plates from tissue extracts of the (**F**) nasal turbinates, (**G**) soft palate, (**H**) trachea, (**I**) left cranial lung, and (**J**) right middle lung of D39-only (day 5 only) and co-infected animals. The blue dotted line indicates the LOD for co-infected animals and the green dotted line indicates the LOD for D39-only animals. The LOD varied by sample and plots show the lowest LOD for each group. Samples with no detectable bacteria were graphed as open symbols just below the LOD. Samples that were not quantifiable were not graphed. Individual bacterial titers and LODs can be found in Table 1 and Table 2. A two-way ANOVA with multiple comparisons was used to determine significance for influenza burden and a t-test was used to determine significance for bacterial burden.

Table 1 LODs for all bacterial samples (CFU/g). LODs were calculated using organ weight, tissue dilution and volume plated to count CFU.

	Animal	Nasal Turbinates	Soft Palate	Trachea	Right Middle Lung	Left Cranial Lung	Spleen	Heart
D39	F69-22	6.667	25	3.636	20	20	20	20
	F70-22	11.765	14.286	4	20	20	20	20
	F85-22	6.25	13.333	NQ	20	20	20	20
H1N1pdm09 + D39	F86-22	151.515	357.143	NQ	500	500	500	500
	F87-22	208.333	333.333	250	500	500	500	500
	F88-22	227.273	NQ	NQ	500	500	500	500
	F143-21	46.512	26.667	19.231	200	200	200	200
	F144-21	24.096	27.397	19.048	200	200	200	200
	F145-21	27.778	27.027	18.868	200	200	200	200
	F146-21	33.333	28.986	18.519	200	200	200	200
	F147-21	25.316	28.169	18.349	200	200	200	200
	F148-21	58.824	29.851	21.505	200	200	200	200
NQ- Sample not quantified due to presence of contamination								

Table 2 LODs for all virus samples (Log_{10} $TCID_{50}$/g). LODs were calculated using organ weight, tissue dilution, and assay limit of detection.

	Animal	Nasal Turbinate	Soft Palate	Trachea	Right Middle Lung	Left Cranial Lung
H1N1pdm09	F149-21	0.784	0.72185	0.487	1.5	1.5
	F150-21	0.8279	0.66115	0.432	1.5	1.5
	F151-21	0.9202	0.6549	0.351	1.5	1.5
	F152-21	0.9202	0.62494	0.536	1.5	1.5
	F153-21	0.7596	0.68046	0.504	1.5	1.5
	F154-21	0.8665	0.6549	0.541	1.5	1.5
	F89-22	1.0086	1.11979	1.199	1.5	1.5
	F90-22	1.085	1.17778	1.199	1.5	1.5
	F91-22	0.9437	1.26955	1.199	1.5	1.5
H1N1pdm09 + D39	F143-21	0.8665	0.62494	0.483	1.5	1.5
	F144-21	0.5809	0.63668	0.479	1.5	1.5
	F145-21	0.6427	0.63077	0.475	1.5	1.5
	F146-21	0.7218	0.66115	0.467	1.5	1.5
	F147-21	0.6024	0.64874	0.463	1.5	1.5
	F148-21	0.9685	0.67393	0.532	1.5	1.5
	F86-22	0.9815	1.35387	1.199	1.5	1.5
	F87-22	1.1198	1.32391	1.199	1.5	1.5
	F88-22	1.1576	1.19897	1.199	1.5	1.5

2.3.3 Tissue site is an important determinant of viral/bacterial titer relationship and host response to infection.

Previous work has suggested that influenza virus and *S. pneumoniae* interact[112,192]. So, we next investigated the relationship between virus titer and bacterial titer in the nasal turbinates, where co-infection and D39-only had high bacterial burden on day 5, the soft palate, where co-infection had a high bacterial burden and D39-only had a low burden, and the lungs, where co-infection and D39-only had no detectable bacteria. We plotted viral titer as a function of bacterial titer in each tissue. Linear regressions were then performed for each tissue (Figure 6A-C).

Analysis of viral titer as a function of bacterial titer indicated a tissue-specific relationship. Linear regression of titers in the nasal turbinates suggested there may be a negative correlation between viral and bacterial titers (Figure 6A), although the p-value for the co-efficient showed there was insufficient evidence to conclude that these variables were negatively associated ($p=0.1275$). In the soft palate, there was a weak positive relationship between viral and bacterial titers ($p=0.4408$, Figure 6B), while the combined data from the right middle lung and left cranial lung demonstrated a trend towards positive correlation ($p=0.0651$, Figure 6C). This trend was primarily driven by the two samples with detectable bacteria, which were determined to be outliers. Further sampling would be needed to determine if this positive trend has biological significance. The importance of tissue site was unexpected, as studies of co-infection in animals have largely focused on analysis of the lungs and extrapolated the results to the rest of the respiratory tract.

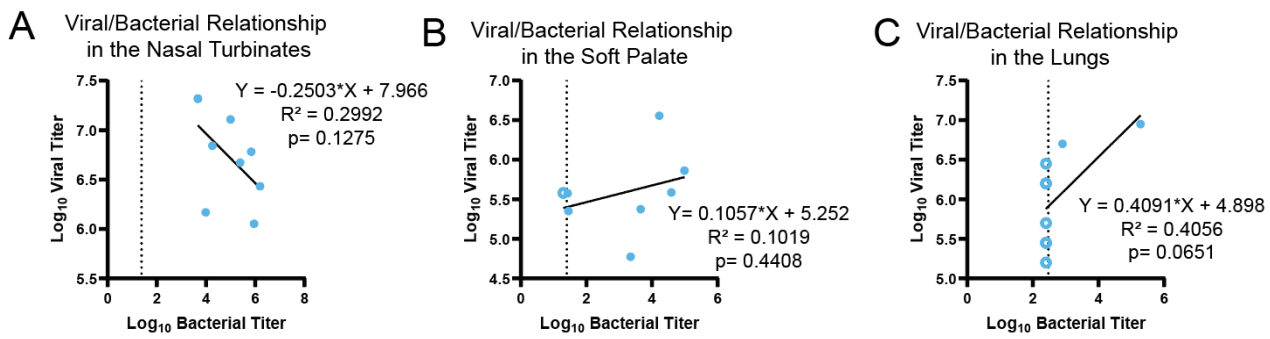

Figure 6. Determination of tissue-specific relationships between viral and bacterial burden. Virus titer plotted against bacterial titer with linear regressions fit for (**A**) the nasal turbinates, (**B**) the soft palate, and (**C**) the lungs using data from Figure 5[82]. Samples with no detectable bacteria were set to just below the limit of detection (shown as the black dotted line) and are shown with an open symbol.

2.3.4 Host response to co-infection varies by tissue

Given the tissue-specific differences in bacterial burden and pathology, we investigated whether host responses to co-infection also varied by tissue. To examine this, mRNA was extracted and sequenced from the nasal turbinates, the soft palate, and the lungs of uninfected, H1N1pdm09-only, and co-infected ferrets. Since nasal turbinates were the only tissue site with a high bacterial burden during D39-only infection, mRNA from this group was also included. Differential expression was assessed using a cut-off of Log_2 Fold Change > |1| and FDR p-value <0.05.

A principal component analysis of all samples indicated that tissue site was a primary driver of variation, as the soft palate clustered separately from other samples (Figure 7A, Table 3). To assess the role of tissue site on host response to co-infection, differentially expressed genes were assessed by comparing co-infected tissues to mock tissues within the nasal turbinates, the soft palate, or the lungs (Figure 7B-C). The nasal turbinates had the greatest number of differentially expressed genes during co-infection with 58.7% of the total number of upregulated

genes in all tissues being exclusive to the nasal turbinates (Figure 7B) and 87.3% of downregulated genes being exclusive to the nasal turbinates (Figure 7C). When examining genes exclusively upregulated in a single tissue, 68.7% of the genes were exclusive to the nasal turbinates, 35.1% were exclusive to the lungs, and 16.4% were exclusive to the soft palate (Figure 7B). Conversely, when examining downregulated genes unique to each tissue, 93.1% of genes downregulated in the nasal turbinates were not altered in the soft palate or lungs, 52.6% of genes were exclusive to the lungs, and 28.0% were exclusive to the soft palate (Figure 7C). These data demonstrate that host responses to pathogens is distinct in different tissues which could explain the pathological changes observed.

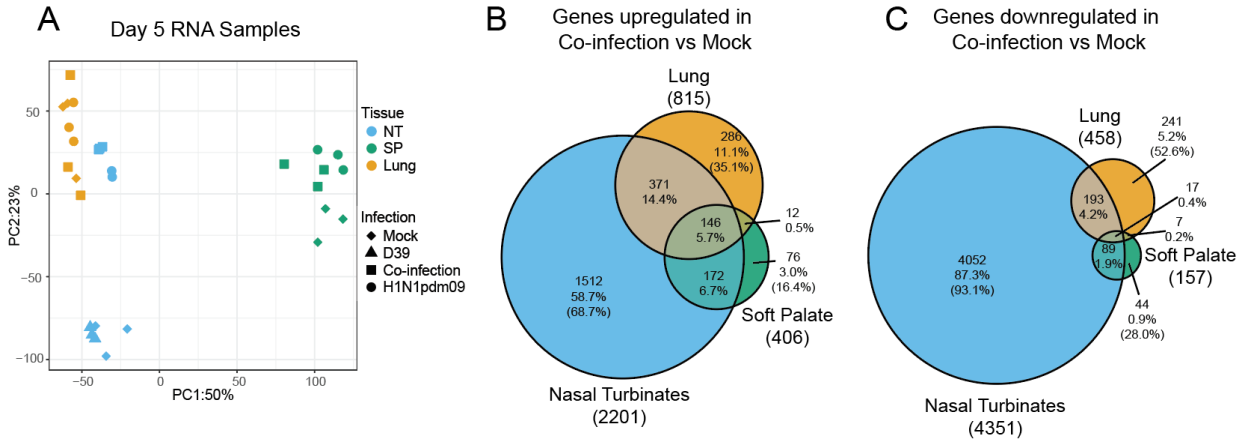

Figure 7. RNA sequencing of infected tissues reveals tissue-specificity. RNA was isolated from nasal turbinate, soft palate, and lung tissue of infected or mock animals on day 5 of the study and mRNA was sequenced. (**A**) A principal component analysis of all samples was performed using the top 2000 genes. In Venn diagrams, upregulated (**B**) and downregulated (**C**) gene counts when comparing co-infection to mock infection are shown with percentage of the total number of genes shown and (percent differentially expressed within the tissue). Differentially expressed genes were determined by FDR p-value < 0.05 and Log_2 Fold Change > |1|.

2.3.5 Host response to co-infection is synergistic compared to mono-infection

We next investigated how the host response to co-infection differed from H1N1pdm09-only or D39-only infection within each tissue. Principal component analysis was performed for each tissue to visualize variation of the samples (Figure 8A-C, Table 3). In all three tissues, co-infection samples clustered with H1N1pdm09-only samples, which suggested that influenza virus infection might be a primary driver of the differential gene expression observed during co-infection.

To begin understanding how the host response to co-infection differed from H1N1pdm09-only, we first assessed differential expression by comparing each infection to mock-infected samples and then generated Venn diagrams for upregulated genes (Figure 8D) and downregulated genes (Figure 8E). When looking at all the genes upregulated by any infection, there was a large overlap between genes upregulated during H1N1pdm09-only and co-infection in all three tissues, ranging from 42.5% to 63.1% (Figure 8D). Suggesting that a significant portion of the host response during a viral bacterial co-infection is driven by the virus.

However, of the genes upregulated during co-infection, between 13.8% and 50.0% were not upregulated during H1N1pdm09-only (Figure 8D). In the nasal turbinates, 21.6% of the genes upregulated during co-infection were not present during H1N1pdm09-only or D39-only infection, suggesting that there is a distinct host response in the nasal turbinates when both pathogens are present albeit though the majority of the response is shared with tissue from H1N1pdm09 infected animals. Given the lack of clinical signs and limited pathology in D39-only animals, it was not surprising that there were relatively few differentially expressed genes (Figure 8D-E). A different pattern of shared downregulated genes was seen between animals infected with H1N1pdm09-only or co-infected. While there was still substantial overlap between H1N1pdm09-only and co-

infection in the genes downregulated in the nasal turbinates, overlap in the soft palate and lungs was only 13.9% and 34.8%, respectively (Figure 8E). In fact, in the soft palate and lungs, there were more genes significantly downregulated during H1N1pdm09-only than during co-infection (Figure 8E).

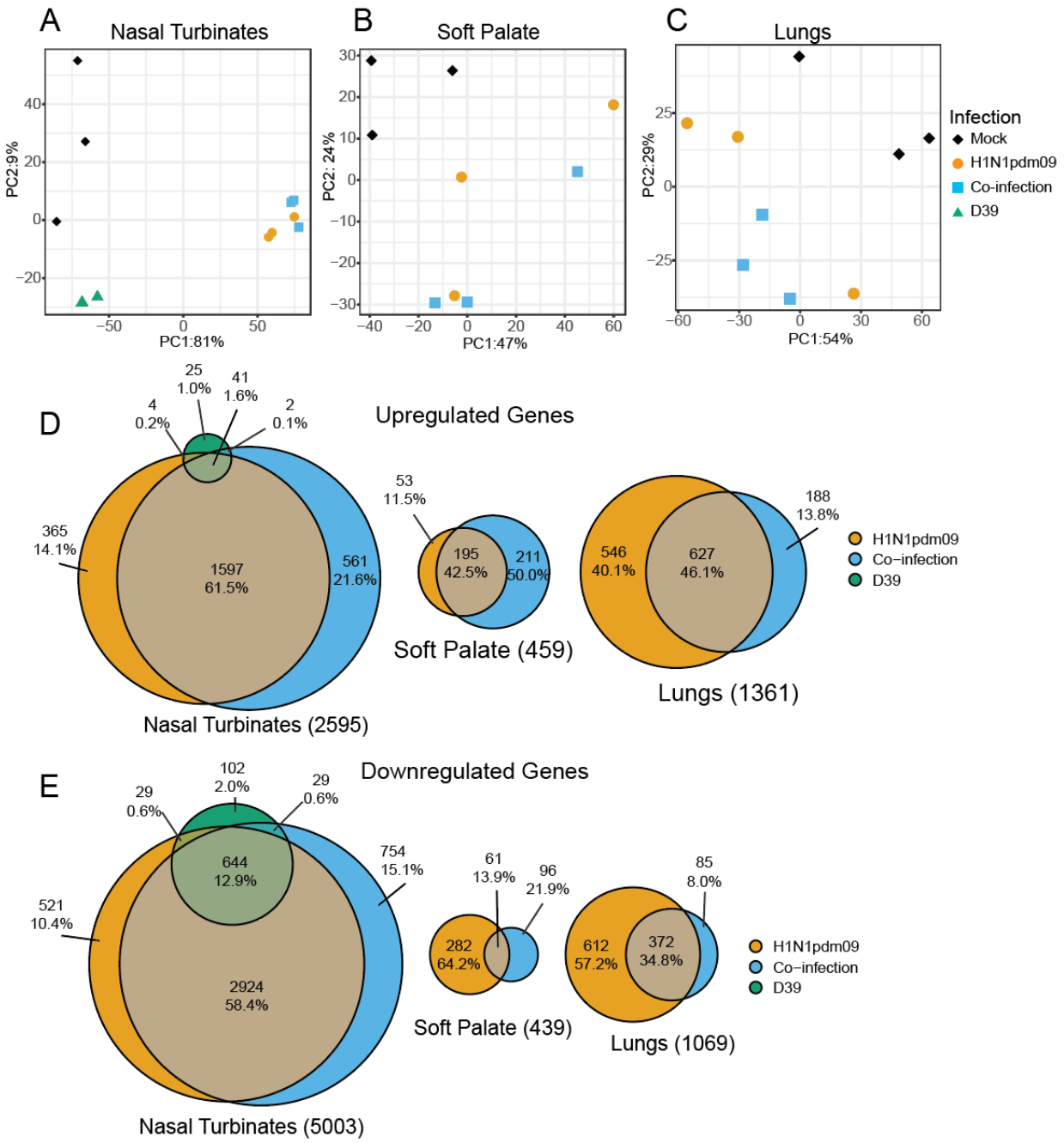

Figure 8. RNAseq in nasal turbinates, soft palate, and lungs shows that many genes differentially expressed during co-infection overlap with genes altered during H1N1pdm09-only infection. Principal component analysis of mRNA sequencing data was performed separately for samples within (**A**) the nasal turbinates, (**B**) the soft palate, or (**C**) the lungs. Each infection was compared to mock, and differentially expressed genes were determined by FDR p-value < 0.05 and Log_2 Fold Change > |1|. (**D**) Upregulated and (**E**) downregulated gene counts

are shown in Venn diagrams with percentage of the total number of genes shown and (percent differentially expressed within the tissue).

Table 3 The top 15 genes driving the principal components analysis results are shown for each PCA plot.

All Tissues		Nasal Turbinates		Soft Palate		Lungs	
PC1 Genes	PC2 Genes	PC1 Genes	PC2 Genes	PC1 Genes	PC2 Genes	PC1 Genes	PC2 Genes
KRT1	BPIFA1	BPIFA1	BPIFB3	CXCL13	CXCL10	BPIFB1	APOBEC3G
BPIFA2	SFTPA1	SCGB1A1	BPIFB4	FCRL1	CXCL11	SCGB3A1	CXCL10
IVL	SFTPC	13334	17860	09806	BATF2	13334	RSAD2
KRT3	VMO1	SEC14L3	LCNL1	MS4A1	ACOD1	BPIFA1	CYP2F1
04938	02820	00381	GPX6	IGHG1	DNAH9	CLCA1	CCL8
CRNN	SFTPB	DNAH9	LCN15	08521	14983	MUC5B	CXCL11
MYH1	13334	10071	UGT2A3	CD22	GBP1	17715	ISG15
RPTN	DNAH9	APOBEC3G	STOML3	ADAMDEC1	12060	CYP1A1	13233
BPIFB2	CYP2F1	BPIFB1	12012	PAX5	CXCL9	TFF3	IFI6
18838	17659	10927	CHGA	CD79B	IDO1	GABRP	12060
ACTA1	SLC27A2	00423	GFY	FCRL5	DYNAP	LPO	ISG20
SPINK5	00381	08923	MMP1	CD79A	RSAD2	AGR2	CCL2
KRT6C	08923	MUC5B	16662	BANK1	CCL2	CAPN13	ANKRD1
KRTDAP	09563	RSPH1	10071	BTLA	CCL8	02887	GZMA
TGM3	CLDN18	SPAG6	CYP1A2	02610	OASL	APOBEC3G	IFIT3

Genes denoted by a five-digit number are not annotated. The corresponding Ensembl ID is "ENSMPUG000000" + the five-digit number.

2.3.6 Co-infection broadly heightens immune response pathways in the nasal turbinates but not the soft palate or lungs

To better appreciate the large-scale host immune responses to each infection, gene set variation analysis (GSVA) was performed using gene sets published by the Molecular Signatures Database (MSigDB) and previously used to examine ferret responses[193] (Figure 9). This analysis revealed that co-infection in the nasal turbinates leads to overall heightened immune responses. Compared to the nasal turbinates from H1N1pdm09-only infected ferrets, there was enrichment in the majority of T cell pathways assessed, including T cell activation, T cell mediated cytotoxicity, and positive regulation of T helper type 1 (Th1) and Th17 responses. Co-infection also contributed to heightened acute inflammatory responses, such as interferon production and response (Figure 9A).

More heterogeneity within host responses was observed in the soft palate and lungs (Figure 9B-C). In the soft palate, the response to co-infection and H1N1pdm09-only was similar, with substantial ferret-to-ferret variation within both groups (Figure 9B). Interestingly, responses to co-infection in ferret lungs appeared to be similar or slightly decreased compared to animals with H1N1pdm09-only (Figure 9C). Genes involved in cytokine production, type 1 interferon signaling, macrophage differentiation, and macrophage migration were decreased in animals infected with both H1N1pdm09 and D39 compared to H1N1pdm09 alone (Figure 9C). Together, these data demonstrate heightened immune responses in the nasal turbinates, comparable responses in the soft palate, and decreased responses in the lungs, although the altered pathways vary by tissue. These findings, in combination with the analysis of viral and bacterial titers based on tissue site (Figure 6), suggest that host responses are associated with the different tissue-specific relationships observed between viral and bacterial burden.

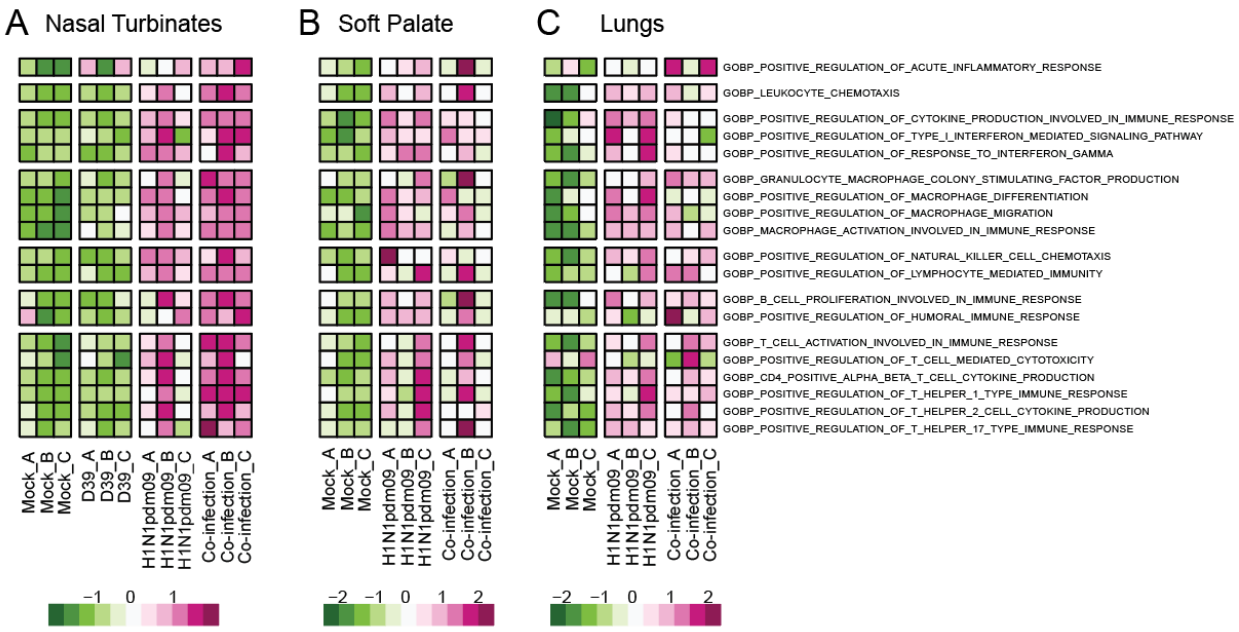

Figure 9. Gene set variation analysis of sequenced RNA samples. Gene set variation analysis was performed using normalized count data from RNA sequenced (**A**) nasal turbinates, (**B**) soft palate, and (**C**) lung samples. Each column represents a different sample and rows correspond to different immune response gene sets selected from MSigDB. Samples are scaled based on row and colored such that pink represents greater enrichment and green represents decreased enrichment of genes within the selected gene set.

2.3.7 Immune cell migration and chemotaxis pathways are highly enriched in the nasal turbinates of co-infected animals

To more fully understand how the host response to co-infection differs from H1N1pdm09, we identified genes that are differentially expressed during co-infection compared to H1N1pdm09 only. There were 218, 35, and 8 genes differentially expressed between co-infection and H1N1pdm09 in the nasal turbinates, the soft palate, and lungs, respectively (Figure 10A-C and Table 4). Some genes lack annotation, as noted by their Ensembl IDs (ENSMPUG) in place of a gene name. When performing gene set enrichment analysis using publicly available gene sets in the nasal turbinates, four of the top nine enriched pathways were for immune cell migration or chemotaxis pathways (Figure 10D), suggesting that there is a significant influx of immune cells to the nasal turbinates during co-infection that is not observed during H1N1pdm09-only. This aligns with the pathology results indicating a large influx of proteinaceous fluid and immune cell infiltrate in the nasal turbinates of co-infected animals. There was also enrichment in Tumor Necrosis Factor (TNF) superfamily cytokine production, inflammatory response, interleukin-6 production, and cell activation pathways (Figure 10D), indicating that there is an overall increase in the magnitude of the host immune response during co-infection which may be contributing to the increased morbidity observed in co-infected animals.

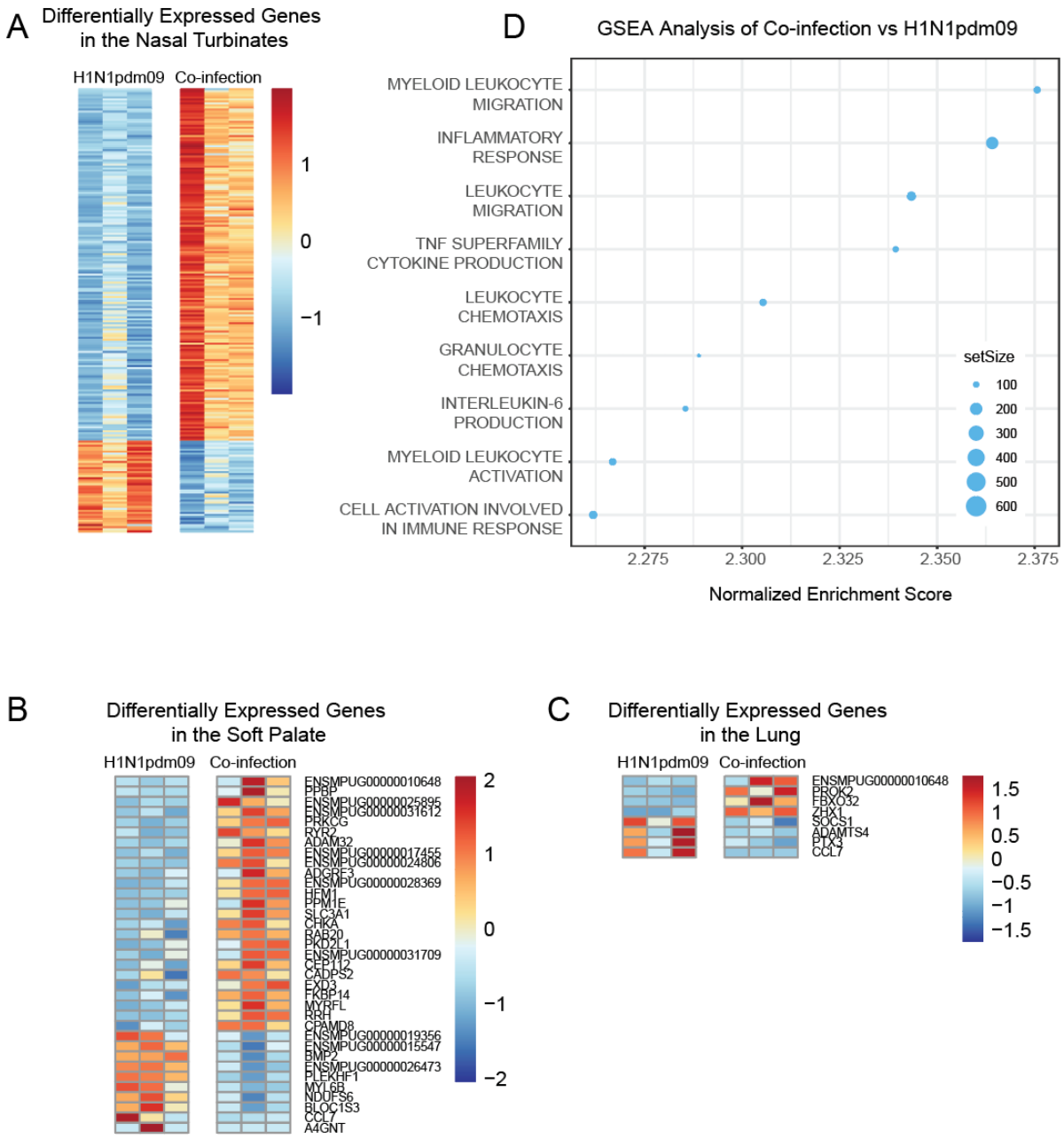

Figure 10. Comparison of co-infection to H1N1pdm09-only in the nasal turbinates shows enrichment of genes involved in immune cell migration. In the (**A**) nasal turbinates, (**B**) soft palate, and (**C**) lungs, co-infection was compared to H1N1pdm09 and differentially expressed genes were assessed by Log_2 Fold Change > |1| and FDR p-value <0.05. Differentially expressed genes are either displayed in Table 4 (nasal turbinates) or alongside the heatmap (soft palate and lungs). (**D**) Gene set enrichment analysis comparing co-infection to H1N1pdm09 was

performed and the 9 categories with the greatest normalized enrichment scores are shown. The size of the dot plot corresponds to the number of genes corresponding contained within the gene set shown on the x-axis.

Table 4 Genes differentially expressed in the nasal turbinates during co-infection as compared to H1N1pdm09 infection.

BPIFB4	TBXAS1	PEAK3	EEPD1
FGB	STBD1	ENSMPUG00000002430	CBS
ENSMPUG00000024261	ENSMPUG00000001362	NFIL3	LPAR2
S100A12	ASAH2B	SLC22A15	GMIP
ENSMPUG00000013359	CPN1	ADORA2A	ENSMPUG00000008900
CLEC4G	ADGRE3	SELP	IL17RA
PROK2	SOAT2	MXD1	CPNE2
SLC26A4	ENSMPUG00000027125	CD101	MBOAT7
ENSMPUG00000001476	PLAT	PTAFR	**CACNA1D**
ENSMPUG00000006864	IL18RAP	CD14	**ANGPT4**
PPBP	CACNA2D4	ENSMPUG00000016737	**KITLG**
ENSMPUG00000030536	G0S2	SOD2	**ENSMPUG00000017326**
S100A8	CSTA	RNASE6	**SYT12**
LCN2	CCNJL	PSTPIP2	**BHLHE41**
S100A9	ENSMPUG00000028121	PRKAG2	**ENSMPUG00000019888**
SLC26A8	DHDH	LIPG	**FABP3**
ENSMPUG00000013724	ENSMPUG00000030831	ALOX5AP	**MAPT**
MCEMP1	ENSMPUG00000016511	RAP1GAP2	**HEYL**
ENSMPUG00000026381	RAB39A	LRRC75B	**ASIP**
ENSMPUG00000025155	IL1B	ADGRF3	**FAT4**
ENSMPUG00000028739	PIGR	VSIR	**GPC1**
MMP8	NOXO1	KBTBD12	**WNT7B**
MGAM	ARG2	JAML	**SCN2A**
MARCO	ENSMPUG00000032004	TMEM171	**ENSMPUG00000013837**
IL1R2	ENSMPUG00000031958	ACSS1	**INSC**
CD177	PLIN5	RGS14	**RCOR2**
ENSMPUG00000000102	CSF3R	ZBTB16	**NEBL**
PADI4	NFE2	CRISPLD2	**MEI4**
KIF1A	ENSMPUG00000024660	TMEM154	**PALM3**
LTF	ENSMPUG00000027560	SSH2	**PPFIA4**
ENSMPUG00000027308	ENSMPUG00000030461	EHD1	**ENSMPUG00000018503**
ENSMPUG00000003859	ENSMPUG00000028257	ENSMPUG00000001347	**ENSMPUG00000011844**
ENSMPUG00000030474	ENSMPUG00000028605	CYTIP	**RBM20**
PRSS57	ENSMPUG00000018165	IRS2	**ENSMPUG00000012100**
P2RY13	TREM1	ZC3H12A	**CLDN11**
PGLYRP1	SLIT1	MAPK13	**GLI1**
ENSMPUG00000002165	ENSMPUG00000009169	DDX50	**PRRT2**
HK3	VSTM1	SH2B2	**SOST**
CD300E	ENSMPUG00000001232	EDNRB	**NPY4R**
IL17F	CASS4	ATP6V0A1	**ENSMPUG00000026616**
ENSMPUG00000003281	IL18	KLF15	**ACADL**

ENSMPUG00000024697	ENSMPUG00000032068	ACSS3	**ST8SIA5**
DGAT2	NLRP12	LPCAT2	**SLC26A7**
GFI1B	ABCC11	PRDM11	**ENSMPUG00000014147**
ENSMPUG00000026133	PLAUR	MMP19	**EPHA7**
ENSMPUG00000031622	FOLR2	IRAK3	**SMCO1**
ENSMPUG00000023976	IGFBP3	SLC16A7	**MUC21**
CTCFL	ENSMPUG00000027382	ABTB1	**PLPPR4**
SFTPA1	RGS2	ENSMPUG00000010930	**RP1L1**
ENSMPUG00000017590	CD24	TTLL3	**ENSMPUG00000012694**
MEFV	ENSMPUG00000028729	ENSMPUG00000002570	**ENSMPUG00000028261**
ENSMPUG00000006623	GMFG	LPIN2	**ENSMPUG00000018741**
MOGAT1	ENSMPUG00000014201	KDM6B	**LRRTM1**
ENSMPUG00000010662	ENSMPUG00000019581	SGK1	
IL18R1	TNFAIP2	PBX2	

Bolded genes indicate genes downregulated during co-infection compared to H1N1pdm09 infection.

2.4 Discussion

An increase in morbidity has long been observed during influenza virus and *S. pneumoniae* co-infection, but the underlying causes have remained elusive. To examine this, we undertook a tissue-specific analysis of co-infected ferrets, analyzing pathology, microbial replication, and gene expression changes. Pathological analysis showed that co-infection caused greater changes in the nasal turbinates than H1N1pdm09 or D39 mono-infection, but pathology of the soft palate and lungs was similar during co-infection and H1N1pdm09. Our results indicated that viral burden is insufficient to explain clinical severity, and co-infection resulted in tissue-specific increases in bacterial load. Gene expression profiles indicate a distinct effect of influenza and *S. pneumoniae* co-infection on the host immune responses, with unique sets of genes up- and downregulated in a tissue-specific manner, which help explain the observed pathology and increased morbidity in ferrets.

Interestingly, the tissue-specific response to co-infection was dominated by gene expression changes in the nasal turbinates, primarily in innate immune response pathways. The increased immune cell infiltration and inflammation observed in co-infected nasal turbinates is consistent with these gene expression profiles and provides a molecular basis for increased morbidity. The soft palate had the least number of differentially expressed genes, and the response to co-infection was variable in the pathways analyzed. Previous work has shown that the soft palate is an important site of influenza virus adaptation[29], and this analysis suggests that increased viral evolution could be due to a smaller magnitude immune response influenza infection at this site compared to the lungs or nasal turbinates.

Recent work examining host responses of primary lung epithelial cells during co-infection complements the work presented here[194]. The authors detected large host expression changes

during influenza infection. Our results similarly found that influenza is a major driver of host response to co-infection. However, unlike our results in the nasal turbinates, the authors observed that the co-infection group clustered with their influenza mono-infection group and the *S. pneumoniae* mono-infection group clustered with the host only[194]. The difference in clustering of the response to each infection condition is likely driven by host responses within immune cells captured in our analysis, that are not present in an ex vivo model of respiratory epithelial cells. This is strengthened by the role of neutrophil influx genes differentially expressed in co-infected tissue compared to H1N1pdm09 mono-infected tissue.

Bacterial gene expression may also contribute to disease severity. Previous studies have examined these changes in *S. pneumoniae*. *S. pneumoniae* undergoes metabolic changes pertaining to ascorbate uptake during pneumonia caused by mono-infection in mice[195] or increased utilization of nitrogen sources (glutamate and threonine) during co-infection of respiratory epithelial cells[194]. Gene knockout indicated that these metabolic alterations facilitated bacterial survival. Altered bacterial protein expression may also play a part in some of the changes in host responses and disease severity we observed here, as co-incubation of *S. pneumoniae* and influenza resulted in increased secretion of six *S. pneumoniae* proteins involved in bacterial virulence and evasion of host responses[196]. These results indicate that *S. pneumoniae* is changed in the presence of a viral infection, which could contribute to the increased morbidity observed in coinfected animals.

Given that there was a trend towards decreased D39 in the nasal wash of D39-infected ferrets compared to co-infected ferrets, it was unexpected that the bacterial burden in the nasal turbinates was similar between the two groups. Previous work suggests that bacterial protein expression shifts from a biofilm phenotype to a planktonic phenotype upon exposure to influenza A virus[196], which may contribute to the increased nasal wash detection of *S. pneumoniae* during

co-infection. Homogenization of tissues for titration is a harsher collection method than nasal washing and will detect bacteria in biofilms while nasal washing may be insufficient to collect these colonies.

In total, these results indicate that characterizing pathogenesis of respiratory microbes by examining only one tissue is insufficient to fully understand the scope of the infection. In fact, tissue-specific differences between virus and bacteria titers may explain some previously published, conflicting results about whether bacterial co-infection leads to increased or decreased viral burden. When sampling the nasopharynx, our group previously found that co-infection led to decreased virus in the nasal wash[82], and another group saw that nasopharyngeal/oral swab with higher bacterial titers correlated with decreased susceptibility to H3N2 virus[73]. Conversely, others examining lung tissue have found that *S. pneumoniae* co-infection contributes to a rebound in influenza virus titer[191]. Future studies may benefit from sampling multiple tissue sites to more clearly delineate influenza virus and *S. pneumoniae* replication differences.

While we are the first to explore the relationship between influenza virus and D39 in multiple regions of the ferret respiratory tract, several limitations exist that should be noted. One limitation of our host response analysis is the weak annotation of the ferret genome. Improved annotation is needed to draw conclusions about many of the differentially expressed genes that currently lack gene names. Additionally, our study only examined a single interval between influenza virus infection and *S. pneumoniae* infection. Studies on *S. pneumoniae* co-infection have tested a large range of intervals, with bacterial co-infection occurring 9 days before influenza out to 16 days after influenza infection[81,82,103,110]. Clinical data supports a large range of co-infection timing as well, and reports during the 2009 H1N1 pandemic suggested that bacterial co-infection occurred anywhere from 1.2 to 11.1 days after influenza infection[32,183]. The primary goal of this

study was to compare co-infection to H1N1pdm09 mono-infection. Thus, we chose to assess viral/bacterial burden and pathology early after co-infection, while infected animals were still shedding virus. Future studies could assess how different timing and infection sequences alter host responses.

In total, this study expands our understanding of influenza and *S. pneumoniae* co-infection by investigating microbial relationships and host responses in multiple tissues of a natural host for influenza and *S. pneumoniae* co-infection. We found that the relationship between virus and host may depend on tissue, and that host responses are tissue specific. In the nasal turbinates, we observed a distinct host response during co-infection that was not observed during either mono-infection. This host response corresponded to increased immune cell infiltration, particularly a neutrophil response. Together, these observations indicate a dynamic relationship between host and microbes during co-infection.

2.5 Materials and Methods

2.5.1 Viruses and bacteria

H1N1 A/CA/07/2009 was grown in Madin-Darby Canine Kidney cells. Quantification of virus was performed using 50% tissue culture infectious dose ($TCID_{50}$) assay on MDCK cells in 96 well or 24 well plates. End point titers were determined using the Spearman-Karber method [197]. *S. pneumoniae* D39 (serotype 2) was provided by Dr. Hasan Yesilkaya and was grown from frozen glycerol stocks [198]. Fresh cultures were generated by streaking on TSA with 5% sheep's blood plates and growing in Columbia Broth incubated at 37˚C without shaking. Bacterial quantification

was performed by plating serial dilutions of samples on blood agar plates and incubating overnight at 37°C. Colonies were then manually counted to determine colony-forming units/mL.

2.5.2 Ferrets

Experiments involving ferrets were performed at the University of Pittsburgh under BSL2 safety conditions (IACUC protocol 19075697). Four to six-month, outbred ferrets were obtained from Triple F Farms and were confirmed to be seronegative for prior influenza infection by hemagglutination inhibition assay before purchase. Ferrets were housed individually throughout the experiment and provided *ad libitum* food and water. Animals were anesthetized prior to intranasal infection with 10^6 $TCID_{50}$ H1N1 A/CA/07/2009 (H1N1pdm09) in 0.5mL or mock infection with 0.5mL cell culture media. Two days after influenza or mock infection, ferrets were intranasally infected with 10^7 CFU *S. pneumoniae* D39 (serotype 2) in 0.5mL PBS or mock infected with 0.5mL PBS. Animals were monitored daily for clinical signs (activity score, weight loss, fever, dehydration, diarrhea, labored breathing, nasal discharge, and sneezing) as shown in Table 5[199]. Animals were provided with additional soft food when weight loss was >10%.

Table 5 Clinical sign scoring criteria

Category	Score	Criteria
Inactivity score	0	Actively initiates play
	1	Initiates play after prompting
	2	Doesn't initiate play even with prompting
Weight loss	0	<10% weight loss
	1	10-15% weight loss
	2	>15% weight loss
Fever	0	Temperature <40C
	1	Temperature >40C
Dehydration	0	Drinking water, no fluid administration needed
	1	Requires administration of subcutaneous fluid
Nasal Discharge	0	No mucus observed
	1	Animal has visible runny nose
	2	Mucus has accumulated and crusted on the nose
	3	Mucus has crusted on the nose and built up on the whiskers
Sneezing	0	No sneezing observed
	1	Sneezing observed
Diarrhea	0	No diarrhea present in cage
	1	Diarrhea observed in cage

2.5.3 Histology and immunohistochemistry

Tissues taken for histology were fixed in 10% neutral buffered formalin. Nasal turbinates were decalcified. Tissues were embedded in paraffin and sectioned. Hemoxylin and eosin staining was performed for pathological analysis and assessed by a blinded veterinary pathologist. Scoring of nasal turbinates was performed by a blinded pathologist with 0 = “none present”, 1 = “mild”, 2 = “moderate”, and 3 = “severe.”

2.5.4 RNA Sequencing

RNA was isolated from ferret tissues using Qiagen Fibrous Tissue kit. RNA quality was assessed using a Bioanalyzer (Agilent) to measure RNA integrity number, and RNA quality ranged from 7.7-9.1. RNA sequencing was performed by the Genomics Research Core at the University of Pittsburgh. Sequencing was performed on a NextSeq2000 (Illumina) with 100bp paired-end reads and $>2x10^7$ reads/sample. Quality checking and read mapping was performed using CLC Genomics Workbench using the ferret genome from Ensembl (GCA_000215625). Analysis of differentially expressed genes was performed in R using DESeq2[200].

2.5.5 Acknowledgements

We also thank members of the lab for providing constructive feedback on this manuscript and Dr. Rachel Duron for critical review and editorial comments. Funding was provided by the National Institute for Allergy and Infectious Diseases (1R01AI158484-01A1, SSL). JF was supported by the University of Pittsburgh Training Program in Antimicrobial Resistance (T32AI138954).

3.0 Detection of Influenza virus and Streptococcus pneumoniae in air sampled from co-infected ferrets and analysis of their influence on pathogen stability

3.1 Abstract

Secondary infection with *Streptococcus pneumoniae* has contributed significantly to morbidity and mortality during multiple influenza virus pandemics and remains a common threat today. During a concurrent infection, both pathogens can influence the transmission of each other, but the mechanisms behind this are unclear. In this study, condensation air sampling and cyclone bioaerosol sampling were performed using ferrets first infected with the 2009 H1N1 pandemic influenza virus (H1N1pdm09) and secondarily infected with *S. pneumoniae* strain D39 (Spn). We detected viable pathogens and microbial nucleic acid in expelled aerosols from co-infected ferrets, suggesting that these microbes could be present in the same respiratory expulsions. To assess whether microbial communities impact pathogen stability within an expelled droplet, we performed experiments measuring viral and bacterial persistence in 1 µL droplets. We observed that H1N1pdm09 stability was unchanged in the presence of Spn. Further, Spn stability was moderately increased in the presence of H1N1pdm09, although the degree of stabilization differed between airways surface liquid collected from individual patient cultures. These findings are the first to collect both pathogens from the air and in doing so, they provide insight into the interplay between these pathogens and their hosts.

3.2 Importance

The impact of microbial communities on transmission fitness and environmental persistence is under-studied. Environmental stability of microbes is crucial to identifying transmission risks and mitigation strategies, such as removal of contaminated aerosols and decontamination of surfaces. Co-infection with *S. pneumoniae* is very common during influenza virus infection, but little work has been done to understand whether *S. pneumoniae* alters stability of influenza virus, or vice versa, in a relevant system. Here, we demonstrate that influenza virus and *S. pneumoniae* are expelled by co-infected hosts. Our stability assays did not reveal any impact of *S. pneumoniae* on influenza virus stability, and a trend towards increased stability of *S. pneumoniae* in the presence of influenza viruses. Future work characterizing environmental persistence of viruses and bacteria should include microbially-complex solutions to better mimic physiologically relevant conditions.

3.3 Observation and Discussion

Environmental stability of respiratory pathogens expelled from an infected host is a key factor impacting transmission[137]. Previous work has shown that several factors (eg. humidity, temperature, and solute concentration) influence microbial stability in droplets[139,146,163,201]. Our understanding of how microbes within the same droplets affect persistence is insufficient, as studies often only examine one microbe at a time. The limited work investigating how bacteria alter viral stability have primarily focused on enteric pathogen stability in feces and found that binding of poliovirus to bacteria increased virus stability[171,172,202,203]. However, these studies did

not examine how viruses alter bacterial stability. So, it remains unclear whether multiple microbes exist within the same aerosols, and if so, whether they influence each other to impact environmental persistence.

Bacterial co-infection is a common occurrence for viral respiratory pathogens: bacterial co-infection rates during influenza virus infection in humans range from 4.2-32.7% and cause significant illness in critically ill patients[5,69,78]. Studies of influenza virus and *S. pneumoniae* secondary infection in animals have shown that influenza virus facilitates transmission of *S. pneumoniae*[82,104,107], while *S. pneumoniae* may decrease viral transmission[82,107]. Other groups have found that *S. pneumoniae* can increase influenza transmission after antibiotic administration[112]. A study on the interaction of nasopharyngeal bacteria on influenza virus observed that influenza virus binds *S. pneumoniae*[192], suggesting that these pathogens may travel in the same aerosols. These observations indicate a complex interplay between these pathogens that requires further investigation to understand how their interactions affect environmental persistence and transmission.

3.3.1 Co-infected ferrets shed H1N1pdm09 and Spn into expelled aerosols.

Co-infections can lead to high titers of virus and bacteria in infected hosts [82,103,107], suggesting that multiple microbes could be present within expelled respiratory droplets. To characterize environmental shedding of H1N1pdm09 and Spn, ferrets were first infected with H1N1pdm09 and then infected with Spn 2 days later. Nasal washes were collected, and air sampling was performed for 3 days after co-infection.

Nasal wash titers from co-infected ferrets showed that all three animals shed H1N1pdm09 on days 3 and 4 post-H1N1pdm09 infection, but only two animals shed virus on day 5, while all

animals shed Spn throughout the time course (Figure 11A). We next assessed whether infectious microbes were released from co-infected ferrets by air sampling with a condensation sampler (Figure 12). Aerosolized infectious H1N1pdm09 was detected from all ferrets on day 3, but from fewer animals on days 4 and 5 (Figure 11B). Despite measurable levels of Spn in nasal washes, only one animal had viable Spn collected from the condensation sampler (Figure 11B). This may be underrepresenting expelled bacteria in the air, as previous work has shown that not all viable bacteria form colonies after aerosolization[204]. Cyclone bioaerosol sampling, used to collect microbial genomic material, detected H1N1pdm09 in air samples from all co-infected ferrets for both the >4 μm and 1-4 μm fractions on all days (Figure 11C-D). The small <1 μm fraction had measurable H1N1pdm09 from one or two of three co-infected ferrets on any day (Figure 11E). Spn was only detectable in the >4 μm fraction in two animals (Figure 11C), which is unsurprising given that *S. pneumoniae* ranges from 5-10x greater in diameter than influenza and is, therefore, less likely to be found in smaller aerosols. This result may also underrepresent the amount of aerosolized Spn, since sample processing was not optimized for encapsulated bacterial DNA. Our results are the first to detect infectious H1N1pdm09 and viable Spn in expelled aerosols from co-infected animals.

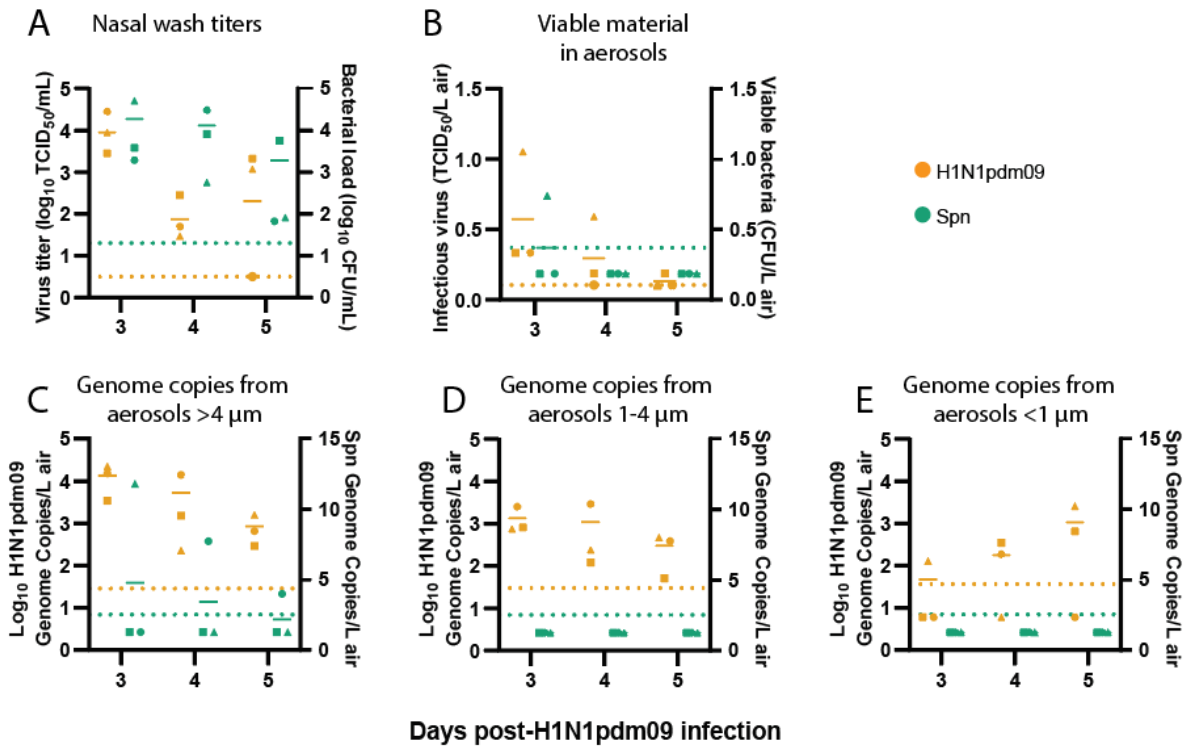

Figure 11. Co-infected ferrets shed H1N1pdm09 and Spn. Ferrets were infected with 10^6 $TCID_{50}$ of H1N1pdm09 and subsequently infected 2 days later with 10^7 CFU *S. pneumoniae* D39. (**A**) Nasal wash loads of H1N1pdm09 and Spn are shown for the days following initial H1N1pdm09 infection. (**B**) Condensation sampling with a Liquid Spot Sampler was used to collect infectious virus and bacteria shed by co-infected animals. Viral and bacterial loads were measured by $TCID_{50}$ and CFU assays, respectively. (**C-E**) Cyclone based air samplers were used to fractionate and collect microbial genomic material shed from co-infected ferrets in (**C**) >4 µm droplets, (**D**) 1-4 µm droplets, and (**E**) <1 µm droplets. Quantitative PCR was used to measure genome copies for each microbe. For all graphs, orange symbols represent H1N1pdm09 (N=3) and green symbols represent Spn (N=3), with each animal indicated by a unique shape and the mean indicated by short, solid lines. Dotted lines denote the limit of detection for H1N1pdm09 (orange) and Spn (green). Samples without infectious virus were placed at the LOD, and viable bacteria samples below the LOD were placed at ½ LOD. Samples without detectable genome copies were placed at ½ LOD (see materials and methods).

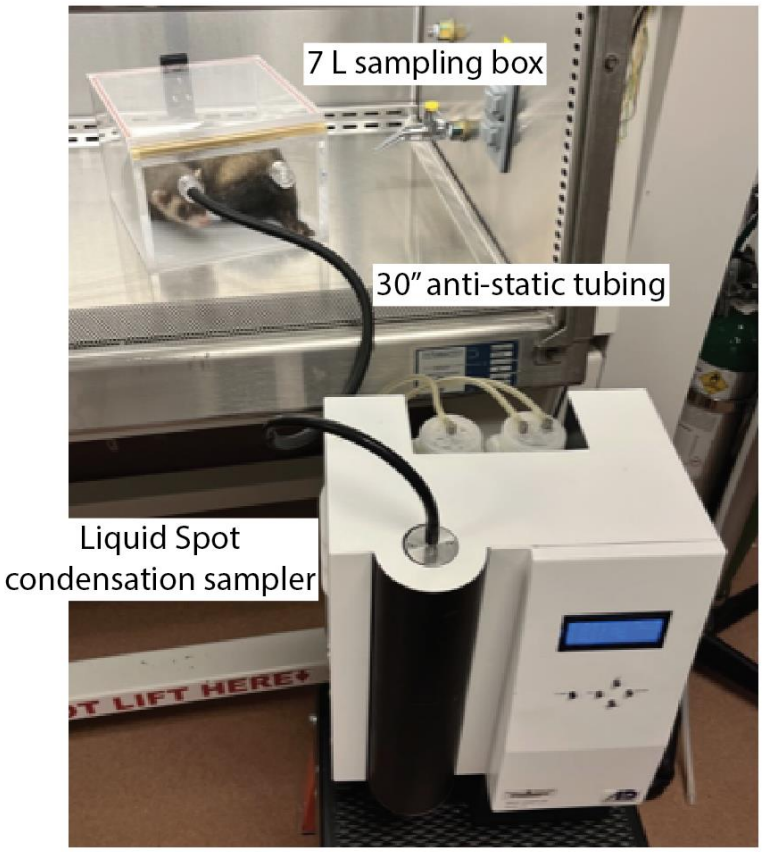

Figure 12. Condensation air sampling. The Liquid Spot condensation sampler was used to collect infectious material from co-infected animals. Co-infected animals were placed in a sampling box for 15 minutes while sampling was performed. Anti-static tubing connected the sampling box to the inlet of the sampler.

3.3.2 Environmental stability of H1N1pdm09 is not impacted by the presence of Spn.

Given the observation that H1N1pdm09 and Spn are shed from co-infected ferrets, we questioned whether these microbes might influence each other's environmental stability in respiratory droplets. Spn has been shown to potentially alter influenza A transmission[82,107], suggesting that Spn might decrease H1N1pdm09 environmental stability. H1N1pdm09, on the other hand, has been shown to increase transmission of Spn[82,104,107], which might indicate enhanced Spn stability with H1N1pdm09. To test this, we measured microbial persistence in droplets containing H1N1pdm09, Spn, or a 1:1 ratio of both pathogens in the presence of airway surface liquid (ASL) collected from four different human bronchial epithelial (HBE) cell donors (Figure 13). ASL is an important component of the respiratory tract and has been shown to increase stability of influenza viruses in the environment[146]. After aging 1 µL droplets of each solution in a humidified chamber for 2 hours, infectious H1N1pdm09 or Spn was measured and compared to bulk solution controls (Figure 13A-B). Experiments were performed at 43% relative humidity (Figure 13E), as viruses and Gram-positive bacteria are more susceptible to decay at intermediate relative humidity[162]. After 2 hours, there was no significant difference ($p= 0.721$) in H1N1pdm09 stability with or without Spn (average decay of 1.19 $\log_{10}$ $TCID_{50}$/mL versus 1.34 $\log_{10}$ $TCID_{50}$/mL, respectively) (Figure 13C). In contrast, there was a trend of increased stability for Spn in the presence of H1N1pdm09. Improved Spn stability was clearly observed in ASL from one patient culture (284), as Spn alone decayed an average of 3.71 $\log_{10}$ CFU/mL and H1N1pdm09/Spn decayed an average of 2.81 $\log_{10}$ CFU/mL ($p=0.078$, Figure 13D, Table 6). More modest stabilization for Spn was observed in one other culture (223) and no difference was observed in ASL from two patients (259 and 305) (Table 6). Together, these results suggest that H1N1pdm09 infectivity is not impacted by Spn at the environmental conditions tested. There may

be a modest impact of Spn stability in the presence of H1N1pdm09, although this may be more sensitive to variations in the ASL (or mucus composition) per individual. Further research should explore the impact of mucus and lung disease states on the relationship between influenza viruses and *S. pneumoniae*.

Co-infection with pathogens can impact the transmissibility to subsequent hosts. Concurrent infections of influenza virus and *S. pneumoniae* result in increased morbidity and a greater risk of bacterial transmission[82,104]. The work here shows that co-infected animals expel both influenza virus and *S. pneumoniae* into air and can be collected using a condensation air-sampler or cyclone bioaerosol sampler. In this study we employed two distinct air sampling methods: a cyclone air sampler (the NIOSH BC251) and a condensation air sampler (Aerosol Devices Liquid Spot). The limitations of these samplers include only a short sampling period from 15 minutes to 1 hour, which captures only a snapshot of what is in the air, and a lack of detection does not mean that these pathogens are not expelled into the air. In addition to the sampling time, the amount of virus detected in the air will be limited by the flow rate of the specific sampling strategy, the amount of virus expelled by an infected ferret, and the distance of the infected source to the sampling device. These factors contribute to the observed heterogeneity in microbial detection observed in our study and necessitate the need for thoughtful use of specific air sampling devices or incorporation of multiple air sampling devices at varying flow rate and times.

No impact was observed for influenza virus in the presence of *S. pneumoniae*, but a trend towards increased *S. pneumoniae* stability in the presence of influenza virus may help explain augmented *S. pneumoniae* transmission in addition to the increased bacterial shedding observed during co-infection[82,104]. Investigation of microbial stability using polymicrobial populations is not widely performed and could help elucidate the complexity of pathogen transmission seen in the

human population. In addition, identifying host specific factors underlying microbial stability in the environment could increase our understanding of individual transmission risks and strategies mitigating the spread of pathogens in the population. At this point, the association between pathogen detection in air samples, transmission frequency, and virulence remains to be investigated. In the long term, it may be possible to perform air-sampling patients with identified co-infection to characterize microbes present in respiratory expulsions, and these may provide insight into complex transmission events and improve infection prevention measures.

Table 6 Average lo_{10} decay for H1N1pdm09 or Spn in droplets

		Log_{10} Decay H1N1pdm09 ± SEM		Log_{10} Decay Spn ± SEM	
ASL Donor	HBE Donor Condition	H1N1pdm09	H1N1pdm09/Spn	Spn	H1N1pdm09/Spn
223	COPD	2.333 ± 0.068*	1.667 ± 0.068*	3.187 ± 0.067*	2.565 ± 0.002*
259	COPD	1.083 ± 0.136	1.125 ± 0.118	3.071 ± 0.101	2.577 ± 0.033
284	IPF	0.958 ± 0.180	1.292 ± 0.180	4.544 ± 0.248*	2.848 ± 0.148*
305	COPD	1.00 ± 0.118	0.708 ± 0.272	4.034 ± 0.167	3.256 ± 0

An asterisk indicates FDR p-value <0.05 when comparing droplets of individual microbes to droplets with both microbes using Welch's unpaired t-tests with Benjamini-Hochberg correction for multiple comparisons.

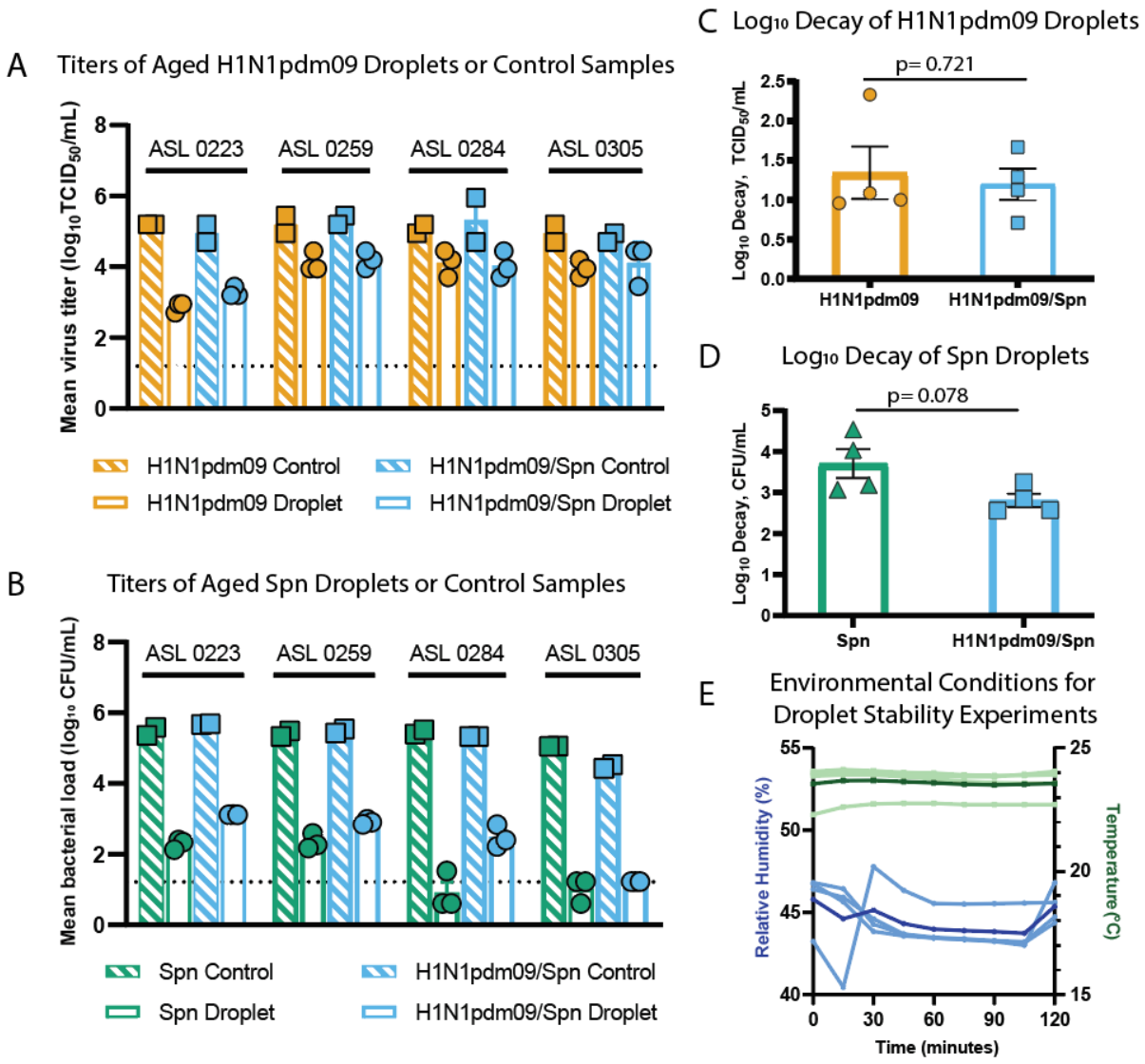

Figure 13. Stability of S. pneumoniae and influenza viruses in droplets. (**A-D**) Viral and bacterial loads of H1N1pdm09 and Spn were assessed after exposure of 10x1 µL droplets to 43% relative humidity (RH) at room temperature for 2 hours. Microbes were suspended in ASL from four different HBE cell donors as indicated in **A** and **B**. Control titers were determined using 10 µL of bulk solutions in closed tubes at room temperature. (**A**) The stability of H1N1pdm09 in droplets containing H1N1pdm09 or H1N1pdm09/Spn measured by $TCID_{50}$ assay, and (**C**) log_{10} decay for each individual ASL culture were determined. (**B**) The stability of Spn in droplets containing Spn or H1N1pdm09/Spn measured by CFU assay, and (**D**) log_{10} decay for each individual ASL culture were determined. Differences were assessed using Welch's unpaired t-test. (**E**) The RH and temperature were recorded every 15 minutes during stability experiments. Temperature (light green) and RH (light blue) for each ASL replicate are shown. The

average temperature (dark green) and RH (dark blue) for all experiments are also included. Bacterial samples with no detection were placed at ½ the LOD.

3.4 Materials and Methods

3.4.1 Virus and Bacteria

A/California/07/2009 (H1N1pdm09) was grown in minimum essential media in Madin-Darby Canine Kidney (MDCK) cells at 37°C for 48 hours and collected by centrifuging supernatant to remove cell debris. Quantification of virus was performed using the 50% tissue culture infectious dose assay ($TCID_{50}$) of 10-fold serial dilution on MDCK cells in 96-well and/or 24-well plates with subsequent assessment for cytopathic effects 4 days after plating. Samples with no detectable virus were placed at 1.2 $\log_{10}(TCID_{50}/mL)$ if titered on 96-well plates or 0.5 $\log_{10}(TCID_{50}/mL)$ if titered on 24-well plates, in accordance with the Spearman Karber method for $TCID_{50}$ determination[197].

S. pneumoniae D39 (Spn) was grown in Columbia broth at 37°C. Quantification of bacterial burden was performed by plating 10-fold serial dilutions on blood agar plates and counting colony-forming units after incubation at 37°C overnight. Samples with no detectable bacteria were placed at ½ the LOD to differentiate between samples at the LOD and those with no detection.

3.4.2 Animals

Experiments involving ferrets were performed at the University of Pittsburgh under BSL2 safety conditions (IACUC protocol 19075697). Four to six-month male ferrets were confirmed to be seronegative for influenza infection prior to purchase. Animals were intranasally infected with 10^6 $TCID_{50}$ of H1N1pdm09 in 500 µL total volume and 10^7 CFU of Spn in 500 µL. Ferrets were

sedated using isoflurane prior to nasal wash collection, performed by collecting the flow-through of PBS passed through the nostrils.

3.4.3 Air Sampling

Infectious virus and bacteria were collected using the Liquid Spot Sampler (Aerosol Devices Inc, Series 110), which uses condensation to collect aerosols into a collection vial. Air was collected from infected animals in a 7 liter chamber connected to the Spot sampler via anti-static tubing for 15 minutes each day at a rate of 1.4L/minute (Figure 12). Sampling was performed on days 3, 4, and 5 post-H1N1pdm09 infection (days 1, 2, and 3 post-Spn infection) and prior to nasal wash collection. Condensed aerosols were collected in 700µL 0.5% BSA in PBS. Samples were immediately plated to quantify expelled bacteria and the remaining sample was used for virus titration as described above.

Aerosol sampling of H1N1pdm09/Spn-infected ferrets was performed using cyclone-based air samplers (BC251 developed by NIOSH) on days 3, 4, and 5 post-H1N1pdm09 infection to collect microbial genomic material. Samplers, calibrated to collect 3.5L of air per minute, were placed downwind of infected animals in cages with directional airflow and were run for 1 hour. Samplers fractionated aerosols into three sizes: aerosols >4µm, 1-4µm, and <1µm diameter. After aerosol collection, samplers were washed with isopropanol and allowed to air-dry to avoid contamination.

RNA was isolated using 500µL MagMAX Lysis/Binding Solution Concentrate in each collection tube with thorough vortexing. QIAamp viral RNA mini kit was used to isolate DNA and RNA from lysis solution. Viral and bacterial genome copies were quantified using RT-qPCR with primers against influenza M gene (Forward 5’-AGATGAGTCTTCTAACCGAGGTCG-3’ ;

Reverse 5’-GCAAAGACACTTTCCAGTCTCTG-3’ ; Probe 5’-[FAM]TCAGGCCCCCTCAAAGCCGA[3BHQ1] -3’) or *S. pneumoniae* lytA gene (Forward 5’-ACGCAATCTAGCAGATGAAGCA-3’ ; Reverse 5’-TCGTGCGTTTTAATTCCAGCT-3’ ; Probe 5’-[HEX]GCCGAAAACGCTTGATACAGGGAG[BHQ1]-3’). *In vitro* transcribed RNA was used to make a standard curve for influenza virus, and *S. pneumoniae* genomic DNA was serially diluted to generate a standard curve for Spn. Limits of detection were determined by a Ct = 40 or a positive day 0 sample. Samples without amplification in both wells or with Ct greater than the day 0 sample were considered as below the LOD and therefore placed at ½ LOD. qPCR was run using iTaq Universal Probes One-Step kit for influenza (Bio-Rad) and SsoAdvanced Universal Probes Supermix for *S. pneumoniae.* Influenza was amplified for 10 minutes at 50°C, 2 minutes at 95°C, then 40 cycles of 10 seconds at 95°C and 20 seconds at 60°C. *S. pneumoniae* was amplified for 10 minutes at 95°C, and 40 cycles of 15 seconds at 95°C and 1 minute at 60°C.

3.4.4 Stability Experiments

Inside a biosafety cabinet, a saturated salt solution of K_2CO_3 was used to condition a glass chamber to 43% relative humidity, and a HOBO UX-100-011 logger was used to record temperature and humidity conditions during each ASL replicate (Figure 13E). Experimental solutions were generated using $10^{7.15}$ CFU/mL Spn, $10^{7.15}$ $TCID_{50}$/mL H1N1pdm09, and a 1:5 dilution in PBS of airway surface liquid collected from human bronchial epithelial cells. Ten 1 µL droplets were incubated on polystyrene tissue culture plates in the conditioned chamber for two hours. Controls were 10 µL samples of each microbial solution in closed tubes that were incubated for 2 hours at ambient temperature during the chamber experiments. Log_{10} decay was calculated as previously described and represents the loss in virus or bacterial infectivity[145]. Log_{10} decay was

determined for each droplet replicate by subtracting the titer of the droplets from the average of the controls for the corresponding ASL. Experiments were performed using technical triplicates for droplets and technical duplicates for controls.

Human lung tissue collected using an approved protocol was used to differentiate human bronchial epithelial cells as previously described[167]. Airway surface liquid was collected by washing differentiated cells with 150 µL PBS and collecting the wash[146]. All HBE donors were diagnosed with chronic obstructive pulmonary disease (COPD), except for HBE 0284, which came from a patient diagnosed with idiopathic pulmonary fibrosis.

3.4.5 Data Availability

The data that supports the findings shown here will be made openly available in FigShare at https://doi.org/10.6084/m9.figshare.c.6469438 upon publication. Some of the stability experiments were previously made available on BioRxiv at https://doi.org/10.1101/2020.11.10.376442

3.4.6 Acknowledgements

We thank members of the Lakdawala and Hiller lab for providing constructive feedback of this manuscript and Dr. Rachel Duron for editorial comments. This work was supported in part with Federal funds from NIAID, NIH, and DHHS (75N93021C00015, SSL). Additional funding was provided by Flu Lab (SSL) and NIAID (R01 AI158484 for SSL and R01 AI139077 for NLH). JF was supported by the University of Pittsburgh Training Program in Antimicrobial Resistance

(T32AI138954). We would also like to acknowledge the Research Development Program from the Cystic Fibrosis Foundation to the University of Pittsburgh (MM and SF).

4.0 Environmental stability of enveloped viruses is impacted by the initial volume and evaporation kinetics

4.1 Abstract

Efficient spread of respiratory viruses requires the virus to maintain infectivity in the environment. Environmental stability of viruses can be influenced by many factors, including temperature and humidity. Our study measured the impact of initial droplet volume (50, 5, and 1 µL) and relative humidity (RH: 40%, 65%, and 85%) on the stability of influenza A virus, bacteriophage, Phi6, a common surrogate for enveloped viruses, and SARS-CoV-2 under a limited set of conditions. Our data suggest that the drying time required for the droplets to reach quasi-equilibrium (i.e. a plateau in mass) varied with RH and initial droplet volume. The macroscale physical characteristics of the droplets at quasi-equilibrium varied with RH but not with the initial droplet volume. Virus decay rates differed between the wet phase, while the droplets were still evaporating, and the dry phase. For Phi6, decay was faster in the wet phase than in the dry phase under most conditions. For H1N1pdm09, decay rates between the two phases were distinct and initial droplet volume had an effect on virus viability within 2 hours. Importantly, we observed differences in virus decay characteristics by droplet size and virus. In general, influenza virus and SARS-CoV-2 decayed similarly, whereas Phi6 decayed more rapidly under certain conditions. Overall, this study suggests that virus decay in media is related to the extent of droplet evaporation, which is controlled by RH. Importantly, accurate assessment of transmission risk requires the use of physiologically relevant droplet volumes and careful consideration of the use of surrogates.

4.2 Introduction

Respiratory viruses, such as influenza A virus and SARS-CoV-2, contribute to high morbidity and mortality. These viruses must remain infectious in the environment for transmission to the next host to succeed. Understanding how environmental, host, and virus factors impact the stability of expelled virus will lead to a better assessment of virus transmission risk and ways to reduce it.

Many factors can impact virus stability in the environment, including virion structure, temperature, relative humidity (RH), droplet composition, solute concentration, and fomite surface material[146,205–208]. However, the relationship between droplet volume and virus stability is not well understood, even though droplet volume plays an important role in virus transmission. Droplet volume impacts the distance traveled by respiratory expulsions[140]. Smaller droplets, or aerosols, can travel further from the infected host, while larger droplets settle to the ground more quickly due to their increased mass[140]. Droplet volume can also be a determinant of host infection site, as particles smaller than 10 μm in diameter are more likely to deposit deeper in the respiratory tract[209]. Given the importance of droplet volume to initiating infection, understanding how volume affects virus stability is critical to mitigating transmission of respiratory viruses such as influenza virus and coronaviruses.

Studies measuring virus stability in the environment typically use one of two methods to generate droplets: nebulizers to produce aerosols, or pipettes to create droplets with as much as 50 μL per droplet. While large droplets are commonly used to assess environmental virus stability, they do not mimic a physiological volume of a droplet created by an expulsion. The vast majority of expelled droplets from the respiratory tract are less than 0.5 μL in volume (approximately 1 mm in diameter for a sphere), in contrast a droplet of 50 μL (approximately 4.6 mm in diameter for a

sphere) is about 5 times larger and 100 times greater in volume[174]. Studies measuring the stability of SARS-CoV-2 on surfaces have examined the virus in 5[210], 10[211], 20[212], or 50 µL droplets[205,206,213], all larger than most expelled droplets. These initial studies into SARS-CoV-2 stability were used widely for policy decisions and to assert the importance of contaminated surfaces on transmission. However, little work has been done to understand whether virus decay in large droplets is representative of decay in smaller, more physiologically relevant, droplet volumes.

This study primarily used the 2009 pandemic influenza H1N1 virus (H1N1pdm09, A/CA/07/2009) and bacteriophage Phi6, a commonly used virus surrogate, to examine environmental stability of enveloped viruses in three different droplet volumes at three different RHs over time. Specifically, we measured the viability of each virus in 50, 5, and 1 µL droplets on surfaces over time at 40%, 65%, and 85% RH. We observed that virus within smaller droplets decays quickly regardless of RH, while virus decay occurs more slowly in larger droplets. We also explored droplet evaporation rates and found that virus decay is closely correlated with the extent of evaporation, which is likely a proxy for the solute concentration in the droplet. Additionally, limited experiments with SARS-CoV-2 showed that influenza virus decayed similarly to SARS-CoV-2 at an intermediate 55-60% RH in 50, 5, and 1 µL droplets. Overall, our results suggest that virus stability studies should use smaller, more physiologically relevant droplet volumes and should recognize the limitations of surrogate viruses.

4.3 Results

4.3.1 Relative humidity alters morphology of evaporating droplets and drying kinetics

We expect the physical and chemical characteristics of droplets to influence decay of viruses within each droplet. Some of these physical and chemical characteristics may be reflected in the morphology of droplets after they have dried[208]. Furthermore, fluid dynamics within droplets could lead to increased aggregation of virus, which can enhance virus stability[214,215]. We investigated whether droplet morphology and drying pattern at 24 hours differed between 1x50, 5x5, or 10x1 µL droplets (i.e., one droplet of volume 50 µL, five droplets of volume 5 µL, ten droplets of volume 1 µL). Droplets of media (DMEM) were placed on polystyrene plastic and incubated at 40%, 65%, or 85% RH for 24 hours (Figure 14, see Movies 1-3 at https://doi.org/10.6084/m9.figshare.21711119, https://doi.org/10.6084/m9.figshare.21711122 and https://doi.org/10.6084/m9.figshare.21711116). These RHs were selected to match values in other published work[206]. We reported RH instead of absolute humidity because the former is more directly related to virus inactivation[15]. Droplet morphology in droplets containing virus was the same as droplets of media alone (data not shown). The effect of RH on dried droplet morphology was independent of initial droplet volume (Figure 14). This suggests that observed differences in viral decay by droplet size would not be due to final physico-chemical differences. Our results show that the droplet drying pattern at 24 hours depends on RH, but not initial droplet volume.

Evaporation leads to the concentration of solutes, which can influence virus stability in droplets[201]. To investigate the drying kinetics, we recorded the mass of 1x50 µL, 5x5 µL, or 10x1 µL droplets of DMEM containing Phi6 for 24 hours at ambient temperature and three RHs: 40%, 65%, and 85% RH (as shown in Figure 14). The droplets at all RHs lost mass linearly over time

before reaching a plateau, referred to as a quasi-equilibrium (Figure 15, Table 7, and Table 8)[205]. We defined this state as quasi-equilibrium because it is likely that very slow evaporation continues over a much longer time scale until complete dryness occurs, or until a crust or shell forms that blocks further water loss. To simplify discussion, we refer to the time period before this as the "wet" phase and the period after this as the "dry" phase. The drying time required for the droplets to reach quasi-equilibrium ranged from 0.5 hours for 1 µL droplets at 40% RH to 11 hours for 50 µL droplets at 85% RH. These data indicate that droplets of different volumes undergo different drying kinetics. We have previously shown that the presence of a virus in a droplet has a negligible effect on its evaporation rate.[162] If the kinetics of drying affect virus stability, then it could differ by initial droplet volume.

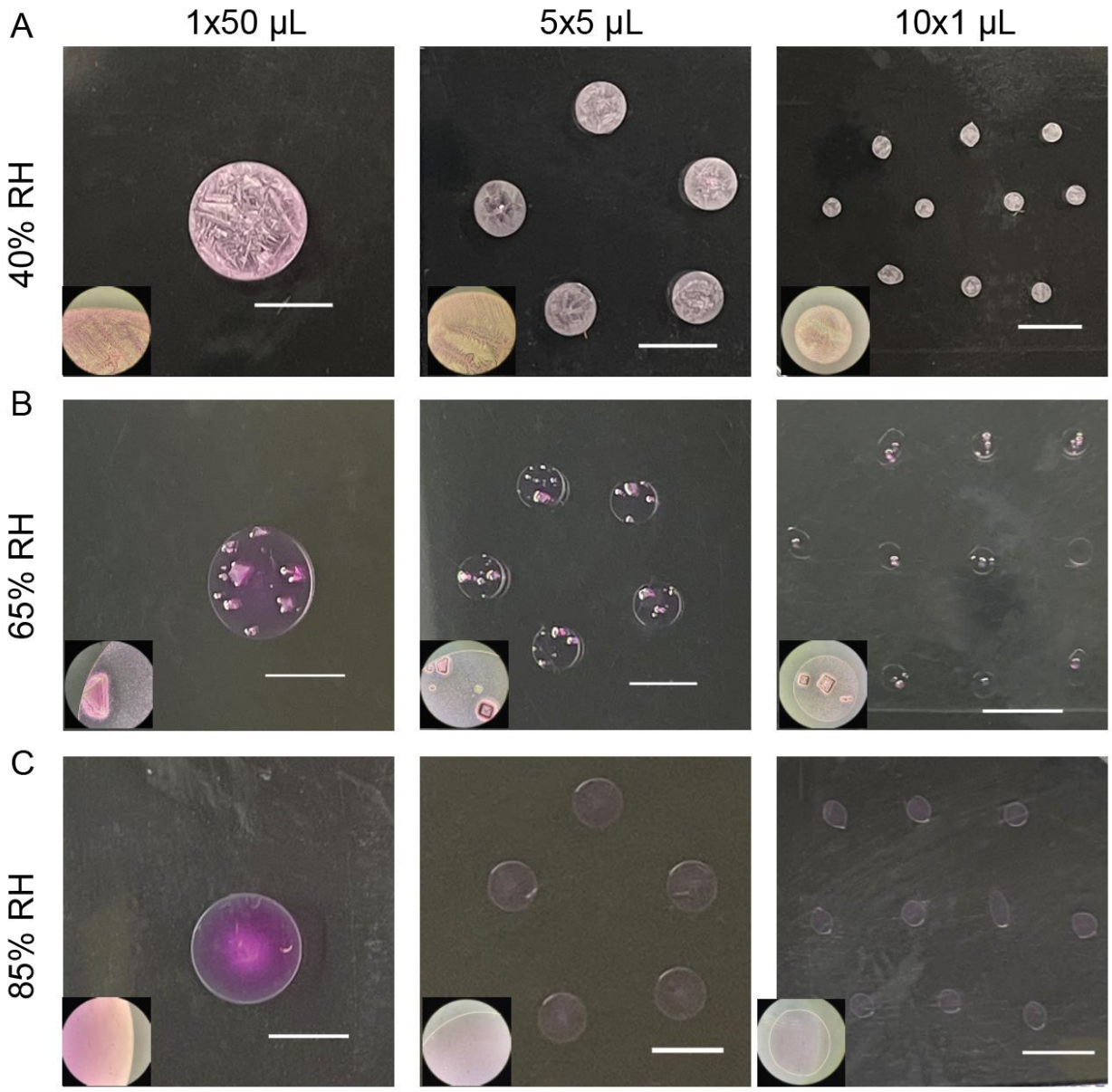

Figure 14. Macroscale physico-chemical characteristics of DMEM droplets vary with RH but not initial volume. Inset images taken with 10x objective. Scale bars indicate 5 mm. **A.** At 40% RH, droplets become concentrated at the border and develop interior feather-like crystals. **B.** At 65% RH, droplets develop distinct crystals within the interior. **C.** At 85% RH, droplets maintain moisture and do not crystallize.

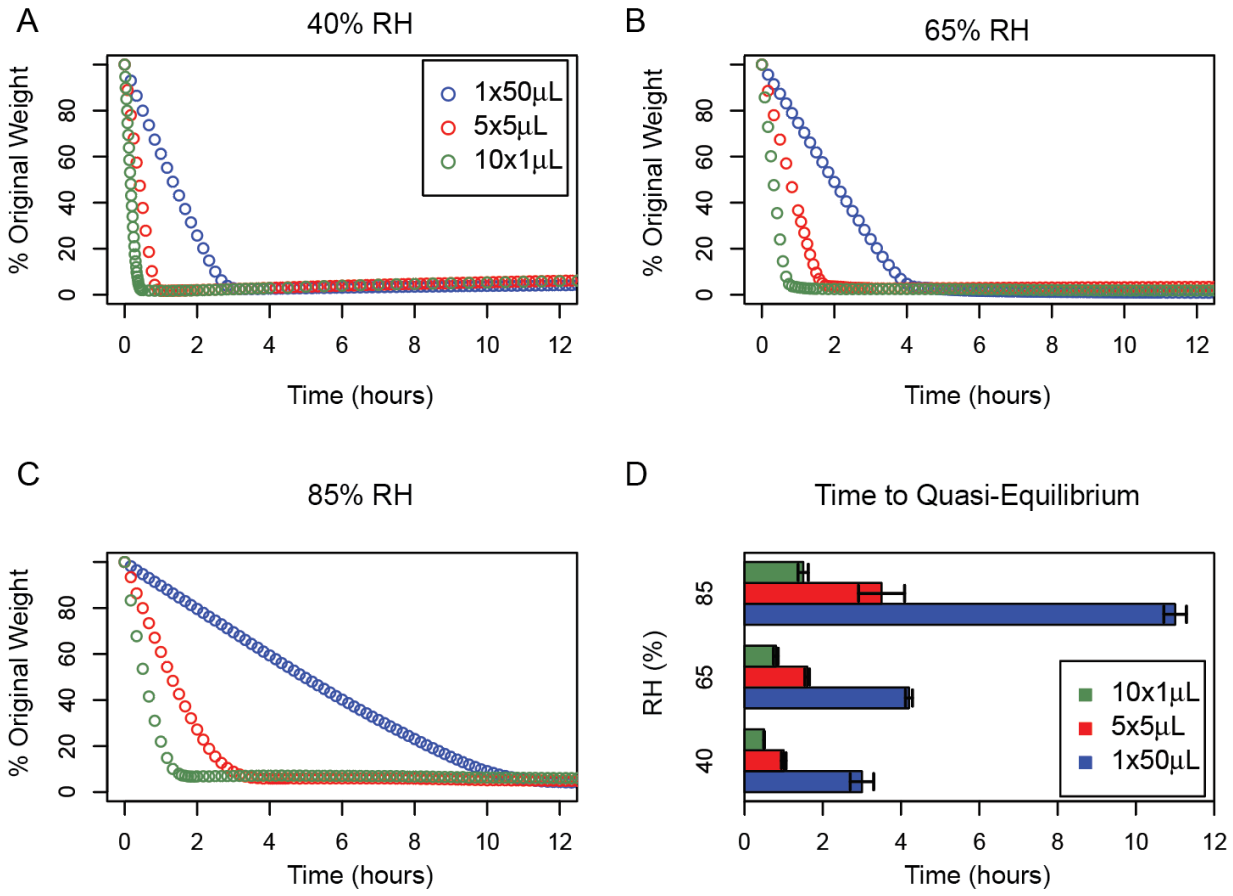

Figure 15. Initial droplet volume impacts drying kinetics. **A-C.** Mass normalized to starting mass for all droplet volumes at (**A**) 40%, (**B**), 65% (**C**), or 85% RH over time. **D**. Summary data showing the time (mean and standard deviation, n = 2) for droplets to reach quasi-equilibrium at each RH. Droplet mass was measured on a micro-balance in an environmental chamber and recorded every minute.

Table 7 The evaporation rates for 1x50 µL, 5x5 µL, or 10x1 µL droplets at 40%, 65%, or 85% RH were determined by fitting a line to the mass over time.

RH (%)	Initial Volume (µL)	Slope ± Std. Error (mg/hour)
40	50	17.9482 ± 0.164
	5	29.9237 ± 0.376
	1	30.1360 ± 0.438
65	50	12.3290 ± 0.102
	5	15.0284 ± 0.301
	1	18.6950 ± 0.601
85	50	5.0560 ± 0.009
	5	8.8678 ± 0.105
	1	10.7260 ± 0.417

Table 8 1x50 µL, 5x5 µL, or 10x1 µL droplets were weighed over time. The time of quasi-equilibrium was determined and the mass at quasi-equilibrium was measured.

RH (%)	Initial Volume (µL)	Mean Time at Quasi-Equilibrium ± Std. Error (hours)	Mean Mass at Quasi-Equilibrium. ± Std. Error	
			mg	% Original
40	50	3.0 ± 0.30	1.392 ± 0.38	2.805 ± 0.56
	5	1.0 ± 0.06	0.425 ± 0.15	1.731± 0.74
	1	0.5 ± 0.01	0.202 ± 0.07	1.994 ± 0.82
65	50	4.2 ± 0.09	1.787 ± 0.05	3.559 ± 0.33
	5	1.6 ± 0.06	1.037 ± 0.05	4.044 ± 0.32
	1	0.8 ± 0.06	0.487 ± 0.06	3.699 ± 0.32
85	50	11 ± 0.30	2.813 ± 0.05	5.565 ± 0.09
	5	3.5 ± 0.59	1.492 ± 0.32	6.273 ± 1.29
	1	1.5 ± 0.13	0.978 ± 0.03	7.983 ± 0.415

4.3.2 Virus decay is more sensitive to relative humidity in large droplets

To directly examine how RH and droplet volume impact virus stability in the environment, we applied virus in droplets of different volumes to a polystyrene surface and quantified recovery of infectious virus over time[216]. We compared decay of H1N1pdm09 and Phi6 at each RH in 1x50

µL, 5x5 µL, or 10x1 µL droplets at 40%, 65%, and 85% RH (Figure 16, Figure 17, and Table 9). In 50 µL droplets, Phi6 decayed fastest at 40% RH and slowest at 85% RH (Figure 16A). The impact of RH on the decay of H1N1pdm09 in 50 µL droplets over the first 8 hours was similar as for Phi6 but less pronounced, with the greatest decay occurring at 40% RH (Figure 16B). Decay of H1N1pdm09 in the 1x50 µL droplet was first detected at 4 hours at 40% RH, 8 hours at 65% RH, and 24 hours at 85% RH, indicating that early virus decay was inversely related to RH (i.e., more decay at lower RH) in large 50 µL droplets (Table 10). Decay of Phi6 in 5 µL droplets differed by RH only at 1 hour, when decay at 40% was greater than at 85%. In 1 µL droplets, decay differed between 40 minutes and 4 hours by RH but was not significantly different at 8 hours or afterward (Figure 16A). H1N1pdm09 in 1 µL and 5 µL droplets decayed at a similar rate within each droplet volume regardless of RH (Figure 16B). Phi6 was more unstable after drying in the intermediate RHs whereas H1N1pdm09 tended to be more stable. This accounts for differences in decay at the smaller droplet sizes. These findings show that the impact of RH on virus decay in droplets depends on the virus and the initial volume of the droplets.

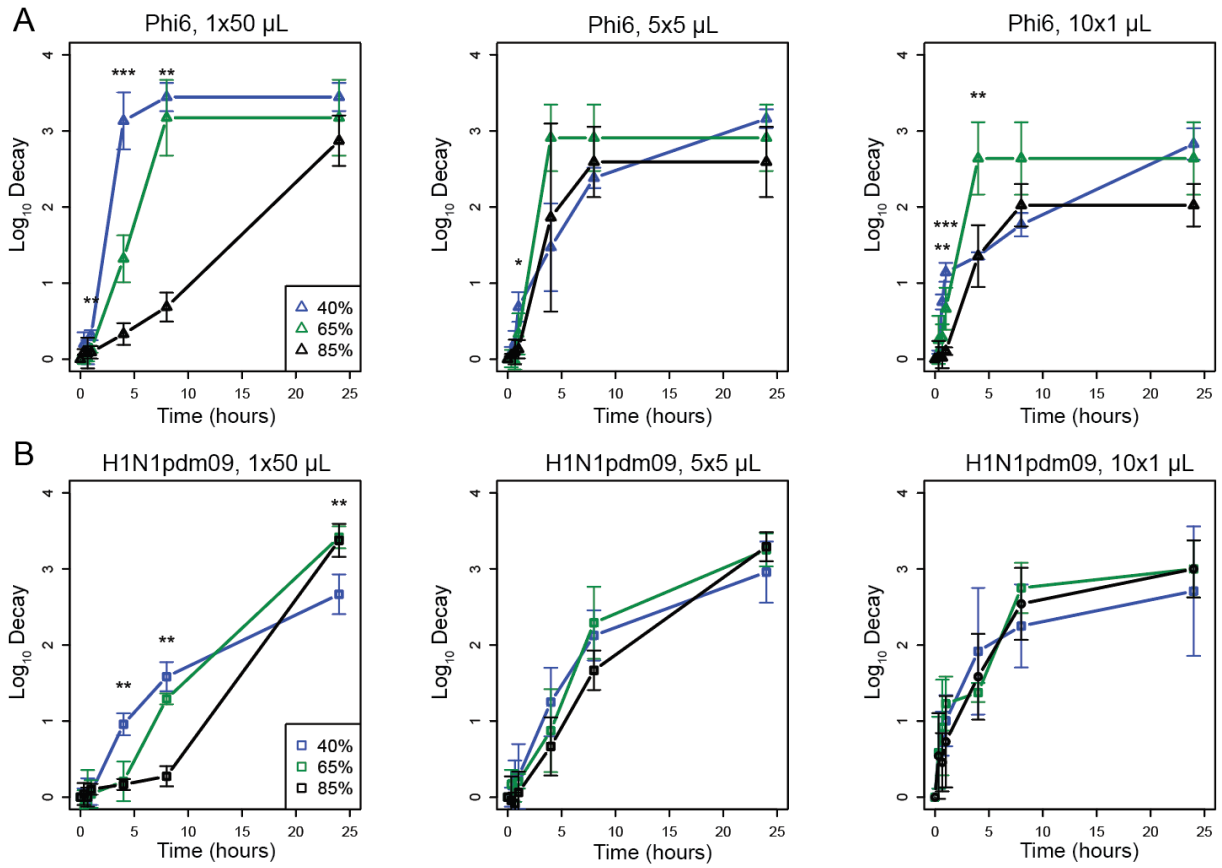

Figure 16. Virus decay varies more with relative humidity in large droplets than in small droplets. A. Titers of Phi6 in 1x50 µL, 5x5 µL, or 10x1 µL droplets compared at 40%, 65%, and 85% RH in terms of $\log_{10}$ decay. **B.** Titers of H1N1pdm09 in 1x50 µL, 5x5 µL, or 10x1 µL droplets compared at 40%, 65%, and 85% RH in terms of $\log_{10}$ decay. Error bars show standard deviation. Asterisks indicate significant differences between two or three RHs. For all graphs N=3 except at 1 hour where H1N1pdm09 N=6. One-way ANOVA tests were conducted between the RHs at each time point. A Tukey HSD test was conducted to determine between which RHs the significant differences ($p < 0.05$) occurred. Statistical details can be found in Table 9.

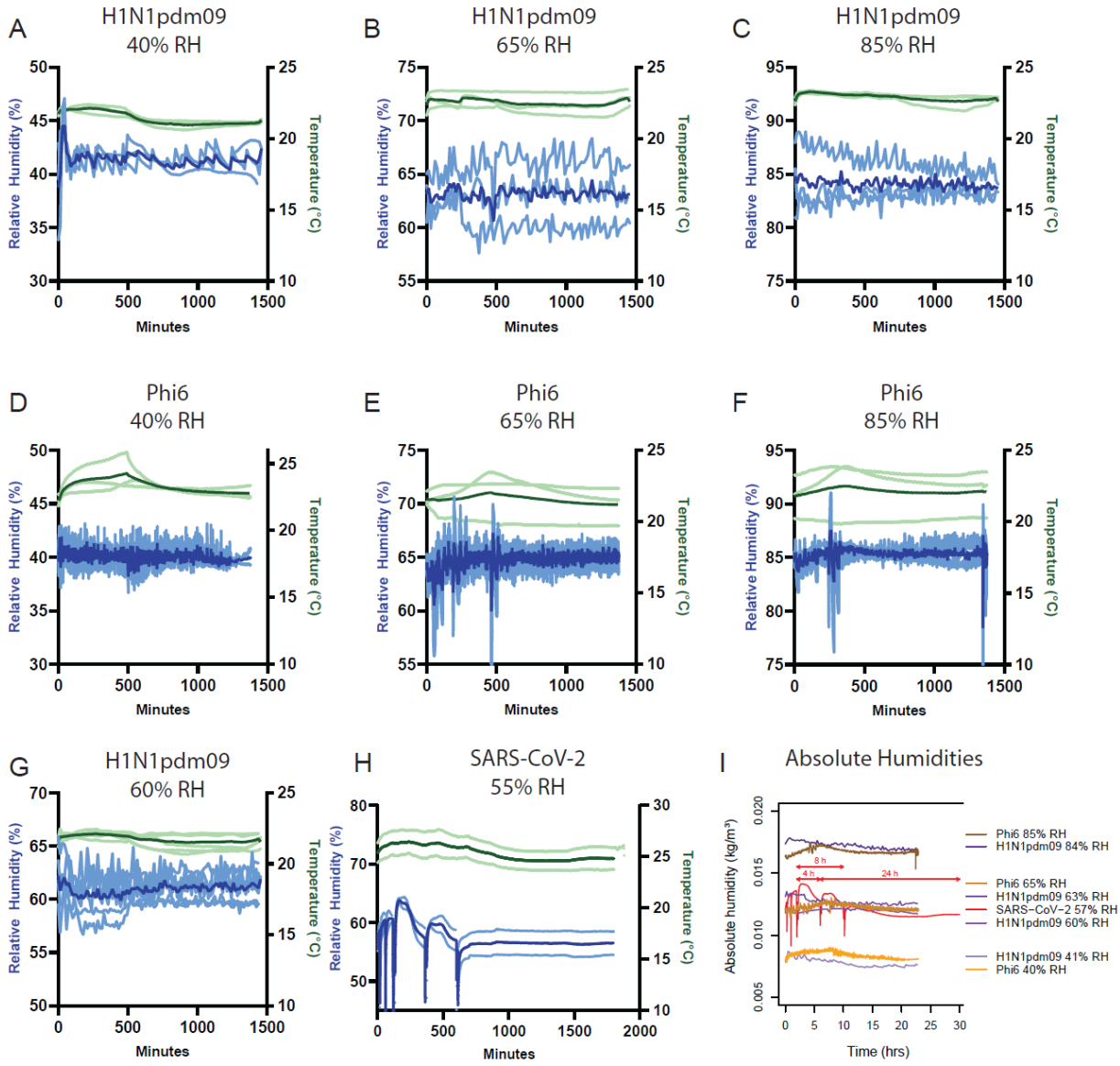

Figure 17. Environmental conditions of H1N1pdm09 and Phi6 droplets were within an average of 5% of the target RH and maintained temperatures between 20 and 25°C. The RH and temperature of the environmental chamber were recorded every 15 minutes during H1N1pdm09 stability experiments at (**A**) 40%, (**B**) 65%, (**C**) and 85% RH. The RH and temperature of the environmental chamber were recorded every minute during Phi6 stability experiments at (**D**) 40%, (**E**) 65%, (**F**) and 85% RH. The RH and temperature data for comparing decay of (**G**) H1N1pdm09 at 60% with (**H**) SARS-CoV-2 at 55% were recorded every 15 minutes or 1 minute, respectively. Light green shows the temperature at each replicate, and dark green indicates the average temperature for the 3 independent replicates. Light blue shows the RH for each replicate, and dark blue indicates the average RH for the 3

independent replicates. (**I**) Absolute humidities were calculated for all experiments. The legends show the corresponding average RH for each condition instead of targeted RH. Conditions for data previously published in van Doremalen et al are unknown[206].

Table 9 Log_{10} decay for each virus was compared between RH for each droplet volume and p-values were determined.

Virus	Initial Volume (µL)	Time (hr)	RH 1 (%)	RH 2 (%)	p-value
Phi6	50	0.33	40	65	0.074
		0.33	40	85	0.42
		0.33	65	85	0.40
		0.67	40	65	0.79
		0.67	40	85	0.99
		0.67	65	85	0.84
		1	40	65	0.033*
		1	40	85	0.014*
		1	65	85	0.75
		4	40	65	<0.001*
		4	40	85	<0.001*
		4	65	85	0.014*
		8	40	65	0.59
		8	40	85	<0.001*
		8	65	85	<0.001*
		24	40	65	0.65
		24	40	85	0.21
		24	65	85	0.59
Phi6	5	0.33	40	65	0.51
		0.33	40	85	0.88
		0.33	65	85	0.78
		0.67	40	65	0.18
		0.67	40	85	0.59
		0.67	65	85	0.60
		1	40	65	0.17
		1	40	85	0.037*
		1	65	85	0.49
		4	40	65	0.16
		4	40	85	0.84
		4	65	85	0.33
		8	40	65	0.27
		8	40	85	0.78
		8	65	85	0.58
		24	40	65	0.70
		24	40	85	0.23
		24	65	85	0.58
Phi6	1	0.33	40	65	0.66
		0.33	40	85	0.94
		0.33	65	85	0.47
		0.67	40	65	0.015*
		0.67	40	85	0.002*
		0.67	65	85	0.13
		1	40	65	0.036*
		1	40	85	<0.001*
		1	65	85	0.020*
		4	40	65	0.012*
		4	40	85	1.0
		4	65	85	0.012*
		8	40	65	0.050
		8	40	85	0.72
		8	65	85	0.14
		24	40	65	0.78
		24	40	85	0.062
		24	65	85	0.15

Table 9 Log_{10} decay for each virus was compared between RH for each droplet volume and p-values were determined. (continued)

Virus	Initial Volume (µL)	Time (hr)	RH 1 (%)	RH 2 (%)	p-value
H1N1pdm09	50	0.33	40	65	0.44
		0.33	40	85	1
		0.33	65	85	0.44
		0.67	40	65	0.92
		0.67	40	85	0.98
		0.67	65	85	0.98
		1	40	65	0.98
		1	40	85	0.94
		1	65	85	0.86
		4	40	65	0.005*
		4	40	85	0.004*
		4	65	85	0.96
		8	40	65	0.096
		8	40	85	<0.001*
		8	65	85	<0.001*
		24	40	65	0.012*
		24	40	85	0.015*
		24	65	85	0.97
H1N1pdm09	5	0.33	40	65	0.65
		0.33	40	85	0.97
		0.33	65	85	0.53
		0.67	40	65	0.32
		0.67	40	85	0.065
		0.67	65	85	0.46
		1	40	65	0.96
		1	40	85	0.68
		1	65	85	0.82
		4	40	65	0.61
		4	40	85	0.34
		4	65	85	0.85
		8	40	65	0.85
		8	40	85	0.34
		8	65	85	0.17
		24	40	65	0.47
		24	40	85	0.38
		24	65	85	0.98
H1N1pdm09	1	0.33	40	65	1
		0.33	40	85	0.99
		0.33	65	85	0.99
		0.67	40	65	0.97
		0.67	40	85	0.60
		0.67	65	85	0.48
		1	40	65	0.82
		1	40	85	0.74
		1	65	85	0.41
		4	40	65	0.53
		4	40	85	0.77
		4	65	85	0.90
		8	40	65	0.43
		8	40	85	0.73
		8	65	85	0.85
		24	40	65	0.82
		24	40	85	0.82
		24	65	85	1
A one-way ANOVA and Tukey HSD test was used to determine significance.					

Table 10 Log_{10} decay for each virus was compared to 0 decay at each time point in 1x50 µL droplets.

Virus	RH (%)	Time	p-value
Phi6	40	0	NA
		0.33	0.15
		0.67	0.42
		1	0.014*
		4	<0.01*
		8	<0.001*
		24	<0.001*
	65	0	NA
		0.33	0.78
		0.67	0.66
		1	0.037*
		4	0.018*
		8	<0.01*
		24	<0.01*
	85	0	NA
		0.33	0.040*
		0.67	0.56
		1	0.19
		4	0.057
		8	0.025*
		24	<0.01*
H1N1pdm09	40	0	NA
		0.33	0.42
		0.67	0.83
		1	0.58
		4	<0.01*
		8	<0.01*
		24	<0.01*
	65	0	NA
		0.33	0.42
		0.67	0.84
		1	0.73
		4	0.30
		8	<0.01*
		24	<0.001*
	85	0	NA
		0.33	0.67
		0.67	1
		1	0.13
		4	0.057
		8	0.069
		24	<0.01*
A t-test was used to determine statistical significance.			

4.3.3 Virus decay rates differ during the wet and dry phases and depend on droplet volume and virus

The pattern of decay for Phi6 and H1N1pdm09 appeared distinct for different droplet volumes. This led us to investigate whether drying time impacts virus decay and whether different

viruses behave similarly across different droplet volumes. Virus decay often follows first-order kinetics[217]. Following a previously developed mechanistic model of virus inactivation in droplets, we fit an exponential decay curve model (see Materials and Methods for details) to virus titers in droplets during the wet phase (prior to quasi-equilibrium) and a separate curve during the dry phase to create a biphasic model (Figure 18, Figure 19, and Table 11)[4]. The model accounts for changing solute concentrations in the droplets as they evaporate during the wet phase[205]. Because of this, the model fit for the initial decay rate shown in the figures does not match the data points. Rather, the model indicates what the decay rate would be if the droplets remained the same size and did not evaporate throughout the wet phase.

Virus decay appeared to be biphasic. In most cases for Phi6, decay was faster in the wet phase than in the dry phase. For H1N1pdm09, differences in decay rates between the two phases were not consistent. Figure 18 shows viability as a function of time for two conditions: 5x5 µL droplets at 40% RH (Figure 18A-B) and 10x1 µL droplets at 65% RH (Figure 18C-D). The insets show the detail during the first 1.5 hours (Figure 18B, D), when the droplets transitioned from wet to dry. Similar patterns are evident in most of the nine combinations of initial volume and RH for both viruses (Figure 19 and Table 11).

Among the 18 total combinations of RH, initial droplet volume, and virus, there were 12 combinations for which the decay rate constant could be compared between the wet phase and dry phase. Decay rates were greater in magnitude during the wet phase than the dry phase in 7 of 12 cases and significantly greater in 3 of 12 of these cases (Table 11): Phi6 in 5x5 µL droplets at 40% RH (Figure 18A), H1N1pdm09 in 5x5 µL droplets at 40% RH (Figure 18A), and Phi6 in 5x5 µL droplets at 65% RH (Figure 19B). Because there were only two time points during the wet phase for the 10x1 µL droplets at 40% RH and only one or two time points during the dry phase for 1x50

µL droplets at 65% and 85% RH, it was not possible to compare decay rates for these conditions (Table 11). Multivariate analysis, described in greater detail in the materials and methods, revealed a significant interaction between initial droplet volume and RH during wet phase decay for H1N1pdm09 but not Phi6.

The decay rate constant was significantly higher for Phi6 than H1N1pdm09 in two cases during the wet phase and was significantly different in two cases—higher for H1N1pdm09 in both cases—during the dry phase (Figure 19, Table 11). Significant differences were not observed in the 1 µL droplets. These results indicate that different enveloped RNA viruses may decay differently.

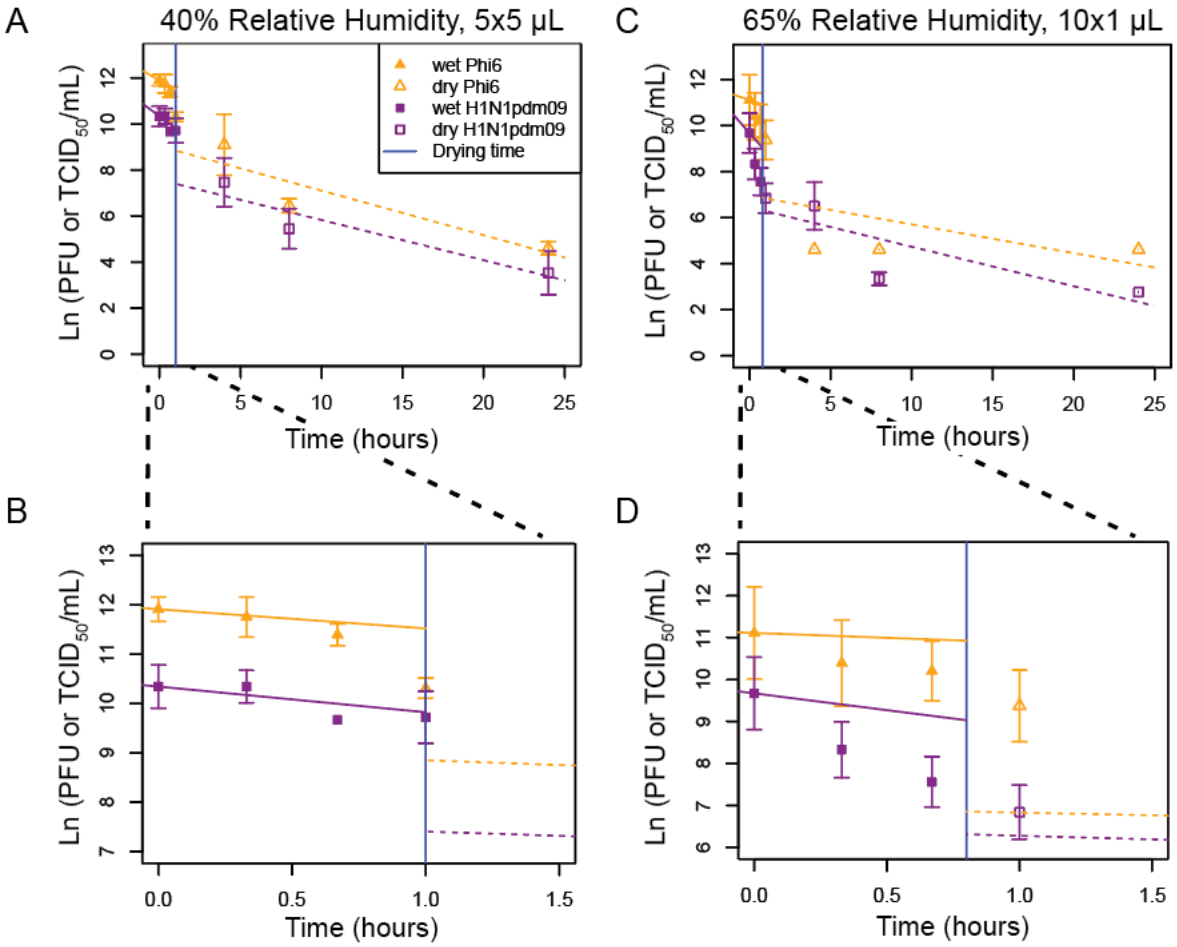

Figure 18. Mechanistic first-order decay modeling of viral decay in 5x5 µL droplets at 40% RH and 10x1 µL droplets at 65% RH shows that viral decay during the wet phase is greater than decay during the dry phase. **A-D**. First order exponential decay models, accounting for increasing solute concentrations over time during the wet phase, were fit to ln(PFU or $TCID_{50}$/mL) over time for (**A-B**) 5x5 µL at 40% RH or (**C-D**) 10x1 µL droplets at 65% RH. B,D A magnification of A,C from 0 to 1.5 hours is shown. For the wet phase, the fitted line represents the initial decay rate, what it would be if the droplets remained the same size and did not evaporate. Actual RH were ±2% from targeted RH, see Figure 17. For all graphs N=3 except at 1 hour where H1N1pdm09 N=6. The vertical blue line indicates the time of transition from the wet phase to the dry phase. A t-test was used to compare the slopes between the evaporation and dry phases for each virus at each droplet volume and between the phases for each virus at each droplet volume ($p < 0.05$). Statistical details can be found in Table 11 and Table 12.

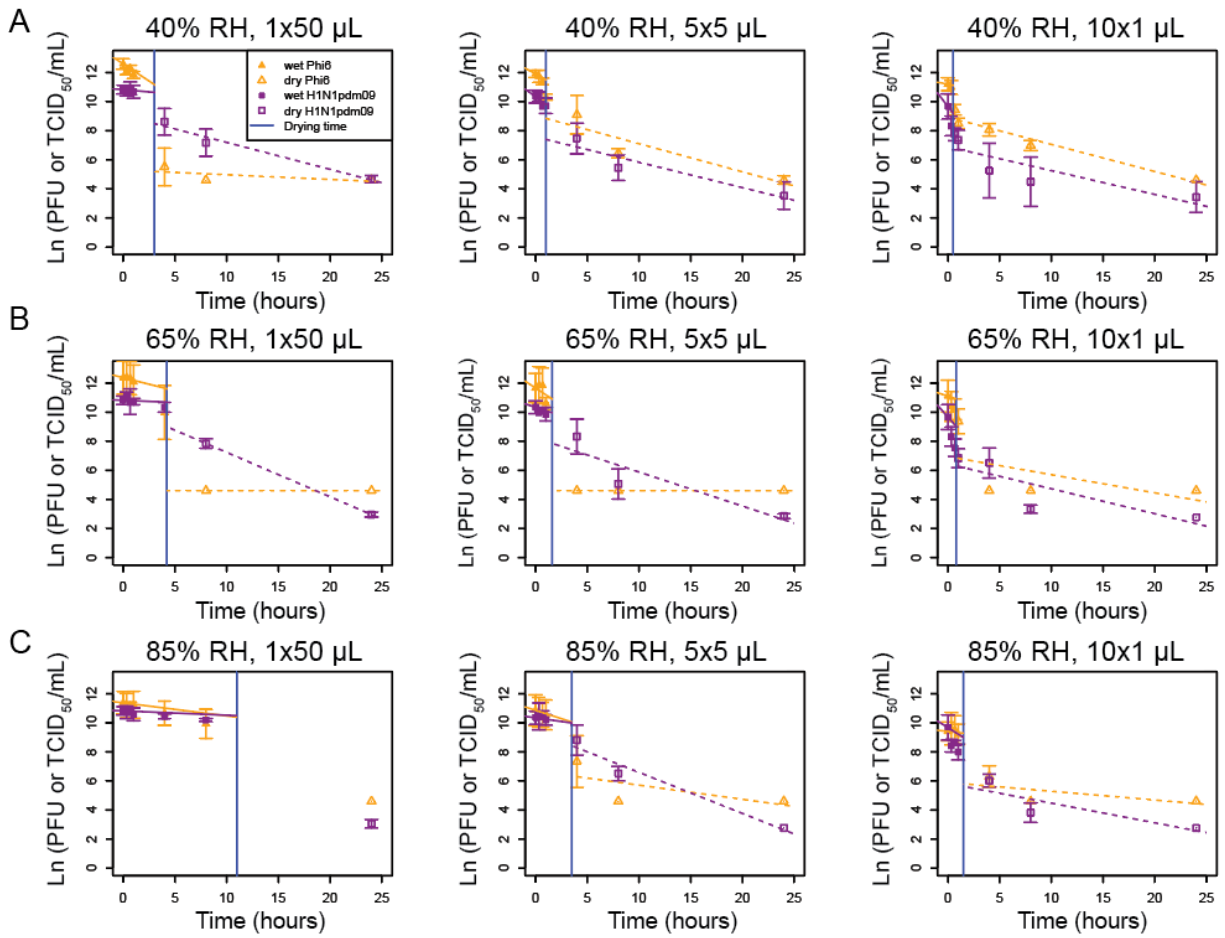

Figure 19. Mechanistic, first-order exponential decay modeling shows that the decay during the wet phase is greater or similar to the rate of decay the dry phase. A-C. First-order exponential decay models, accounting for increasing solute concentrations over time during the wet phase, were fit to ln(PFU or $TCID_{50}$/mL) over time for 1x50 µL, 5x5 µL, or 10x1 µL droplets at (**A**) 40% RH, (**B**), 65% RH, (**C**) or 85% RH. For the wet phase, the fitted initial decay rate is shown. For all graphs N=3 except at 1 hour where H1N1pdm09 N=6. The vertical blue line indicates the time of transition from the wet phase to the dry phase. A t-test was used to compare the slopes between the evaporation and dry phases for each virus at each droplet volume and between the phases for each virus at each droplet volume ($p < 0.05$). Statistical details can be found in Table 11 and Table 12.

Table 11 First-order exponential decay curves were fit to virus decay data of Phi6 and H1N1pdm09 in 1x50 µL, 5x5 µL, and 10x1 µL droplets at 40%, 65%, and 85% RH.

RH (%)	Initial Volume (µL)	Exponential Decay Rate Constants ($\frac{1}{hour}$)			
		Phi6		H1N1pdm09	
		Wet Phase	Dry Phase	Wet Phase	Dry Phase
40	50	0.47 ± 0.23	0.03 ± 0.04^{+}	0.06 ± 0.13	0.19 ± 0.03^{+}
40	5	0.39 ± 0.02*	0.19 ± 0.09*	0.52 ± 0.16*	0.17 ± 0.06*
40	1	0.14 ± NA	0.19 ± 0.03	0.92 ± NA	0.16 ± 0.06
65	50	0.18 ± 0.01^{+}	<0.01 ± NA	0.03 ± 0.01^{+}	0.31 ± NA
65	5	0.47 ± 0.23*	<0.01 ± 0.00*$^{+}$	0.23 ± 0.15	0.23 ± 0.11^{+}
65	1	0.23 ± 0.21	0.13 ± 0.14	0.80 ± 0.43	0.17 ± 0.08
85	50	0.09 ± 0.01^{+}	NA ± NA	0.03 ± 0.01^{+}	NA ± NA
85	5	0.23 ± 0.03	0.10 ± 0.11	0.10 ± 0.17	0.28 ± 0.06
85	1	0.08 ± 0.02	0.06 ± 0.07	0.45 ± 0.25	0.14 ± 0.08

NA indicates that a line could not be fit due to only 1 point occurring during the dry phase or that standard error could not be calculated due to having only 2 points to fit.

An asterisk indicates significant differences in slope between the wet and dry phase for the given volume and virus.

A cross indicates a significant difference between Phi6 and H1N1pdm09 for the given phase and volume.

Table 12 Decay constants for each phase and virus were compared within each RH and droplet volume to characterize how phase and virus impact virus decay.

Initial Volume (µL)	RH (%)	Virus 1	Virus 2	Phase 1	Phase 2	p-value
50	40	Phi6	Phi6	Wet	Dry	0.059
5	40	Phi6	Phi6	Wet	Dry	0.037*
1	40	Phi6	Phi6	Wet	Dry	NA
50	40	H1N1pdm09	H1N1pdm09	Wet	Dry	0.37
5	40	H1N1pdm09	H1N1pdm09	Wet	Dry	0.045*
1	40	H1N1pdm09	H1N1pdm09	Wet	Dry	NA
50	40	Phi6	H1N1pdm09	Wet	Wet	0.12
50	40	Phi6	H1N1pdm09	Dry	Dry	<0.01*
5	40	Phi6	H1N1pdm09	Wet	Wet	0.41
5	40	Phi6	H1N1pdm09	Dry	Dry	0.86
1	40	Phi6	H1N1pdm09	Wet	Wet	NA
1	40	Phi6	H1N1pdm09	Dry	Dry	0.71
50	65	Phi6	Phi6	Wet	Dry	NA
5	65	Phi6	Phi6	Wet	Dry	0.044*
1	65	Phi6	Phi6	Wet	Dry	0.69
50	65	H1N1pdm09	H1N1pdm09	Wet	Dry	NA
5	65	H1N1pdm09	H1N1pdm09	Wet	Dry	0.98
1	65	H1N1pdm09	H1N1pdm09	Wet	Dry	0.15
50	65	Phi6	H1N1pdm09	Wet	Wet	<0.001*
50	65	Phi6	H1N1pdm09	Dry	Dry	NA
5	65	Phi6	H1N1pdm09	Wet	Wet	0.39
5	65	Phi6	H1N1pdm09	Dry	Dry	0.036*
1	65	Phi6	H1N1pdm09	Wet	Wet	0.22
1	65	Phi6	H1N1pdm09	Dry	Dry	0.77
50	85	Phi6	Phi6	Wet	Dry	NA
5	85	Phi6	Phi6	Wet	Dry	0.24
1	85	Phi6	Phi6	Wet	Dry	0.76
50	85	H1N1pdm09	H1N1pdm09	Wet	Dry	NA
5	85	H1N1pdm09	H1N1pdm09	Wet	Dry	0.30
1	85	H1N1pdm09	H1N1pdm09	Wet	Dry	0.23
50	85	Phi6	H1N1pdm09	Wet	Wet	<0.001*
50	85	Phi6	H1N1pdm09	Dry	Dry	NA
5	85	Phi6	H1N1pdm09	Wet	Wet	0.43
5	85	Phi6	H1N1pdm09	Dry	Dry	0.14
1	85	Phi6	H1N1pdm09	Wet	Wet	0.15
1	85	Phi6	H1N1pdm09	Dry	Dry	0.48
A t-test was used to determine statistical significance.						

4.3.4 H1N1pdm09 decays similarly to SARS-CoV-2 at intermediate RH

Given the observed differences in the decay rate constants of H1N1pdm09 and Phi6 (Figure 19 and Table 11), we further investigated how the stability of these two enveloped RNA viruses compared to the stability of SARS-CoV-2 using both original and previously published data[206]. To determine whether these viruses undergo similar patterns of decay at 40%, 65%, and 85% RH, we compared our results for H1N1pdm09 and Phi6 in 50 µL droplets to published results for SARS-

CoV-2 (Figure 20A-C, Table 13)[206]. Consistent droplet composition, temperature, and RH between our study and the published results facilitated this comparison. While the published work started with 10^5 $TCID_{50}$/mL for SARS-CoV-2 and our viruses were 10^6 PFU or $TCID_{50}$/mL, we believe this difference to be negligible[1]. There were significant differences for each pairwise comparison of the decay of H1N1pdm09, Phi6, and SARS-CoV-2 at 40% RH at 4 and 8 hours; SARS-CoV-2 was most stable, followed by H1N1pdm09 and then Phi6 (Figure 20A). At 65% RH, there were fewer differences: only Phi6 was significantly different (less stable) from H1N1pdm09 and SARS-CoV-2 again at 4 and 8 hours (Figure 20B). At 85% RH, there were no significant differences for the decay of any pairwise comparison (Figure 20C). Significance at 24 hours was not assessed due to virus decay reaching the limit of detection for at least one of the viruses tested. This suggests that in large 50 µL droplets, virus specific differences are greater at lower RH. To validate the use of the previously published data, we compared original SARS-CoV-2 experiments at a targeted 55% RH (actual 57% RH) to the previously published SARS-CoV-2 data at a targeted 65% RH[206] (actual RH not known) (Figure 20D). Comparison of the original and published SARS-CoV-2 decay show similar trends and statistical differences are likely due to the difference in RH (Figure 20D).

To understand the role of droplet volume on decay of different enveloped respiratory viruses, we assessed titers of SARS-CoV-2 and H1N1pdm09 in 50 µL, 5x5 µL, and 10x1 µL droplets at 55% and 60% RH, respectively. Due to technical limitations, we were not able to test the exact same RH, but we consider these conditions to be similar, as their actual RHs were 57% and 60% (Figure 17G-I). SARS-CoV-2 stability in 50 µL, 5 µL, and 1 µL droplets at 55% RH was similar to that of H1N1pdm09 at 60% RH (Figure 21A-C, Table 13). While the decay of H1N1pdm09 in the 50 µL droplet at 65% RH appeared greater at 8 hours compared to SARS-

CoV-2, this difference was not significant (Figure 20B). The $\log_{10}$ decay in 10x1 µL droplets between H1N1pdm09 and SARS-CoV-2 was significantly different only at 8 hours, and their decay was similar again at 24 hours. Taken together with Figure 20, these results show that SARS-CoV-2 and H1N1pdm09 decay similarly at intermediate RH and that differences in virus decay may occur in larger droplets at low RH.

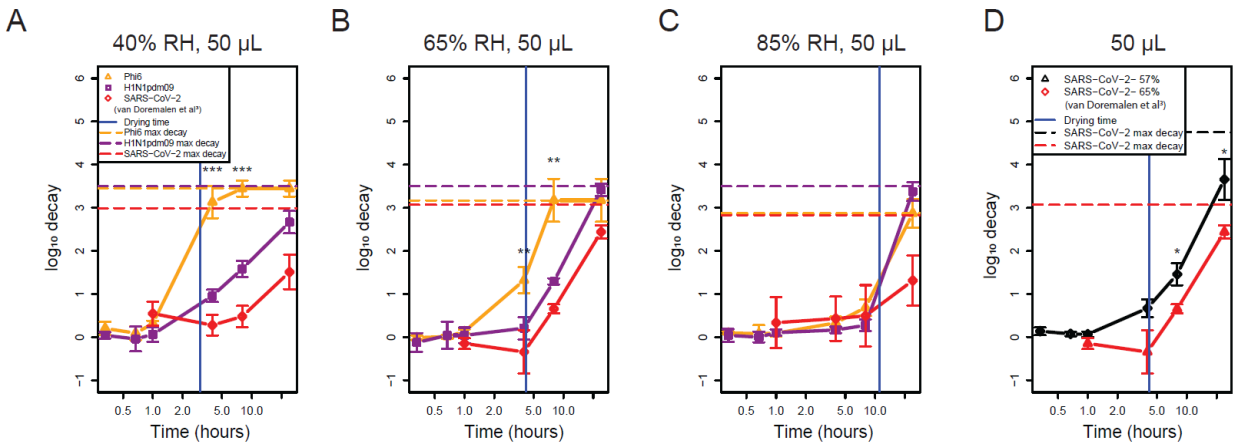

Figure 20. SARS-CoV-2 and H1N1pdm09 decay similarly across RH in 1x50 µL droplets. A-C. SARS-CoV-2, H1N1pdm09, and Phi6 stability were measured at (**A**) 40%, (**B**) 65%, (**C**) and 85% RH in 50 µL droplets using SARS-CoV-2 data originally published in van Doremalen et al[206]. **D.** Original data for SARS-CoV-2 at 55% were compared to the previously published data[206] at a targeted RH of 65%. Actual environmental conditions for original work can be found in Figure 17. Environmental conditions for van Doremalen et al SARS-CoV-2 data were not available. The vertical blue line indicates the time of transition from the wet phase to the dry phase. A one-way ANOVA and Tukey TSD test were used to determine statistical significance. Statistical details can be found in Table 13.

Table 13 Log10 decay within 1x50 µL droplets was compared between Phi6, H1N1pdm09, and SARS-CoV-2 at 40%, 65%, and 85% RH over time. Log10 decay within 50 µL, 5 µL, or 1 µL droplets was compared between H1N1pdm09 and SARS-CoV-2. Log10 decay of H1N1pdm09 and SARS-CoV-2 were compared across time for each droplet volume at 55-60% RH. Comparisons between H1N1pdm09 at 60% and 65% are also shown.

RH (%)	Time (hours)	Droplet Volume (µL)	Virus 1	Virus 2	p-value
40	0.33	50	Phi6	H1N1pdm09	0.17
	0.67	50	Phi6	H1N1pdm09	0.52
	1	50	Phi6	H1N1pdm09	0.42
		50	Phi6	SARS-CoV-2 (van Doremalen et al[206])	0.67
		50	H1N1pdm09	SARS-CoV-2 (van Doremalen et al[206])	0.15
	4	50	Phi6	H1N1pdm09	<0.001*
		50	Phi6	SARS-CoV-2 (van Doremalen et al[206])	<0.001*
		50	H1N1pdm09	SARS-CoV-2 (van Doremalen et al[206])	0.021*
	8	50	Phi6	H1N1pdm09	<0.001*
		50	Phi6	SARS-CoV-2 (van Doremalen et al[206])	<0.001*
		50	H1N1pdm09	SARS-CoV-2 (van Doremalen et al[206])	<0.01*
65	0.33	50	Phi6	H1N1pdm09	0.42
	0.67	50	Phi6	H1N1pdm09	0.88
	1	50	Phi6	H1N1pdm09	0.69
		50	Phi6	SARS-CoV-2 (van Doremalen et al[206])	0.087
		50	H1N1pdm09	SARS-CoV-2 (van Doremalen et al[206])	0.25
	4	50	Phi6	H1N1pdm09	0.024*
		50	Phi6	SARS-CoV-2 (van Doremalen et al[206])	<0.01*
		50	H1N1pdm09	SARS-CoV-2 (van Doremalen et al[206])	0.24
	8	50	Phi6	H1N1pdm09	<0.001*
		50	Phi6	SARS-CoV-2 (van Doremalen et al[206])	<0.001*
		50	H1N1pdm09	SARS-CoV-2 (van Doremalen et al[206])	0.086
85	0.33	50	Phi6	H1N1pdm09	0.55
	0.67	50	Phi6	H1N1pdm09	0.59
	1	50	Phi6	H1N1pdm09	1.0
		50	Phi6	SARS-CoV-2 (van Doremalen et al[206])	0.68
		50	H1N1pdm09	SARS-CoV-2 (van Doremalen et al[206])	0.71
	4	50	Phi6	H1N1pdm09	0.80
		50	Phi6	SARS-CoV-2 (van Doremalen et al[206])	0.92
		50	H1N1pdm09	SARS-CoV-2 (van Doremalen et al[206])	0.58
	8	50	Phi6	H1N1pdm09	0.51
		50	Phi6	SARS-CoV-2	0.86

				(van Doremalen et al[206])	
		50	H1N1pdm09	SARS-CoV-2 (van Doremalen et al[206])	0.81
55-60	1	50	H1N1pdm09	SARS-CoV-2 (VT)	0.847
	4	50	H1N1pdm09	SARS-CoV-2 (VT)	0.095
	8	50	H1N1pdm09	SARS-CoV-2 (VT)	0.571
	1	5	H1N1pdm09	SARS-CoV-2 (VT)	0.729
	4	5	H1N1pdm09	SARS-CoV-2 (VT)	0.409
	8	5	H1N1pdm09	SARS-CoV-2 (VT)	0.5
	1	1	H1N1pdm09	SARS-CoV-2 (VT)	0.117
	4	1	H1N1pdm09	SARS-CoV-2 (VT)	0.0712
	8	1	H1N1pdm09	SARS-CoV-2 (VT)	0.822
55-65	1	50	SARS-CoV-2 (van Doremalen et al[206])	SARS-CoV-2 (VT)	0.393
	4	50	SARS-CoV-2 (van Doremalen et al[206])	SARS-CoV-2 (VT)	0.426
	8	50	SARS-CoV-2 (van Doremalen et al[206])	SARS-CoV-2 (VT)	0.0169*
	24	50	SARS-CoV-2 (van Doremalen et al[206])	SARS-CoV-2 (VT)	<0.001*

A one-way ANOVA and Tukey TSD test were used to determine statistical significance. SARS-CoV-2 (van Doremalen et al[206]) data was originally published in van Doremalen et al[206]. SARS-CoV-2 (VT) data is original data collected by JP and NKD.

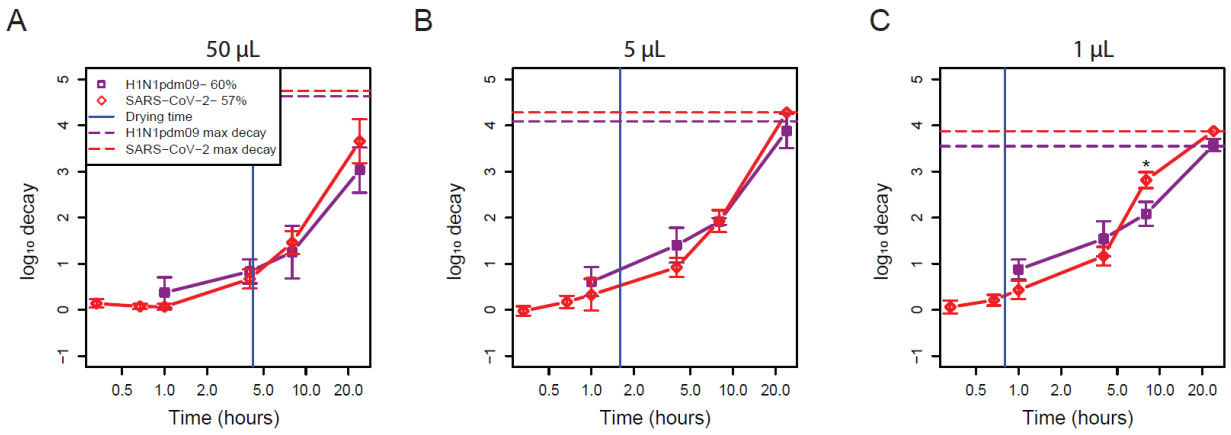

Figure 21. SARS-CoV-2 and H1N1pdm09 decay similarly across droplet volume at intermediate RH. A-C. SARS-CoV-2 stability was compared to H1N1pdm09 at 55-60% RH in 1 or 2x50 µL (**A**), 5x5 µL (**B**), and 10x1 µL (**C**) droplets over time. The vertical blue line indicates the time of transition from the wet phase to the dry phase. A one-way ANOVA was used to determine statistical significance. Statistical details can be found in Table 13. Experiments were conducted in 2 or 3 independent replicates each with technical duplicates. Data from both replicate studies is presented here.

4.4 Discussion

The studies detailed here characterize the interplay of droplet volume and RH on the stability of three enveloped RNA viruses: Phi6, H1N1pdm09, and SARS-CoV-2. Our results showed that RH has a greater impact on viral decay in large 50 µL droplets than in small 1 µL droplets, that decay rates during the wet phase are greater than or similar to decay rates during the dry phase regardless of droplet size and RH, and that differences in virus decay are more common in 50 µL droplets than in 1 µL droplets and at low RH.

Our results raise questions about the relevance of prior studies on stability of viruses that employ large droplet volumes. For example, one study derived a half-life (~0.3-log decay) of 6.8 hours for SARS-CoV-2 in 50 µL droplets on polypropylene plastic [206]. Another used 5 µL droplets to evaluate the lifetime of SARS-CoV-2 on different materials and reported 0.5-log decay in 3 hours and 1.1-log decay in 6 hours on plastic, similar to the results shown here (Figure 21B)[210]. The conclusions reached within these studies might have differed had they used smaller, more physiologically relevant droplet volumes. In our study, after 4 hours, we observed no significant decay in 50 µL droplets, ~1-log decay in 5 µL droplets, and ~1.5-log decay in 1 µL droplets at 55-60% RH. Over longer time periods, results converged, as we observed at least 3-log decay in all three droplet volumes after 24 hours. These differences are likely controlled by physical and chemical properties of the droplets as they undergo evaporation at different rates, depending on their initial volume and ambient humidity.

We have attempted to study viruses in a more realistic droplet volume compared to those used in past research, but even a 1 µL droplet is at the extremely large end of the range of droplet volumes observed in respiratory emissions. During talking, coughing, and sneezing, droplets of this volume are emitted in much lower numbers, by many orders of magnitude, compared to those that are 100-1000 times smaller in diameter and that behave as aerosols[140]. While we observed differences between 1x50 µL and 10x1 µL droplets in this study, previous work has shown that virus in 10x1 µL droplets undergoes similar decay to that in aerosols at 23% to 98% RH and 22°C[161]. Other techniques, such as a droplet-on-demand dispenser, are needed to study smaller droplet volumes on surfaces and determine whether there are fewer meaningful differences as droplets further decrease in size from 1 µL.

Our results also suggest caution in the use of surrogates to study the stability of pathogenic viruses and their potential for transmission. Surrogates that require fewer biosafety precautions are attractive for obvious reasons[218]. They can be useful for evaluating sampling and analysis methods, studying physico-chemical processes such as mechanisms of decay and transport in complex media, or eliciting trends in survival in complex media. For example, we have used Phi6 to study the fate and transport of Ebola virus in wastewater systems and to examine how survival of viruses in droplets and aerosols varies with humidity and media composition[146,161,163,219]. However, we should be cautious about extrapolating survival times from surrogates to other viruses. In the present study, we found that Phi6 decayed more quickly than did influenza virus and SARS-Cov-2 under our experimental conditions. In order to place viruses in the same droplet solution, Phi6 had to be ultracentrifuged, which may have contributed to differences in virus stability. This further emphasizes the need to use relevant viruses that can be grown in culture conditions that produce droplets similar to those that might be expelled from an infected host. Relying on only Phi6 data could lead to incorrect, and potentially hazardous, conclusions about pathogenic viruses that are more persistent. Strain selection should also be considered when using influenza virus as a surrogate for characterization of emerging virus decay, as previous work has shown that avian influenza viruses undergo more rapid decay compared to human influenza viruses[145]. Decay of enveloped viruses is likely dependent upon many complex changes to the viral glycoprotein after droplet drying or interactions between the glycoprotein and media composition. Thus, variations in glycoprotein content and density per virus family or strain likely influence the stability within droplets. On the other hand, H1N1pdm09 decayed more similarly to SARS-CoV-2 and could be useful surrogate to extrapolate the latter's persistence in more physiologically relevant conditions.

One limitation of this study is that we investigated virus persistence in culture medium, DMEM, that may not be representative of real respiratory fluid. We chose to use this medium for the purpose of comparing results with prior studies of SARS-CoV-2 in DMEM[205,206]. Prior studies have shown that virus survival in droplets, including suspended aerosols, is strongly dependent on the chemical composition of the suspending medium[146,163,220]. In particular, we have previously shown that H1N1pdm09 in aerosols and 1 µL droplets survived better when the suspending medium was supplemented with extracellular material from human bronchial epithelial cells[146]. Further studies will be required to characterize whether extracellular material from airway cells alters the biphasic decay patterns (increased decay during the wet phase followed by slower decay during the dry phase) observed in this study.

Extrapolating our results to smaller droplet sizes and combining them with the findings of other studies may provide mechanistic insight into the dynamics of virus inactivation in droplets and aerosols. The biphasic virus decay that is readily observed in droplets likely occurs in aerosols, too[205,210,221,222]. While a droplet/aerosol is wet and evaporation is still occurring, the virus is subject to a faster decay rate than after the droplet/aerosol reaches a solid or semi-solid state at quasi-equilibrium, as we observed for all droplet sizes tested[208]. At the point of efflorescence (the crystallization of salts as water evaporates), if it occurs, there appears to be a step-change loss in infectivity. With aerosols, the first phase occurs quickly, within seconds, and further observations of decay are dominated by the quasi-equilibrium phase. Thus, the first phase of decay is important for transmission at close range, when exposure occurs within seconds, while both phases are important for transmission at farther range. While the residence time of aerosols in indoor air will typically not exceed a few hours before they are removed by ventilation, droplets that are deposited

on surfaces could remain there for much longer. So, virus on surfaces could persist for longer time scales than virus within aerosols.

Although virus stability in droplets and aerosols appears to be a complex function of droplet size, composition, humidity, and other variables, mechanistically their role is to modulate the microenvironment surrounding a virion[208,222,223]. Ultimately, molecular-scale interactions are what lead to virus inactivation. We combined results for all droplet sizes and all RHs and plotted virus decay as a function of extent of evaporation of a droplet (Figure 22), a proxy for its instantaneous physical and chemical characteristics. There appeared to be less separation in results at different experimental conditions than in plots considering initial droplet size (Figure 16) and RH (Figure 19). This observation supports our hypothesis that the critical factor controlling virus decay is a virion's microenvironment and that initial droplet size and RH are indicators of this factor. The exact mechanisms of virus inactivation—the biochemical changes that occur—remain unknown. Determination of viral gene copies in a subset of samples at 1 hour and 24 hours revealed no appreciable genome loss (Table 14), indicating that genome instability is not contributing to this inactivation. As such, virus inactivation mechanisms are ripe for further investigation.

Due to our findings on the sensitivity of virus persistence to both droplet volume and composition, we urge a shift toward the use of more realistic conditions in future studies. They should employ droplets as close in volume as possible to those released from the respiratory tract (sub-micron up to several hundred microns in diameter), and whose chemical composition closely mimics that of real respiratory fluid. These findings are critical for pandemic risk assessment of emerging pathogens and useful to improve public policy on optimal transmission mitigation strategies.

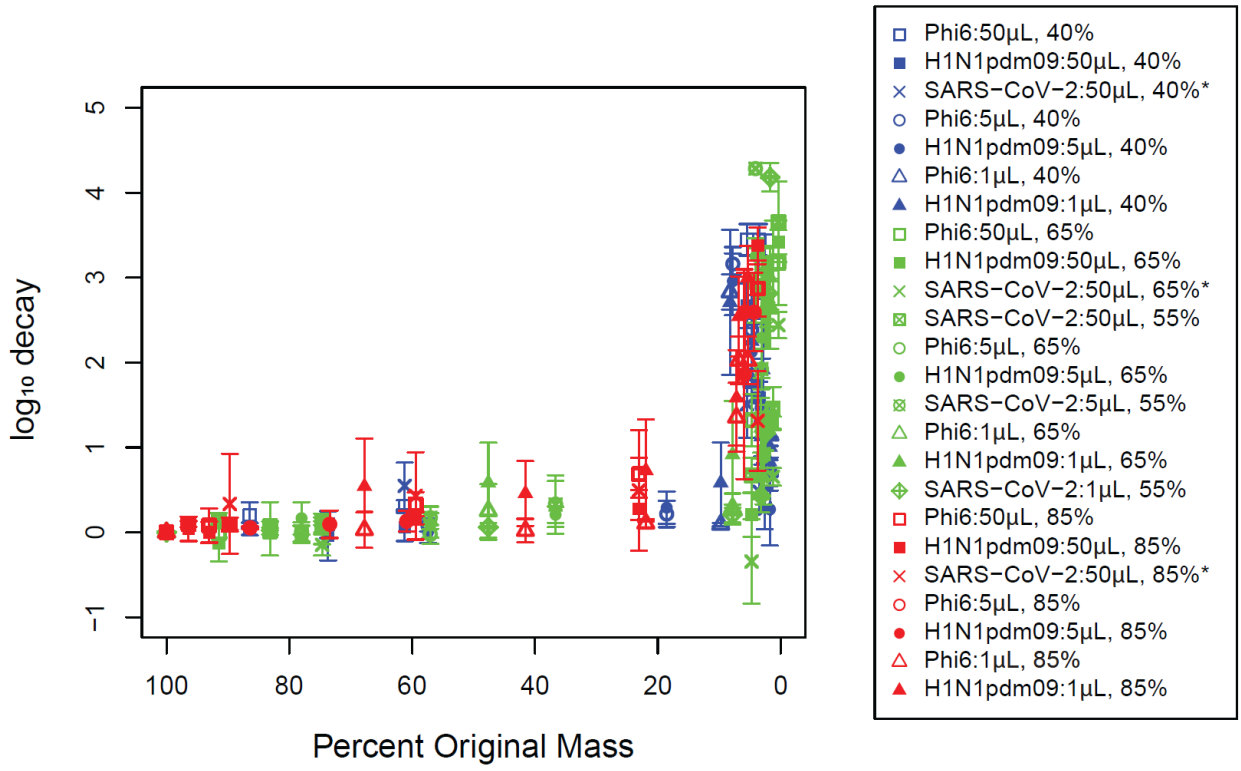

Figure 22. Evaporation is major determinant of virus decay regardless of initial droplet volume Log_{10} virus decay was plotted against percent original mass for Phi6, H1N1pdm09, and SARS-CoV-2 in 1x50 µL, 5x5 µL, and 10x1 µL at 40% RH (**A**), 65% RH (**B**), and 85% RH, (**C**). Percent original mass was determined by determining droplet mass at 0, 20, and 40 minutes, then 1, 4, 8, and 24 hours. RH listed in the legend show the targeted RH. Actual RH data are available in Figure 17, except for data previously published in van Doremalen et al[206], for which actual RH values are unavailable.

Table 14 Genome copies for limited SARS-CoV-2 and H1N1pdm09 experiments demonstrate consistent recovery and genome stability.

Virus	RH (%)	Time (hours)	Droplet volume (µL)	Log_{10} Genome Copies (per mL)[+]	Log_{10} Infectious Units (per mL)[*]	Log_{10} Decay of Infectious Units[*]
H1N1pdm09	40	1	50	7.61	4.64	0.06
		24	50	7.89	2.03	2.67
		1	5	7.23	4.22	0.27
		24	5	7.51	1.53	2.96
		1	1	6.78	3.20	1.00
		24	1	7.00	1.49	2.71
	60	1	50	7.70	4.70	0.38
		24	50	7.80	2.04	3.03
		1	5	7.41	4.03	0.61
		24	5	7.43	0.82	3.88
		1	1	6.82	3.20	0.88
		24	1	6.86	0.46	3.58
	65	1	50	7.71	4.66	0.04
		24	50	7.61	1.28	3.42
		1	5	7.36	4.28	0.21
		24	5	7.39	1.24	3.25
		1	1	6.92	2.97	1.23
		24	1	6.94	1.20[&]	3.00
	85	1	50	7.72	4.60	0.10
		24	50	7.46	1.33	3.38
		1	5	7.44	4.43	0.13
		24	5	7.17	1.20[&]	2.59
		1	1	6.77	3.47	0.73
		24	1	6.93	1.20[&]	3.00
SARS-CoV-2	55	1	50	8.12	5.40	0.07
		24	50	7.90	1.83	3.66
		1	5	7.42	4.66	0.33
		24	5	7.11	0.70[&]	4.28
		1	1	6.87	4.22	0.43
		24	1	6.92	0.70[&]	3.88

H1N1pdm09 infectious units are in $TCID_{50}$/mL while SARS-CoV-2 infectious units are in PFU/mL.
[+]A cross symbol indicates samples isolated from one replicate.
[*]The asterisk symbol indicates average data as shown in the main text.
[&]The ampersand symbol indicates values at the limit of detection

4.5 Materials and Methods

4.5.1 Cells and viruses

MDCK cells (obtained from ATCC) were grown at 37°C in 5% CO_2 in Minimum Essential Medium containing 10% FBS, penicillin/streptomycin, and L-glutamine. Influenza A virus

A/CA/07/2009 was derived from reverse genetics and grown in MDCK cells for 48 hours in DMEM (D6546-500ML, Sigma) containing 2% FBS, antibiotic-antimycotic, and L-glutamine. Stocks were diluted to 10^6 $TCID_{50}$/mL using DMEM containing 2% FBS, penicillin/streptomycin, and L-glutamine for use in experiments. Virus titers were measured using the 50% tissue culture infectious dose assay on MDCK cells and calculated using the Spearman-Karber method[197].

Phi6 was propagated in Luria-Bertani media from stock suspensions according to established methods[224]. The virus was then ultracentrifuged and resuspended in the same Dulbecco's Modified Eagle Medium as previously described using the Optima XPN-100 Ultracentrifuge. While ultracentrifugation of virus can cause aggregation, Phi6 can't be grown in DMEM, ultracentrifugation had to be done to maintain a constant droplet composition. Stocks were diluted to 10^6 PFU/mL for use in experiments. Virus titers were quantified by plaque assay[219].

SARS-CoV-2 strain USA-WA1/2020 (NR-52281, BEI Resources, Manassas, VA) was passaged in Vero cells once before receipt and subsequently in Vero cells once upon receipt. Vero cells were grown in DMEM (10-017-CV, Corning) supplemented with 5% FBS (97068-086, VWR), 100 units/mL penicillin and 100 mg/mL streptomycin (15140122, Gibco) and maintained at 37°C and 5% CO_2. Virus titers were quantified by plaque assay as described previously[225]. Stocks were diluted to 10^6 PFU/mL in DMEM (D6546-500ML, Sigma) containing 2% FBS, antibiotic-antimycotic, and L-glutamine for use in experiments. All SARS-CoV-2-related work was conducted in BSL-3 laboratories.

Given that $TCID_{50}$ and plaque assay have a linear relationship, virus decay should be comparable between virus quantification methods[226].

4.5.2 Evaporation experiment

We measured the evaporation kinetics of DMEM droplets containing Phi6 under the same humidity conditions as in the virus stability experiments. We tested each droplet volume independently by measuring the mass of the droplets every 10 minutes for up to 24 hours using a micro-balance (Sartorius MSE3.6P-000-DM, readability 0.0010 mg) placed in the environmental chamber.

4.5.3 Stability studies

We measured virus stability for Phi6 and H1N1pdm09 in a temperature and humidity controlled environmental chamber (Electro-Tech Systems) at room temperature and three (40%, 65%, and 85%) or four RHs (also 60% for H1N1pdm09). A logger (HOBO UX100-011) placed inside the chamber recorded temperature and relative humidity. The temperature and humidity for all experiments is presented in Figure 17. Briefly, the temperature ranged between 21 and 25°C in all studies and ±5% of the desired RH. The average measured RH was within ±2% of the targeted RH (Figure 17). The absolute humidities (AH) corresponding to the four targeted RHs (40%, 60%, 65%, 85%) were approximately 0.008, 0.011, 0.012, and 0.017 kg/m^3, respectively (Figure 17I). Droplets (1x50 µL, 5x5 µL, or 10x1 µL) were pipetted onto 6-well polystyrene tissue culture-coated plates (Thermo Scientific) in technical duplicates. Droplets were resuspended at seven different time points (0 minutes, 20 minutes, 40 minutes, 1 hour, 4 hours, 8 hours, and 24 hours), or four time points (1, 4, 8 and 24 hours) for the experiment at 60% RH, using 500 µL of DMEM containing 2% FBS, penicillin/streptomycin, and L-glutamine.

We measured the stability of SARS-CoV-2 in an airtight desiccator at room temperature and 55% RH as described previously.[161] The measured temperature ranged between 23 and 28°C. In short, we filled one polyethylene Petri dish with 10 to 20 mL of saturated magnesium nitrate solution and placed it at the bottom of the desiccator to control the humidity. A battery-powered fan was also placed inside to enhance air mixing and thus accelerate the establishment of equilibrium, which was usually within 5 to 10 minutes. A logger recorded temperature and relative humidity. After RH equilibrium was reached, 2x50 µL, 5x5 µL, or 10x1 µL droplets were deposited and suspended as described previously. Plaque assay on Vero cells was used to measure virus titers.

All H1N1pdm09 and Phi6 collections were performed in technical duplicates and independent triplicates. Due to biosafety constraints and the additional resources required, the SARS-CoV-2 work was performed in technical duplicates with two independent replicates. Data from all replicates are presented for each virus.

4.5.4 Calculations and modeling

We measured the initial mass (m(0)) immediately after the droplets were deposited onto the polystyrene surface. We calculated the percent original mass of the droplet over time using the following equation:

$$\%\, Original\, mass \;=\; 100 - \frac{\big(m(0) - m(t)\big)}{m(0)} \cdot 100 \qquad \textbf{Equation 1}$$

We defined the time to quasi-equilibrium state, also referred to as the drying time, as the time to reach a value that did not increase or decrease by more than 2%.

Virus decay was calculated as follows:

N(0)= titer at time 0

N(t)= titer at time t

$$\text{Log}_{10}\text{ Decay} = \log\frac{\overline{N(0)}}{N(t)} \qquad \textbf{Equation 2}$$

Because virus decay was measured by comparing to titer at time 0, we have already accounted for potential loss due to resuspension.

We modeled the decay of viruses using first-order exponential decay curves separately for the wet phase and the dry phase. The first order decay equation is as follows.

$$N(t) = N(0)e^{-kt} \qquad \textbf{Equation 3}$$

We ran a linear regression in R through the log-transformed equation to find the decay rate. For wet decay, we adjusted for the increasing concentrations of solutes over time, as shown in the following equation[205]

$$\log_{10}\big(N(t)\big) = \log_{10}(\text{N}(0)) + \frac{k_0}{B}\log_{10}(1 - Bt) \qquad \textbf{Equation 4}$$

N(0) is the initial virus titer, N(t) is the titer at time t, k0 is the initial first-order rate constant during the evaporation phase, and B equals the slope of the wet change in mass divided by the initial water mass.

4.5.5 Quantitative RT-PCR

We performed qRT-PCR on one independent replicate each of H1N1pdm09 and SARS-CoV-2 to address genome instability as a possible mechanism of inactivation. For SARS-CoV-2 the Qiagen QIAamp Viral RNA Mini kit was used to isolate RNA according to the manufacturer's protocol. The 2019-nCoV RUO primer/probe kit targeting the N1 gene (IDT) was used in combination with iTaq Universal Probes One-Step kit. Synthetic SARS-CoV-2 RNA (BEI Resources) was used as a standard. For H1N1pdm09, the Qiagen QIAamp Viral RNA Mini Kit was used to isolate RNA according to the manufacturer's protocol. The influenza M gene was targeted using the iTaq Universal Probes One-Step kit with primers (Forward 5'-AGATGAGTCTTCTAACCGAGGTCG-3' ; Reverse 5'-GCAAAGACACTTTCCAGTCTCTG-3') and probe (5'-[FAM]TCAGGCCCCCTCAAAGCCGA[3BHQ1] -3'). In vitro transcribed RNA served as standards to determine genome copies. Each qPCR plate contained duplicates of standards, samples, and no-template controls.

4.5.6 Multivariate analysis

We conducted a multivariate analysis (manova) to determine if there was an interaction between initial droplet volume and RH that would account for differences in the wet phase decay of the viruses. There was no statistically significant amount of variance ($p = 0.339$) for Phi6 wet phase decay, but there was statistically significant variance for H1N1pdm09 wet phase decay ($p = 0.037$) indicating there is an interaction between initial droplet volume and RH that affects wet phase decay.

4.5.7 Data Availability

All raw data associated with this study is available on figshare at the following doi https://doi.org/10.6084/m9.figshare.c.6458767 . In addition, movies corresponding to the droplet drying over time at 3 different relative humidities can be found within the collection and at these individual links: https://doi.org/10.6084/m9.figshare.21711119; https://doi.org/10.6084/m9.figshare.21711122; https://doi.org/10.6084/m9.figshare.21711116 .

4.5.8 Acknowledgements and funding

We thank Dylan Morris for sharing the SARS-CoV-2 data previously published in van Doremalen et al. and Morris et al[205,206]. This work was supported by NIAID (CEIRS HHSN272201400007C, SSL and LCM), and in part with Federal funds from NIAID, NIH, and DHHS (75N93021C00015, SSL). Additional funding was provided by Flu Lab (SSL and LCM), an ICTAS Junior Faculty Award (NKD), and NIH NINDS R01NS124204 (NKD). JF was supported by the University of Pittsburgh Training Program in Antimicrobial Resistance (T32AI138954). We thank Dr. Rachel Schwartz for critical review and feedback. We would also like to thank Dr. Douglas Reed and his lab for allowing us access to the humidity cabinet used in these experiments.

5.0 Summary and Implications

5.1 Summary

This dissertation examined host and environmental factors influencing transmission of the 2009 H1N1 pandemic influenza A virus. Prior, it was not known how co-infection led to increased morbidity or the effect it had on microbial release into the air. It was also not known whether co-infection or droplet size had an impact on microbial stability in the environment. Thus, this dissertation explored these questions to broadly improve understanding of influenza transmission. In chapter two, we determined that host responses were a critical component of the increased morbidity observed during co-infection (Figure 23A). In chapters three and four, we explored environmental factors of transmission. We found that co-infected ferrets release detectable influenza virus and *S. pneumoniae* into the air and that there is a trend towards increased stability of *S. pneumoniae* in the presence of influenza virus (Figure 23B). We also found that droplet size has important implications for viral stability in the environment and viral surrogates don't always replicate the same decay kinetics as the virus of interest (Figure 23C).

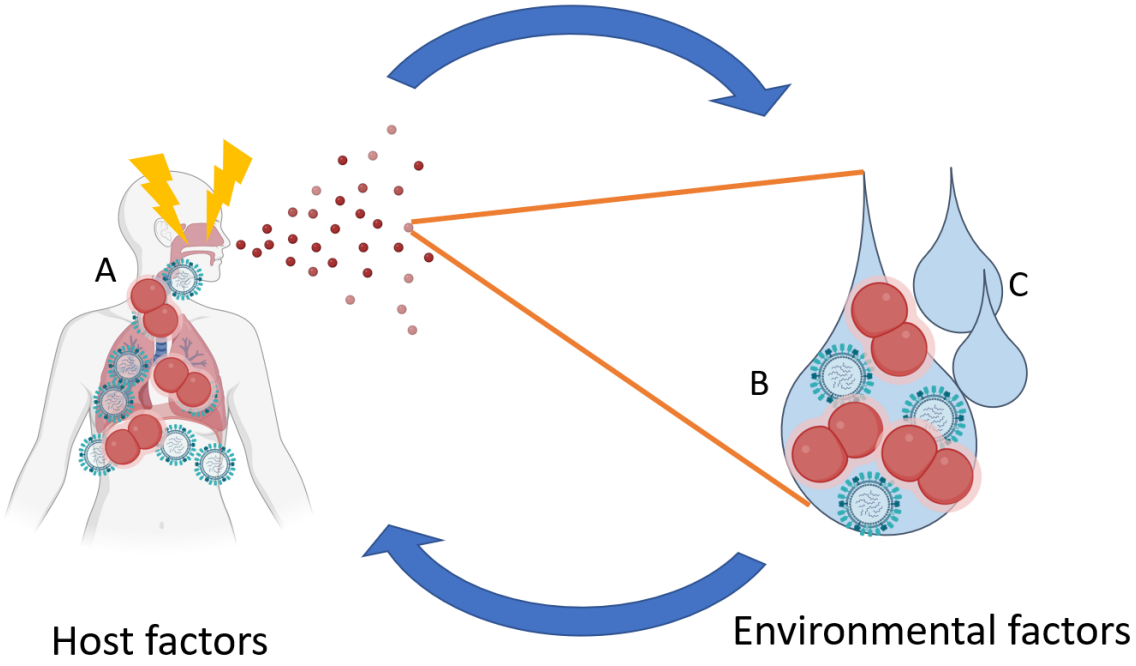

Figure 23. Disseration summary. Exploration of factors influencing influenza transmission involved (**A**) how co-infection contributes to increased morbidity, (**B**) examination of viral and bacterial release into the environment during co-infection, and (**C**) the effect of droplet size and virus on decay in the environment.

5.1.1 Influenza virus and *S. pneumoniae* co-infection has complex impacts on pathogenesis

First, we wanted to explore how co-infection might impact transmission by assessing its impact on the pathogenesis of influenza virus. In chapter two, I hypothesized that co-infection would lead to severe pathology in infected tissues, possibly corresponding to high levels of viral and bacterial burden. However, no differences in viral burden were observed in upper or lower respiratory tissue during co-infection compared to influenza-only infection even though significant morbidity was observed in co-infected ferrets. I observed trends towards increased bacterial burden in the soft palate and trachea, but there were no differences in the nasal turbinates, where co-infection and *S. pneumoniae* mono-infection had high burden, or the lungs, where co-infection and *S. pneumoniae* mono-infection had no detectable bacteria. Interestingly, even though viral and bacterial loads were not different in the nasal turbinate there was significant pathological changes in co-infected animals compared to mono-infected animals. These pathological changes are likely to be the cause of increased clinical signs in ferrets co-infected with influenza virus and bacteria.

Since detection of increased clinical signs was not dependent upon viral or bacterial load, but pathological changes were observed we proceeded to explore host immune responses. We observed enrichment in immune cell migration, acute inflammatory responses, and IL-6 production in the nasal turbinates when comparing tissue from co-infection animals to those infected only with influenza. The nasal turbinates were unique, as the soft palate and lungs did not display the same uniform upregulation of host immune responses, which corresponds with the lack of significant pathological changes in lung and soft palate tissue.

In total, this work improves our understanding of how co-infection drives morbidity and mortality. We see that host responses contribute to this morbidity, suggesting that clinical care during co-infection could consider inclusion of therapy to alleviate the burden of strong immune responses. Therapies may want to focus on the nasal passages, as this site seemed to be a primary location of immunopathology in our study.

5.1.2 Analysis of microbial stability in the environment requires careful consideration of experimental conditions

One of the goals of this dissertation was to improve our understanding of transmission of influenza A viruses using the 2009 pandemic H1N1 influenza virus. Environmental stability is an important factor for transmission of respiratory pathogens, as a pathogen cannot initiate infection if it has become inactivated while outside of a host. Studies measuring viral persistence in the environment have used an array of microbes[162,163,221], droplet sizes[205,206,210–213] and compositions[146,163,227] to determine half-lives.

In chapters three and four, I focused on factors that influence environmental persistence of influenza virus. First, in chapter three, I assessed the role of a second microbe, the common co-infector *S. pneumoniae*, on influenza virus stability. My first approach to characterizing environmental stability during co-infection was to quantify the prevalence of pathogens released into the air. Both influenza and *S. pneumoniae* were detected in aerosols from co-infected animals, indicating that they could exist within the same droplets. Subsequently, stability experiments were performed to assess whether *S. pneumoniae* altered influenza virus stability or the reverse. Airway surface liquid collected from human bronchial epithelial cells was used in these experiments to create a more physiologically relevant droplet composition. No effect was observed on influenza

virus stability when *S. pneumoniae* was added to droplets. However, there seemed to be a trend towards increased stability of *S. pneumoniae* in the presence of influenza. However, this effect was more prominent in the presence of airway surface liquid from a single donor, the only donor with idiopathic pulmonary fibrosis. Future studies should examine whether airway surface liquid from donors with idiopathic pulmonary fibrosis contributes to enhanced stability of *S. pneumoniae* in the presence of influenza.

Next, I examined the role of droplet size on stability of influenza virus and compared my results to stability of Phi6 under identical conditions. I found that larger droplets take longer to reach quasi-equilibrium than smaller droplets. This suggested that evaporation-dependent decay may lead to differences in virus stability based on droplet size. Consequently, I also found that relative humidity has a greater impact on virus decay in large droplets and decay rates are greater during the wet phase. There were also differences between the decay rates for influenza virus and for Phi6, which led us to compare our results against SARS-CoV-2, an enveloped respiratory virus. Decay of SARS-CoV-2 was similar to influenza virus, which indicated that surrogates may not always accurately estimate absolute decay times of other viruses. Collectively, these findings demonstrated that studies performed to inform policy decisions surrounding decontamination procedures of contaminated surfaces need to use relevant droplet sizes and ideally the virus of interest. However, when biosafety procedures limit the use of the virus of interest, a very similar virus should be used.

Collectively my work advances our understanding of environmental persistence of respiratory pathogens by addressing the role of droplet size and the role of additional microbes. Characterizing microbial resistance requires the use of physiologically relevant droplet sizes and should consider inclusion of common co-infecting pathogens when deciding the droplet

composition. If we apply my findings to the transmission cycle, the work presented here suggests that modulation of relative humidity as an engineering control might not reduce transmission, as small droplets are less sensitive to relative humidity-mediated decay. Additionally, co-infection may alter the stability of *S. pneumoniae*, providing further evidence for the increased transmission observed for *S. pneumoniae* during influenza co-infection[81,82].

5.2 Future Directions

5.2.1 Bacterial evolution during co-infection

In chapter two, there were no differences between viral burden in co-infection or influenza mono-infection, but there were trends towards increased bacterial burden in the trachea and soft palate of co-infected animals compared to *S. pneumoniae* mono-infection. We also observed synergistic host responses in the nasal turbinates during co-infection that were not observed in influenza or *S. pneumoniae* mono-infection. These observations could be the exclusive result of tissue-specific host responses, but previous work found that *S. pneumoniae* has organ-specific gene expression during mono-infection[228]. So, the relative contribution of altered *S. pneumoniae* gene expression to the tissue-specificity observed during influenza co-infection is unknown, and comparison of gene expression between multiple tissues and multiple infection types may inform drug targets to prevent high bacterial burden during influenza infection.

Therefore, future work should address this by isolating bacteria from homogenized tissue during *S. pneumoniae* mono-infection and co-infection and performing RNA sequencing to assess differential gene expression. Simultaneously, bacteria could be isolated for whole genome

sequencing to determine whether bacteria undergo evolution during co-infection that is different than mono-infection. This information could provide additional insight into the selective pressures exerted by the host during co-infection and how *S. pneumoniae* circumvents this host response.

5.2.2 Sampling aerosols to assess for presence of commensal bacteria during influenza infection

In chapter three, I detected both influenza and *S. pneumoniae* in the air using culture methods and PCR detection of their genomes. We experimentally infected ferrets with these microbes, but the nasal turbinates contain a complex microbiome, inhabited by many microbes that are also present on the skin[173]. Analysis of microbiome changes during influenza infection have also shown that the nasal microbiome changes during influenza infection before returning to a state similar to before influenza infection[229]. Previous studies have examined the presence of bacteria in aerosols from hospital wards[230], bacteria in expectorated sputum from cystic fibrosis patients[231], or the presence of influenza in aerosols[232], but never respiratory tract bacteria and influenza in the same aerosols. So, it's not clear whether commensal microbes are also emitted in respiratory expulsions from influenza-infected hosts or if there is a correlation between commensal abundance in nasal wash and presence in respiratory emissions.

The work presented here demonstrates a role for modulation of microbial stability by other microbes. So, future work should address the gap in knowledge concerning whether commensal microbes from the respiratory tract are present in aerosols with influenza virus and then whether they modulate the stability of influenza in the environment. Experiments could be done to collect aerosols from influenza-infected patients and perform whole genome sequencing for low abundance species[233]. Any microbes detected in the aerosols would be candidates for subsequent

droplet and aerosol stability experiments. Given that the *Pseudomonas* genus has been observed as one of the most abundant operational taxonomic units in nasal washes of ferrets during influenza infection[229], I would hypothesize that this genus would be detected in aerosols from influenza-infected ferrets. These experiments could help the field move microbial stability closer to physiologically relevant conditions and unveil possible microbial interactions.

5.2.3 Impact of droplet size on microbial stability in the presence of biologically relevant solutions

One limitation of my work examining the impact of droplet size on viral persistence was that we used a medium not relevant to transmission. The droplet media was chosen to allow comparison between our study and the results of a previously published study with SARS-CoV-2[206]. The cell culture media in which Phi6 and H1N1pdm09 were suspended is unlike the solutions emitted from an infected host. Whether droplet size contributes to different virus decay in saliva or airway surface liquid secreted from bronchial epithelial cells remains unknown. Given that airway surface liquid protect virus from relative humidity-mediated decay[146], I would hypothesize that droplet size would have a reduced impact on virus stability in this solution. However, further study needs to be performed to determine the impact of droplet size with airway surface liquid and saliva.

5.3 Conclusion

The goal of this dissertation was to better understand factors influencing severe disease and transmission of influenza virus. The results of my research describe how co-infection promotes high morbidity, define a role for influenza to promote *S. pneumoniae* transmission through airway surface liquid dependent means, and outline droplet size as a determinant for virus stability in the environment (Figure 23). In the end, there is a lot of room for continued study of environmental stability and co-infection pathogenesis. Better understanding of these fields will allow for improved engineering controls and health interventions to reduce influenza transmission and disease burden.

Appendix A

Publication List

French, AJ[*], Longest, AK[*], Pan, J, Vikesland, PJ, Duggal, NK, Marr, LC, Lakdawala, SS (2023). Environmental Stability of Enveloped Viruses is Impacted by the Initial Volume and Evaporation Kinetics of Droplets. *mBio.*

[*]Co-first authors

French, AJ, Rockey, NC, Mueller Brown K., Shephard, MJ, Myerburg, MM, Hiller, NL, Lakdawala, SS (2023). Detection of Influenza virus and *Streptococcus pneumoniae* in air sampled from co-infected ferrets and analysis of their influence on pathogen stability. *mSphere*.

French, AJ, Rockey, NC, Le Sage, VM, Mueller Brown, K, Walters, SG, Shephard, MJ, Jones, JE, Rigatti, L, Hiller, NL, Lakdawala, SS (2023). Tissue-specific responses and microbial relationships during influenza virus and *Streptococcus pneumoniae* co-infection in the ferret model. (In preparation).

Mueller Brown, K[*], Le Sage, VM[*], **French, AJ**, Jones, JE, Padovani, GE, Avery, AJ, Schultz-Cherry, S, Rosch, JW, Hiller, NL, & Lakdawala, SS (2022). Secondary infection with *Streptococcus pneumoniae* decreases influenza virus replication and is linked to severe disease. *FEMS Microbes*, *3*.

Bibliography

1. Johnson, N. P. A. S. & Mueller, J. Updating the Accounts: Global Mortality of the 1918-1920 'Spanish' Influenza Pandemic. *Bull Hist Med* **76**, 105–115 (2002).
2. Girard, M. P., Tam, J. S., Assossou, O. M. & Kieny, M. P. The 2009 A (H1N1) influenza virus pandemic: A review. *Vaccine* **28**, 4895–4902 (2010).
3. Shinde, V. *et al.* Triple-Reassortant Swine Influenza A (H1) in Humans in the United States, 2005–2009. *New England Journal of Medicine* **360**, 2616–2625 (2009).
4. Munster, V. J. *et al.* Pathogenesis and transmission of swine-origin 2009 A(H1N1) influenza virus in ferrets. *Science (1979)* **325**, 481–483 (2009).
5. Louie, J. K. *et al.* Factors associated with death or hospitalization due to pandemic 2009 influenza A(H1N1) infection in California. *JAMA - Journal of the American Medical Association* **302**, 1896–1902 (2009).
6. Swayne, D. E., Hill, R. E. & Clifford, J. Safe application of regionalization for trade in poultry and poultry products during highly pathogenic avian influenza outbreaks in the USA. *Avian Pathology* **46**, 125–130 (2017).
7. United States Department of Agriculture: Animal and Plant Health Inspection Service. 2022-2023 Confirmations of Highly Pathogenic Avian Influenza in Commercial and Backyard Flocks. https://www.aphis.usda.gov/wcm/connect/APHIS_Content_Library/SA_Our_Focus/SA_Animal_Health/SA_Animal_Disease_Information/Avian/avian-influenza/hpai-2022/2022-hpai-commercial-backyard-

flocks?presentationtemplate=APHIS_Design_Library%2FPT_Print_Friendly (2023).

8. Chen, C. & Zhuang, X. Epsin 1 is a cargo-specific adaptor for the clathrin-mediated endocytosis of the influenza virus. *Proc Natl Acad Sci U S A* **105**, 11790 (2008).
9. White, J., Helenius, A. & Gething, M. J. Haemagglutinin of influenza virus expressed from a cloned gene promotes membrane fusion. *Nature* **300**, 658–659 (1982).
10. Martin, K. & Heleniust, A. Nuclear transport of influenza virus ribonucleoproteins: The viral matrix protein (M1) promotes export and inhibits import. *Cell* **67**, 117–130 (1991).
11. Eisfeld, A. J., Neumann, G. & Kawaoka, Y. At the centre: influenza A virus ribonucleoproteins. *Nat Rev Microbiol* **13**, 28 (2015).
12. Cros, J. F., García-Sastre, A. & Palese, P. An Unconventional NLS is Critical for the Nuclear Import of the Influenza A Virus Nucleoprotein and Ribonucleoprotein. *Traffic* **6**, 205–213 (2005).
13. Dou, D., Revol, R., Östbye, H., Wang, H. & Daniels, R. Influenza A Virus Cell Entry, Replication, Virion Assembly and Movement. *Front Immunol* **9**, 1 (2018).
14. Huang, S. *et al.* A Second CRM1-Dependent Nuclear Export Signal in the Influenza A Virus NS2 Protein Contributes to the Nuclear Export of Viral Ribonucleoproteins. *J Virol* **87**, 767 (2013).
15. Lakdawala, S. S. *et al.* Influenza A Virus Assembly Intermediates Fuse in the Cytoplasm. *PLoS Pathog* **10**, (2014).

16. Palese, P. & Compans, R. W. Inhibition of influenza virus replication in tissue culture by 2-deoxy-2,3-dehydro-N- trifluoroacetylneuraminic acid (FANA): mechanism of action. *Journal of General Virology* **33**, 159–163 (1976).

17. Moscona, A. Neuraminidase Inhibitors for Influenza. *New England Journal of Medicine* **353**, 1363–1373 (2005).

18. Zhuang, Q. *et al.* Diversity and distribution of type A influenza viruses: An updated panorama analysis based on protein sequences. *Virol J* **16**, 1–38 (2019).

19. Leung, H. S. Y. *et al.* Entry of Influenza A Virus with a α2,6-Linked Sialic Acid Binding Preference Requires Host Fibronectin. *J Virol* **86**, 10704 (2012).

20. Gulati, S., Smith, D. F. & Air, G. M. Deletions of neuraminidase and resistance to oseltamivir may be a consequence of restricted receptor specificity in recent H3N2 influenza viruses. *Virol J* **6**, (2009).

21. Maines, T. R. *et al.* Local innate immune responses and influenza virus transmission and virulence in ferrets. *J Infect Dis* **205**, 474–485 (2012).

22. Krammer, F. The human antibody response to influenza A virus infection and vaccination. *Nature Reviews Immunology 2019 19:6* **19**, 383–397 (2019).

23. Carrat, F. *et al.* Time Lines of Infection and Disease in Human Influenza: A Review of Volunteer Challenge Studies. *Am J Epidemiol* **167**, 775–785 (2008).

24. Memoli, M. J. *et al.* Validation of the Wild-type Influenza A Human Challenge Model H1N1pdMIST: An A(H1N1)pdm09 Dose-Finding Investigational New Drug Study. *Clin Infect Dis* **60**, 693 (2015).

25. Gustin, K. M. *et al.* Influenza virus aerosol exposure and analytical system for ferrets. *Proc Natl Acad Sci U S A* **108**, 8432–8437 (2011).

26. Hayden, F. G. *et al.* Safety and Efficacy of the Neuraminidase Inhibitor GG167 in Experimental Human Influenza. *JAMA* **275**, 295–299 (1996).

27. Alford, R., Kasel, J., Gerone, P. & Knight, V. Human influenza resulting from aerosol inhalation. *Proceedings of the Society for Experimental Biology and Medicine* **122**, 800–804 (1966).

28. Manicassamy, B. *et al.* Analysis of in vivo dynamics of influenza virus infection in mice using a GFP reporter virus. *Proc Natl Acad Sci U S A* **107**, 11531–11536 (2010).

29. Lakdawala, S. S. *et al.* The soft palate is an important site of adaptation for transmissible influenza viruses. *Nature* **526**, 122–125 (2015).

30. Fraňková, V., Jirásek, A. & Tůmová, B. Type A influenza: Postmortem virus isolations from different organs in human lethal cases. *Arch Virol* **53**, 265–268 (1977).

31. Guarner, J. *et al.* Histopathologic and immunohistochemical features of fatal influenza virus infection in children during the 2003-2004 season. *Clinical Infectious Diseases* **43**, 132–140 (2006).

32. Rice, T. W. *et al.* Critical Illness from 2009 Pandemic Influenza A (H1N1) Virus and Bacterial Co-Infection in the United States. *Crit Care Med* **40**, 1487 (2012).

33. Belser, J. A., Katz, J. M. & Tumpey, T. M. The ferret as a model organism to study influenza A virus infection. *Dis Model Mech* **4**, 575–579 (2011).

34. Peng, X. *et al.* The draft genome sequence of the ferret (Mustela putorius furo) facilitates study of human respiratory disease. *Nat Biotechnol* **32**, 1250 (2014).

35. Maines, T. R. *et al.* Lack of transmission of H5N1 avian-human reassortant influenza viruses in a ferret model. *Proc Natl Acad Sci U S A* **103**, 12121–12126 (2006).

36. Belser, J. A. *et al.* Robustness of the Ferret Model for Influenza Risk Assessment Studies: a Cross-Laboratory Exercise Working group on the standardization of the ferret model for influenza risk assessment. (2022) doi:10.1128/mbio.01174-22.

37. Moore, I. N. *et al.* Severity of Clinical Disease and Pathology in Ferrets Experimentally Infected with Influenza Viruses Is Influenced by Inoculum Volume. *J Virol* **88**, 13879 (2014).

38. Belser, J. A., Eckert, A. M., Tumpey, T. M. & Maines, T. R. Complexities in Ferret Influenza Virus Pathogenesis and Transmission Models. *Microbiol Mol Biol Rev* **80**, 733 (2016).

39. Le Sage, V. *et al.* Pre-existing heterosubtypic immunity provides a barrier to airborne transmission of influenza viruses. *PLoS Pathog* **17**, (2021).

40. Carolan, L. A. *et al.* Characterization of the Localized Immune Response in the Respiratory Tract of Ferrets following Infection with Influenza A and B Viruses. *J Virol* **90**, 2838–2848 (2016).

41. Meunier, I. *et al.* Virulence differences of closely related pandemic 2009 H1N1 isolates correlate with increased inflammatory responses in ferrets. *Virology* **422**, 125–131 (2012).

42. Ma, J., Rubin, B. K. & Voynow, J. A. Mucins, Mucus, and Goblet Cells. *Chest* **154**, 169–176 (2018).

43. McAuley, J. L. *et al.* The cell surface mucin MUC1 limits the severity of influenza A virus infection. *Mucosal Immunol* **10**, 1581–1593 (2017).

44. Iwasaki, A. & Pillai, P. S. Innate immunity to influenza virus infection. *Nature Reviews Immunology 2014 14:5* **14**, 315–328 (2014).

45. le Goffic, R. *et al.* Cutting Edge: Influenza A virus activates TLR3-dependent inflammatory and RIG-I-dependent antiviral responses in human lung epithelial cells. *J Immunol* **178**, 3368–3372 (2007).

46. McNab, F., Mayer-Barber, K., Sher, A., Wack, A. & O'Garra, A. Type I interferons in infectious disease. *Nature Reviews Immunology 2015 15:2* **15**, 87–103 (2015).

47. Zürcher, T., Pavlovic, J. & Staeheli, P. Nuclear localization of mouse Mx1 protein is necessary for inhibition of influenza virus. *J Virol* **66**, 5059 (1992).

48. Murphy, K. & Weaver, C. *Janeway's Immunobiology*. (Garland Science/Taylor & Francis Group, LLC, 2017).

49. Pothlichet, J. *et al.* Type I IFN Triggers RIG-I/TLR3/NLRP3-dependent Inflammasome Activation in Influenza A Virus Infected Cells. *PLoS Pathog* **9**, 1003256 (2013).

50. Ichinohe, T., Lee, H. K., Ogura, Y., Flavell, R. & Iwasaki, A. Inflammasome recognition of influenza virus is essential for adaptive immune responses. *J Exp Med* **206**, 79–87 (2009).

51. Pang, I. K., Ichinohe, T. & Iwasaki, A. IL-1R signaling in dendritic cells replaces pattern recognition receptors to promote CD8+ T cell responses to influenza A virus. *Nat Immunol* **14**, 246 (2013).

52. Lauder, S. N. *et al.* Interleukin-6 limits influenza-induced inflammation and protects against fatal lung pathology. *Eur J Immunol* **43**, 2613–2625 (2013).

53. Denton, A. E., Doherty, P. C., Turner, S. J. & la Gruta, N. L. IL-18, but not IL-12, is required for optimal cytokine production by influenza virus-specific CD8+ T cells. *Eur J Immunol* **37**, 368–375 (2007).

54. Braciale, T. J., Sun, J. & Kim, T. S. Regulating the adaptive immune response to respiratory virus infection. *Nature Reviews Immunology 2012 12:4* **12**, 295–305 (2012).

55. Hobson, D., Curry, R. L., Beare, A. S. & Ward-Gardner, A. The role of serum haemagglutination-inhibiting antibody in protection against challenge infection with influenza A2 and B viruses. *J Hyg (Lond)* **70**, 767 (1972).

56. Svitek, N. & von Messling, V. Early cytokine mRNA expression profiles predict Morbillivirus disease outcome in ferrets. *Virology* **362**, 404–410 (2007).

57. Carolan, L. A. *et al.* TaqMan real time RT-PCR assays for detecting ferret innate and adaptive immune responses. *J Virol Methods* **205**, 38–52 (2014).

58. Music, N. *et al.* Influenza Vaccination Accelerates Recovery of Ferrets from Lymphopenia. *PLoS One* **9**, 100926 (2014).

59. Music, N., Reber, A. J., Kim, J. H. & York, I. A. Peripheral Leukocyte Migration in Ferrets in Response to Infection with Seasonal Influenza Virus. *PLoS One* **11**, (2016).

60. Walsh, K. B. *et al.* Suppression of cytokine storm with a sphingosine analog provides protection against pathogenic influenza virus. *Proc Natl Acad Sci U S A* **108**, 12018–12023 (2011).

61. La Gruta, N. L., Kedzierska, K., Stambas, J. & Doherty, P. C. A question of self-preservation: immunopathology in influenza virus infection. *Immunol Cell Biol* **85**, 85–92 (2007).

62. le Goffic, R. *et al.* Detrimental Contribution of the Toll-Like Receptor (TLR)3 to Influenza A Virus–Induced Acute Pneumonia. *PLoS Pathog* **2**, 0526–0535 (2006).

63. Kaiser, L., Fritz, R. S., Straus, S. E., Gubareva, L. & Hayden, F. G. Symptom pathogenesis during acute influenza: interleukin-6 and other cytokine responses. *J Med Virol* **64**, 262–268 (2001).

64. Thomas, P. G. *et al.* NLRP3 (NALP3/CIAS1/Cryopyrin) mediates key innate and healing responses to influenza A virus via the regulation of caspase-1. *Immunity* **30**, 566 (2009).

65. Gounder, A. P. & Boon, A. C. M. Influenza Pathogenesis: The role of host factors on severity of disease. *Journal of immunology* **202**, 350 (2019).

66. Haq, K. & McElhaney, J. E. Immunosenescence: influenza vaccination and the elderly. *Curr Opin Immunol* **29**, 38–42 (2014).

67. Frost, W. THE EPIDEMIOLOGY OF INFLUENZA. *Public Health Reports* **34**, 1823–1836 (1919).

68. Santa-Olalla Peralta, P. *et al.* Risk factors for disease severity among hospitalised patients with 2009 pandemic influenza A (H1N1) in Spain, April - December 2009. *Euro surveillance* **15**, 1–9 (2010).

69. Randolph, A. G. *et al.* Critically Ill Children During the 2009–2010 Influenza Pandemic in the United States. *Pediatrics* **128**, e1450 (2011).

70. Fink, A. L., Engle, K., Ursin, R. L., Tang, W. Y. & Klein, S. L. Biological sex affects vaccine efficacy and protection against influenza in mice. *Proc Natl Acad Sci U S A* **115**, 12477–12482 (2018).

71. Balter, S. *et al.* 2009 Pandemic Influenza A (H1N1) in Pregnant Women Requiring Intensive Care --- New York City, 2009. *MMWR* **59**, 321–326 (2010).

72. Harris, J. W. INFLUENZA OCCURRING IN PREGNANT WOMEN A STATISTICAL STUDY OF THIRTEEN HUNDRED AND FIFTY CASES. *JAMA - Journal of the American Medical Association* 978–980 (1919).

73. Tsang, T. K. *et al.* Association Between the Respiratory Microbiome and Susceptibility to Influenza Virus Infection. *Clinical Infectious Diseases* **71**, 1195–1203 (2020).

74. Lee, K. H. *et al.* The respiratory microbiota: Associations with influenza symptomatology and viral shedding. *Ann Epidemiol* **37**, 51 (2019).

75. Ichinohe, T. *et al.* Microbiota regulates immune defense against respiratory tract influenza A virus infection. *Proc Natl Acad Sci U S A* **108**, 5354–5359 (2011).

76. Morens, D. M., Taubenberger, J. K. & Fauci, A. S. Predominant Role of Bacterial Pneumonia as a Cause of Death in Pandemic Influenza: Implications for Pandemic Influenza Preparedness. *J Infect Dis* **198**, 962–970 (2008).

77. Palacios, G. *et al.* Streptococcus pneumoniae Coinfection Is Correlated with the Severity of H1N1 Pandemic Influenza. *PLoS One* **4**, (2009).

78. Martin-Loeches, I. *et al.* Increased incidence of co-infection in critically ill patients with influenza. *Intensive Care Medicine 2016 43:1* **43**, 48–58 (2016).

79. CDC FluView. *https://www.cdc.gov/flu/weekly/fluviewinteractive.htm* https://www.cdc.gov/flu/weekly/fluviewinteractive.htm.

80. McCullers, J. A. & Rehg, J. E. Lethal Synergism between Influenza Virus and Streptococcus pneumoniae: Characterization of a Mouse Model and the Role of Platelet-Activating Factor Receptor. *J Infect Dis* **186**, 341–350 (2002).

81. Peltola, V. T., Rehg, J. E. & McCullers, J. A. A ferret model of synergism between influenza virus and Streptococcus pneumoniae. *Int Congr Ser* **1263**, 486–490 (2004).

82. Mueller-Brown, K. *et al.* Secondary infection with Streptococcus pneumoniae decreases influenza virus replication and is linked to severe disease. *FEMS Microbes* (2022) doi:10.1093/FEMSMC/XTAC007.

83. World Health Organization. Pneumonia in children. https://www.who.int/news-room/fact-sheets/detail/pneumonia (2022).

84. Faden, H. *et al.* Relationship between Nasopharyngeal Colonization and the Development of Otitis Media in Children. *J Infect Dis* **175**, 1440–1445 (1997).

85. World Health Organization. WHO publishes list of bacteria for which new antibiotics are urgently needed. https://www.who.int/news/item/27-02-2017-who-publishes-list-of-bacteria-for-which-new-antibiotics-are-urgently-needed (2017).

86. Chapman, T. J., Morris, M. C., Xu, L. & Pichichero, M. E. Nasopharyngeal colonization with pathobionts is associated with susceptibility to respiratory illnesses in young children. *PLoS One* **15**, (2020).

87. Sleeman, K. L. *et al.* Acquisition of Streptococcus pneumoniae and nonspecific morbidity in infants and their families: A cohort study. *Pediatric Infectious Disease Journal* **24**, 121–127 (2005).

88. Regev-Yochay, G. *et al.* Nasopharyngeal Carriage of Streptococcus pneumoniae by Adults and Children in Community and Family Settings. *Clinical Infectious Diseases* 632–639 (2004).

89. Goldblatt, D. *et al. Antibody Responses to Nasopharyngeal Carriage of Streptococcus pneumoniae in Adults: A Longitudinal Household Study*.

Pneumococcal Immunity after Carriage • JID https://academic.oup.com/jid/article-abstract/192/3/387/833292 (2005).

90. Geno, K. A. *et al.* Pneumococcal capsules and their types: Past, present, and future. *Clin Microbiol Rev* **28**, 871–899 (2015).

91. Klugman, K. P. *et al.* A Trial of a 9-Valent Pneumococcal Conjugate Vaccine in Children with and Those without HIV Infection. *New England Journal of Medicine* **349**, 1341–1348 (2003).

92. Madhi, S. A. & Klugman, K. P. A role for Streptococcus pneumoniae in virus-associated pneumonia. *Nat Med* **10**, 811–813 (2004).

93. Briles, D. E., Crain, M. J., Gray, B. M., Forman, C. & Yother, J. Strong association between capsular type and virulence for mice among human isolates of Streptococcus pneumoniae. *Infect Immun* **60**, 111 (1992).

94. Grabenstein, J. D. & Musey, L. K. Differences in serious clinical outcomes of infection caused by specific pneumococcal serotypes among adults. *Vaccine* **32**, 2399–2405 (2014).

95. Moscoso, M., García, E. & López, R. Pneumococcal biofilms. *International Microbiology* **12**, 77–85 (2009).

96. Wartha, F. *et al.* Capsule and d-alanylated lipoteichoic acids protect Streptococcus pneumoniae against neutrophil extracellular traps. *Cell Microbiol* **9**, 1162–1171 (2007).

97. Bootsma, H. J., Egmont-Petersen, M. & Hermans, P. W. M. Analysis of the in vitro transcriptional response of human pharyngeal epithelial cells to adherent

Streptococcus pneumoniae: Evidence for a distinct response to encapsulated strains. *Infect Immun* **75**, 5489–5499 (2007).

98. Hiller, N. L. & Sá-Leão, R. Puzzling Over the Pneumococcal Pangenome. *Front Microbiol* **9**, (2018).

99. Short, K. R., Reading, P. C., Wang, N., Diavatopoulos, D. A. & Wijburg, O. L. Increased nasopharyngeal bacterial titers and local inflammation facilitate transmission of Streptococcus pneumoniae. *mBio* **3**, (2012).

100. Gonzalez-Juarbe, N. *et al.* Influenza-Induced Oxidative Stress Sensitizes Lung Cells to Bacterial-Toxin-Mediated Necroptosis. *Cell Rep* **32**, (2020).

101. Bogaert, D., De Groot, R. & Hermans, P. W. M. Streptococcus pneumoniae colonisation: the key to pneumococcal disease. *Lancet Infect Dis* **4**, 144–154 (2004).

102. Gray, B. M., Converse, G. M. & Dillon, H. C. Epidemiologic studies of Streptococcus pneumoniae in infants: acquisition, carriage, and infection during the first 24 months of life. *J Infect Dis* **142**, 923–933 (1980).

103. Mifsud, E. J., Farrukee, R., Hurt, A. C., Reading, P. C. & Barr, I. G. Infection with different human influenza A subtypes affects the period of susceptibility to secondary bacterial infections in ferrets. *FEMS Microbes* **3**, 1–8 (2022).

104. McCullers, J. A. *et al.* Influenza Enhances Susceptibility to Natural Acquisition of and Disease due to Streptococcus pneumoniae in Ferrets . *J Infect Dis* **202**, 1287–1295 (2010).

105. Grijalva, C. G. *et al.* The role of influenza and parainfluenza infections in nasopharyngeal pneumococcal acquisition among young children. *Clinical Infectious Diseases* **58**, 1369–1376 (2014).

106. Wadowsky, R. M., Mietzner, S. M., Skoner, D. P., Doyle, W. J. & Fireman, P. Effect of experimental influenza A virus infection on isolation of Streptococcus pneumoniae and other aerobic bacteria from the oropharynges of allergic and nonallergic adult subjects. *Infect Immun* **63**, 1153–1157 (1995).

107. Diavatopoulos, D. A. *et al.* Influenza A virus facilitates Streptococcus pneumoniae transmission and disease. *The FASEB Journal* **24**, 1789–1798 (2010).

108. Mina, M. J., Klugman, K. P. & McCullers, J. A. Live attenuated influenza vaccine, but not pneumococcal conjugate vaccine, protects against increased density and duration of pneumococcal carriage after influenza infection in pneumococcal colonized mice. *Journal of Infectious Diseases* **208**, 1281–1285 (2013).

109. Peltola, V. T., Boyd, K. L., McAuley, J. L., Rehg, J. E. & McCullers, J. A. Bacterial sinusitis and otitis media following influenza virus infection in ferrets. *Infect Immun* **74**, 2562–2567 (2006).

110. Manna, S. *et al.* Synergism and Antagonism of Bacterial-Viral Coinfection in the Upper Respiratory Tract. *mSphere* (2022) doi:10.1128/MSPHERE.00984-21.

111. Smith, A. M. *et al.* Kinetics of Coinfection with Influenza A Virus and Streptococcus pneumoniae. *PLoS Pathog* **9**, (2013).

112. Rowe, H. M. *et al.* Respiratory Bacteria Stabilize and Promote Airborne Transmission of Influenza A Virus. *mSystems* **5**, (2020).

113. Rowe, H. M. *et al.* Bacterial Factors Required for Transmission of Streptococcus pneumoniae in Mammalian Hosts. *Cell Host Microbe* **25**, 884-891.e6 (2019).

114. Weiser, J. N., Ferreira, D. M. & Paton, J. C. Streptococcus pneumoniae: Transmission, colonization and invasion. *Nature Reviews Microbiology* vol. 16 355–367 Preprint at https://doi.org/10.1038/s41579-018-0001-8 (2018).

115. Lees, J. A. *et al.* Genome-wide identification of lineage and locus specific variation associated with pneumococcal carriage duration. *Elife* **6**, (2017).

116. Nakamura, S., Davis, K. M. & Weiser, J. N. Synergistic stimulation of type I interferons during influenza virus coinfection promotes Streptococcus pneumoniae colonization in mice. *Journal of Clinical Investigation* **121**, 3657–3665 (2011).

117. Girardin, S. E. *et al.* Nod2 is a general sensor of peptidoglycan through muramyl dipeptide (MDP) detection. *J Biol Chem* **278**, 8869–8872 (2003).

118. Lemon, J. K. & Weiser, J. N. Degradation products of the extracellular pathogen Streptococcus pneumoniae access the cytosol via its pore-forming toxin. *mBio* **6**, (2015).

119. Davis, K. M., Nakamura, S. & Weiser, J. N. Nod2 sensing of lysozyme-digested peptidoglycan promotes macrophage recruitment and clearance of S. pneumoniae colonization in mice. *J Clin Invest* **121**, 3666 (2011).

120. Andre, G. O. *et al.* Role of Streptococcus Pneumoniae proteins in evasion of complement-mediated immunity. *Front Microbiol* **8**, 224 (2017).

121. Ferreira, D. M. *et al.* Controlled human infection and rechallenge with Streptococcus pneumoniae reveals the protective efficacy of carriage in healthy adults. *Am J Respir Crit Care Med* **187**, 855–864 (2013).

122. Trzciński, K. *et al.* Protection against Nasopharyngeal Colonization by Streptococcus pneumoniae Is Mediated by Antigen-Specific CD4+ T Cells. *Infect Immun* **76**, 2678 (2008).

123. Zhang, Z., Clarke, T. B. & Weiser, J. N. Cellular effectors mediating Th17-dependent clearance of pneumococcal colonization in mice. *J Clin Invest* **119**, 1899 (2009).

124. Mubarak, A. *et al.* A dynamic relationship between mucosal T helper type 17 and regulatory T-cell populations in nasopharynx evolves with age and associates with the clearance of pneumococcal carriage in humans. *Clin Microbiol Infect* **22**, 736.e1-736.e7 (2016).

125. Nagai, M., Moriyama, M. & Ichinohe, T. Oral bacteria combined with an intranasal vaccine protect from influenza a virus and sars-cov-2 infection. *mBio* **12**, (2021).

126. Carniel, B. F. *et al.* Pneumococcal colonization impairs mucosal immune responses to live attenuated influenza vaccine. *JCI Insight* **6**, (2021).

127. Shrestha, S. *et al.* Time and dose-dependent risk of pneumococcal pneumonia following influenza: a model for within-host interaction between influenza and Streptococcus pneumoniae. *J R Soc Interface* **10**, (2013).

128. Levine, A. M., Koeningsknecht, V. & Stark, J. M. *Decreased pulmonary clearance of S. pneumoniae following influenza A infection in mice*. *Journal of Virological Methods* vol. 94 www.elsevier.com/locate/jviromet (2001).

129. Schmitz, N., Kurrer, M., Bachmann, M. F. & Kopf, M. Interleukin-1 is responsible for acute lung immunopathology but increases survival of respiratory influenza virus infection. *J Virol* **79**, 6441–6448 (2005).

130. Bansal, S., Yajjala, V. K., Bauer, C. & Sun, K. IL-1 Signaling Prevents Alveolar Macrophage Depletion during Influenza and Streptococcus pneumoniae Coinfection . *The Journal of Immunology* **200**, 1425–1433 (2018).

131. Ghoneim, H. E., Thomas, P. G. & McCullers, J. A. Depletion of Alveolar Macrophages during Influenza Infection Facilitates Bacterial Superinfections. *The Journal of Immunology* **191**, 1250–1259 (2013).

132. Jochems, S. P. *et al.* Inflammation induced by influenza virus impairs human innate immune control of pneumococcus. *Nat Immunol* **19**, 1299–1308 (2018).

133. Hoffmann, J. *et al.* Viral and bacterial co-infection in severe pneumonia triggers innate immune responses and specifically enhances IP-10: a translational study. *Sci Rep* **6**, 38532 (2016).

134. Liu, Y. *et al.* Outcomes of respiratory viral-bacterial co-infection in adult hospitalized patients. *EClinicalMedicine* **37**, 100955 (2021).

135. Fiore, A. E. *et al.* Antiviral Agents for the Treatment and Chemoprophylaxis of Influenza. *MMWR* **60**, 1–24 (2011).

136. Lakdawala, S. S. & Subbarao, K. The challenge of flu transmission. *Nat Med* **18**, 1468–1471 (2012).

137. Leung, N. H. L. Transmissibility and transmission of respiratory viruses. *Nat Rev Microbiol* **19**, 528 (2021).

138. Principles of Epidemiology | Lesson 1 - Section 10. https://www.cdc.gov/csels/dsepd/ss1978/lesson1/section10.html.

139. Wang, C. C. *et al.* Airborne transmission of respiratory viruses. *Science (1979)* **373**, (2021).

140. Bourouiba, L. Fluid Dynamics of Respiratory Infectious Diseases. *Annu Rev Biomed Eng* (2021) doi:10.1146/annurev-bioeng-111820.

141. Tellier, R. Review of Aerosol Transmission of Influenza A Virus. *Emerg Infect Dis* **12**, 1657 (2006).

142. Killingley, B. & Nguyen-Van-Tam, J. Routes of influenza transmission. *Influenza Other Respir Viruses* **7**, 42 (2013).

143. Bouvier, N. M., Lowen, A. C. & Palese, P. Oseltamivir-resistant influenza A viruses are transmitted efficiently among guinea pigs by direct contact but not by aerosol. *J Virol* **82**, 10052–10058 (2008).

144. Mukherjee, D. V *et al.* Survival of influenza virus on hands and fomites in community and laboratory settings. *Am J Infect Control* **40**, 590–594 (2012).

145. Kormuth, K. A. *et al.* Environmental Persistence of Influenza Viruses Is Dependent upon Virus Type and Host Origin. *mSphere* **4**, 1–14 (2019).

146. Kormuth, K. A. *et al.* Influenza virus infectivity is retained in aerosols and droplets independent of relative humidity. *Journal of Infectious Diseases* **218**, 739–747 (2018).

147. Mubareka, S. *et al.* Transmission of influenza virus via aerosols and fomites in the guinea pig model. *J Infect Dis* **199**, 858–865 (2009).

148. Nguyen-Van-Tam, J. S. *et al.* Minimal transmission in an influenza A (H3N2) human challenge-transmission model within a controlled exposure environment. *PLoS Pathog* **16**, (2020).

149. Killingley, B. *et al.* Use of a Human Influenza Challenge Model to Assess Person-to-Person Transmission: Proof-of-Concept Study. *J Infect Dis* **205**, 35–43 (2012).

150. Calfee, D. P., Peng, A. W., Hussey, E. K., Lobo, M. & Hayden, F. G. Safety and efficacy of once daily intranasal zanamivir in preventing experimental human influenza A infection. *Antivir Ther* **4**, 143–149 (1999).

151. Richard, M. *et al.* Influenza A viruses are transmitted via the air from the nasal respiratory epithelium of ferrets. *Nat Commun* **11**, 1–11 (2020).

152. Houser, K. v, Pearce, M. B., Katz, J. M. & Tumpey, T. M. Impact of prior seasonal H3N2 influenza vaccination or infection on protection and transmission of emerging variants of influenza A(H3N2)v virus in ferrets. *J Virol* **87**, 13480–13489 (2013).

153. Lowen, A. C. *et al.* Blocking interhost transmission of influenza virus by vaccination in the guinea pig model. *J Virol* **83**, 2803–2818 (2009).

154. Edenborough, K. M., Gilbertson, B. P. & Brown, L. E. A mouse model for the study of contact-dependent transmission of influenza A virus and the factors that govern transmissibility. *J Virol* **86**, 12544–12551 (2012).

155. Stefan, K. L. *et al.* Commensal Microbiota Modulation of Natural Resistance to Virus Infection. *Cell* **183**, 1312-1324.e10 (2020).

156. Li, Y. *et al.* Role of ventilation in airborne transmission of infectious agents in the built environment - A multidisciplinary systematic review. *Indoor Air* **17**, 2–18 (2007).

157. Ortigoza, M. B., Blaser, S. B., Ammar Zafar, M., Hammond, A. J. & Weiser, J. N. An Infant Mouse Model of Influenza Virus Transmission Demonstrates the Role of Virus-Specific Shedding, Humoral Immunity, and Sialidase Expression by Colonizing Streptococcus pneumoniae. *mBio* **9**, e02359-18 (2018).

158. Ward, A. & Campoli-Richards, D. M. Mupirocin: A Review of Its Antibacterial Activity, Pharmacokinetic Properties and Therapeutic Use. *Drugs* **32**, 425–444 (1986).

159. Lowen, A. C., Mubareka, S., Steel, J. & Palese, P. Influenza virus transmission is dependent on relative humidity and temperature. *PLoS Pathog* **3**, 1470–1476 (2007).

160. Biryukov, J. *et al.* Increasing Temperature and Relative Humidity Accelerates Inactivation of SARS-CoV-2 on Surfaces. (2020) doi:10.1128/mSphere.00441-20.

161. Prussin, A. J. *et al.* Survival of the Enveloped Virus Phi6 in Droplets as a Function of Relative Humidity, Absolute Humidity, and Temperature. *Appl Environ Microbiol* **84**, (2018).

162. Lin, K. & Marr, L. C. Humidity-Dependent Decay of Viruses, but Not Bacteria, in Aerosols and Droplets Follows Disinfection Kinetics. *Cite This: Environ. Sci. Technol* **2020**, 1024–1032 (2020).

163. Lin, K., Schulte, C. R. & Marr, L. C. Survival of MS2 and Φ6 viruses in droplets as a function of relative humidity, pH, and salt, protein, and surfactant concentrations. *PLoS One* **15**, e0243505 (2020).

164. DUNKLIN, E. W. & PUCK, T. T. THE LETHAL EFFECT OF RELATIVE HUMIDITY ON AIR-BORNE BACTERIA. *J Exp Med* **87**, 87 (1948).

165. Rockey, N. C., Henderson, J. B., Chin, K., Raskin, L. & Wigginton, K. R. Predictive Modeling of Virus Inactivation by UV. *Environ Sci Technol* **55**, 3322–3332 (2021).

166. Cox, C. Airborne bacteria and viruses. *Sci Prog* **73**, 469–499 (1989).

167. Myerburg, M. M., Harvey, P. R., Heidrich, E. M., Pilewski, J. M. & Butterworth, M. B. Acute regulation of the epithelial sodium channel in airway epithelia by proteases and trafficking. *Am J Respir Cell Mol Biol* **43**, 712–719 (2010).

168. Pöhlker, M. L. *et al.* Respiratory aerosols and droplets in the transmission of infectious diseases. (2021) doi:10.48550/arxiv.2103.01188.

169. Humphrey, S. P. & Williamson, R. T. A review of saliva: Normal composition, flow, and function. *J Prosthet Dent* **85**, 162–169 (2001).

170. Tang, J. W. The effect of environmental parameters on the survival of airborne infectious agents. *J R Soc Interface* **6**, (2009).

171. Robinson, C. M., Jesudhasan, P. R. & Pfeiffer, J. K. Bacterial Lipopolysaccharide Binding Enhances Virion Stability and Promotes Environmental Fitness of an Enteric Virus. *Cell Host Microbe* **15**, 36–46 (2014).

172. Aguilera, E. R., Nguyen, Y., Sasaki, J. & Pfeiffer, J. K. Bacterial Stabilization of a Panel of Picornaviruses. *mSphere* **4**, (2019).

173. Man, W. H., De Steenhuijsen Piters, W. A. A. & Bogaert, D. The microbiota of the respiratory tract: gatekeeper to respiratory health. *Nature Reviews Microbiology 2017 15:5* **15**, 259–270 (2017).

174. Johnson, G. *et al.* Modality of human expired aerosol size distributions. *J Aerosol Sci* **42**, 839–851 (2011).

175. Milton, D. K., Fabian, M. P., Cowling, B. J., Grantham, M. L. & McDevitt, J. J. Influenza Virus Aerosols in Human Exhaled Breath: Particle Size, Culturability, and Effect of Surgical Masks. *PLoS Pathog* **9**, (2013).

176. Alsved, M. *et al.* Size distribution of exhaled aerosol particles containing SARS-CoV-2 RNA. *Infect Dis (Lond)* **55**, (2023).

177. Lindsley, W. G. *et al.* Viable Influenza A Virus in Airborne Particles from Human Coughs. *J Occup Environ Hyg* **12**, 107 (2015).

178. Milton, D. K. A Rosetta Stone for Understanding Infectious Drops and Aerosols. *J Pediatric Infect Dis Soc* **9**, 413 (2020).

179. Johnson, G. R. & Morawska, L. The mechanism of breath aerosol formation. *J Aerosol Med Pulm Drug Deliv* **22**, 229–237 (2009).

180. Paget, J. *et al.* Global mortality associated with seasonal influenza epidemics: New burden estimates and predictors from the GLaMOR Project. *J Glob Health* **9**, (2019).

181. Iuliano, A. D. *et al.* Estimates of global seasonal influenza-associated respiratory mortality: a modelling study. *Lancet* **391**, 1285 (2018).

182. Wahl, B. *et al.* Burden of Streptococcus pneumoniae and Haemophilus influenzae type b disease in children in the era of conjugate vaccines: global, regional, and national estimates for 2000–15. *Lancet Glob Health* **6**, e744–e757 (2018).

183. Chertow, D. S. & Memoli, M. J. Bacterial Coinfection in Influenza: A Grand Rounds Review. *JAMA* **309**, 275–282 (2013).

184. Aguilera, E. R. & Lenz, L. L. Inflammation as a Modulator of Host Susceptibility to Pulmonary Influenza, Pneumococcal, and Co-Infections. *Front Immunol* **11**, 105 (2020).

185. Sun, K. & Metzger, D. W. Inhibition of pulmonary antibacterial defense by interferon-γ during recovery from influenza infection. *Nature Medicine 2008 14:5* **14**, 558–564 (2008).

186. McNamee, L. A. & Harmsen, A. G. Both influenza-induced neutrophil dysfunction and neutrophil-independent mechanisms contribute to increased susceptibility to a secondary Streptococcus pneumoniae infection. *Infect Immun* **74**, 6707–6721 (2006).

187. Li, W., Moltedo, B. & Moran, T. M. Type I Interferon Induction during Influenza Virus Infection Increases Susceptibility to Secondary Streptococcus pneumoniae Infection by Negative Regulation of γδ T Cells. *J Virol* **86**, 12304 (2012).

188. van der Sluijs, K. F. *et al.* IL-10 Is an Important Mediator of the Enhanced Susceptibility to Pneumococcal Pneumonia after Influenza Infection. *The Journal of Immunology* **172**, 7603–7609 (2004).

189. Smith, M. W., Schmidt, J. E., Rehg, J. E., Orihuela, C. J. & McCullers, J. A. Induction of pro- and anti-inflammatory molecules in a mouse model of pneumococcal pneumonia after influenza. *Comp Med* **57**, 82–89 (2007).

190. Ellis, G. T. *et al.* TRAIL+ monocytes and monocyte-related cells cause lung damage and thereby increase susceptibility to influenza–Streptococcus pneumoniae coinfection. *EMBO Rep* **16**, 1203–1218 (2015).

191. Smith, A. M. *et al.* Kinetics of Coinfection with Influenza A Virus and Streptococcus pneumoniae. *PLoS Pathog* **9**, e1003238 (2013).

192. Rowe, H. M. *et al.* Direct interactions with influenza promote bacterial adherence during respiratory infections. *Nat Microbiol* **4**, 1328–1336 (2019).

193. Kim, Y. Il *et al.* Age-dependent pathogenic characteristics of SARS-CoV-2 infection in ferrets. *Nature Communications 2022 13:1* **13**, 1–13 (2022).

194. D'Mello, A. *et al.* Influenza A virus modulation of Streptococcus pneumoniae infection using ex vivo transcriptomics in a human primary lung epithelial cell model

reveals differential host glycoconjugate uptake and metabolism. *bioRxiv* 2023.01.29.526157 (2023) doi:10.1101/2023.01.29.526157.

195. D'Mello, A. *et al.* An in vivo atlas of host–pathogen transcriptomes during Streptococcus pneumoniae colonization and disease. *Proc Natl Acad Sci U S A* **117**, 33507–33518 (2020).

196. Platt, M. P. *et al.* A multiomics analysis of direct interkingdom dynamics between influenza A virus and Streptococcus pneumoniae uncovers host-independent changes to bacterial virulence fitness. *PLoS Pathog* **18**, e1011020 (2022).

197. Ramakrishnan, M. A. Determination of 50% endpoint titer using a simple formula. *World J Virol* **5**, 85 (2016).

198. Zhi, X. *et al.* Rgg-Shp regulators are important for pneumococcal colonization and invasion through their effect on mannose utilization and capsule synthesis. *Scientific Reports 2018 8:1* **8**, 1–15 (2018).

199. Reuman, P. D., Keely, S. & Schiff, G. M. Assessment of signs of influenza illness in the ferret model. *J Virol Methods* **24**, 27–34 (1989).

200. Love, M. I., Huber, W. & Anders, S. Moderated estimation of fold change and dispersion for RNA-seq data with DESeq2. *Genome Biol* **15**, (2014).

201. Marr, L. C., Tang, J. W., Mullekom, J. Van & Lakdawala, S. S. Mechanistic insights into the effect of humidity on airborne influenza virus survival, transmission and incidence. *J R Soc Interface* **16**, (2019).

202. Berger, A. K., Yi, H., Kearns, D. B. & Mainou, B. A. Bacteria and bacterial envelope components enhance mammalian reovirus thermostability. *PLoS Pathog* **13**, e1006768 (2017).

203. Olive, M., Gan, C., Carratalà, A. & Kohn, T. Control of Waterborne Human Viruses by Indigenous Bacteria and Protists Is Influenced by Temperature, Virus Type, and Microbial Species. *Appl Environ Microbiol* **86**, (2020).

204. Heidelberg, J. F. *et al.* Effect of aerosolization on culturability and viability of gram-negative bacteria. *Appl Environ Microbiol* **63**, 3585 (1997).

205. Morris, D. H. *et al.* Mechanistic theory predicts the effects of temperature and humidity on inactivation of sars-cov-2 and other enveloped viruses. *Elife* **10**, (2021).

206. Doremalen, N. van *et al.* Aerosol and Surface Stability of SARS-CoV-2 as Compared with SARS-CoV-1. *NEJM* **382**, 1564–1567 (2020).

207. Firquet, S. *et al.* Survival of Enveloped and Non-Enveloped Viruses on Inanimate Surfaces. *Microbes Environ* **30**, 140 (2015).

208. Huynh, E. *et al.* Evidence for a semisolid phase state of aerosols and droplets relevant to the airborne and surface survival of pathogens. *Proc Natl Acad Sci U S A* **119**, (2022).

209. Gralton, J., Tovey, E., McLaws, M. L. & Rawlinson, W. D. The role of particle size in aerosolised pathogen transmission: A review. *Journal of Infection* vol. 62 1–13 Preprint at https://doi.org/10.1016/j.jinf.2010.11.010 (2011).

210. Chin, A. W. H. *et al.* Stability of SARS-CoV-2 in different environmental conditions. *Lancet Microbe* **1**, e10 (2020).

211. Kasloff, S. B., Leung, A., Strong, J. E., Funk, D. & Cutts, T. Stability of SARS-CoV-2 on critical personal protective equipment. *Scientific Reports 2021 11:1* **11**, 1–7 (2021).

212. Newey, C. R. *et al.* Presence and stability of SARS-CoV-2 on environmental currency and money cards in Utah reveals a lack of live virus. *PLoS One* **17**, e0263025 (2022).

213. Liu, Y. *et al.* Stability of SARS-CoV-2 on environmental surfaces and in human excreta. *Journal of Hospital Infection* **107**, 105–107 (2021).

214. Gerba, C. P. & Betancourt, W. Q. Viral Aggregation: Impact on Virus Behavior in the Environment. *Environ Sci Technol* **51**, 7318–7325 (2017).

215. Huang, Q., Wang, W. & Vikesland, P. J. Implications of the Coffee-Ring Effect on Virus Infectivity. *Langmuir* (2021) doi:10.1021/ACS.LANGMUIR.1C01610.

216. Reed, L. J. & Muench, H. A SIMPLE METHOD OF ESTIMATING FIFTY PERCENT ENDPOINTS. *Am J Epidemiol* **27**, 493–497 (1938).

217. Hiatt, C. W. KINETICS OF THE INACTIVATION OF VIRUSES. *Bacteriol Rev* **28**, 150 (1964).

218. Verreault, D., Moineau, S. & Duchaine, C. Methods for Sampling of Airborne Viruses. *Microbiology and Molecular Biology Reviews* **72**, 413–444 (2008).

219. Lin, K. & Marr, L. C. Aerosolization of Ebola Virus Surrogates in Wastewater Systems. *Environ Sci Technol* **51**, 2669–2675 (2017).

220. Yang, W., Elankumaran, S. & Marr, L. C. Relationship between Humidity and Influenza A Viability in Droplets and Implications for Influenza's Seasonality. *PLoS One* **7**, e46789 (2012).

221. Harper, G. Airborne micro-organisms: survival tests with four viruses. *J Hyg (Lond)* **59**, 479–486 (1961).

222. Oswin, H. P. *et al.* The Dynamics of SARS-CoV-2 Infectivity with Changes in Aerosol Microenvironment. *medRxiv* 2022.01.08.22268944 (2022) doi:10.1101/2022.01.08.22268944.

223. Vejerano, E. P. & Marr, L. C. Physico-chemical characteristics of evaporating respiratory fluid droplets. *J R Soc Interface* **15**, (2018).

224. Daugelavičius, R. *et al.* Penetration of Enveloped Double-Stranded RNA Bacteriophages φ13 and φ6 into Pseudomonas syringae Cells. *J Virol* **79**, 5017–5026 (2005).

225. Hawks, S. A. *et al.* Infectious SARS-CoV-2 Is Emitted in Aerosol Particles. *mBio* **12**, (2021).

226. Hollý, J. *et al.* Comparison of infectious influenza A virus quantification methods employing immuno-staining. *J Virol Methods* **247**, 107–113 (2017).

227. Smither, S. J., Eastaugh, L. S., Findlay, J. S. & Lever, M. S. Experimental aerosol survival of SARS-CoV-2 in artificial saliva and tissue culture media at medium and high humidity. *Emerg Microbes Infect* **9**, 1415–1417 (2020).

228. D'Mello, A. *et al.* An in vivo atlas of host–pathogen transcriptomes during Streptococcus pneumoniae colonization and disease. *Proc Natl Acad Sci U S A* **117**, 33507–33518 (2020).

229. Kaul, D. *et al.* Microbiome disturbance and resilience dynamics of the upper respiratory tract during influenza A virus infection. *Nat Commun* **11**, 1–12 (2020).

230. Zhang, W. *et al.* Community structure of environmental microorganisms associated with COVID-19 affected patients. *Aerobiologia (Bologna)* **37**, 575 (2021).

231. Ku, D. N. *et al.* Ability of device to collect bacteria from cough aerosols generated by adults with cystic fibrosis. *F1000Res* **5**, (2016).

232. Yan, J. *et al.* Infectious virus in exhaled breath of symptomatic seasonal influenza cases from a college community. *Proc Natl Acad Sci U S A* **115**, 1081–1086 (2018).

233. Luhung, I. *et al.* Experimental parameters defining ultra-low biomass bioaerosol analysis. *NPJ Biofilms Microbiomes* **7**, 1–11 (2021).